AD-A159 312 SPANWISE REDISTRIBUTION OF ENERGY AND LOSS IN AN AXIAL FLOW COMPRESSOR BY..(U) GENERAL ELECTRIC CO CINCINNATI OH AIRCRAFT ENGINE BUSINESS GR.. C W WHITFIELD ET AL. 1/2

UNCLASSIFIED MAY 85 R84AEB460 AFWAL-TR-84-2109 F/G 20/4 NL

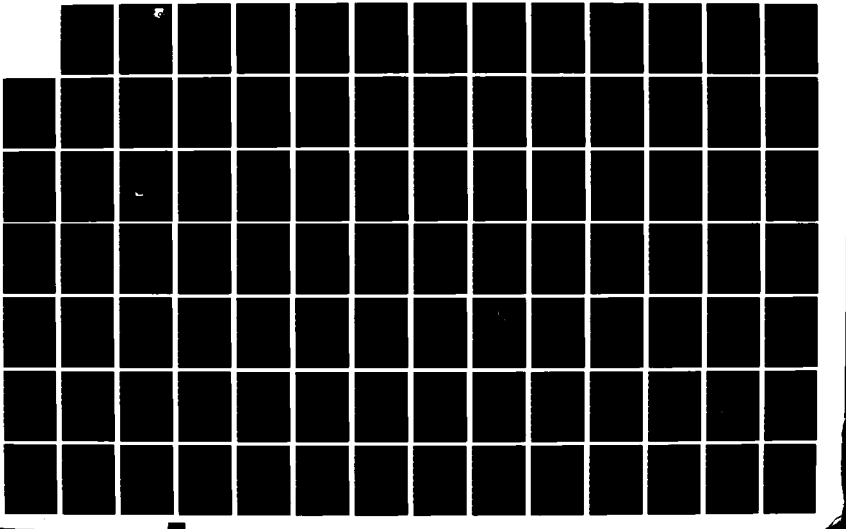

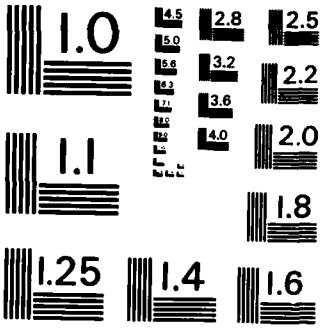

MICROCOPY RESOLUTION TEST CHART
NATIONAL BUREAU OF STANDARDS - 1963 - A

(2)

AFWAL-TR-84-2109

AD-A159 312

SPANWISE REDISTRIBUTION OF ENERGY AND LOSS IN AN AXIAL FLOW COMPRESSOR BY WAKE CENTRIFUGATION

C.W. Whitfield
J.S. Keith

General Electric Company
Aircraft Engine Business Group
Advanced Technology Programs Department
Cincinnati, Ohio 45215

~~February~~ May 1985

Final Report for Period 15 September 1981 through 15 March 1984

Approved for public release; distribution unlimited

DTIC FILE COPY

DTIC ELECTE SEP 19 1985 S

AERO PROPULSION LABORATORY
AIR FORCE WRIGHT AERONAUTICAL LABORATORIES
AIR FORCE SYSTEMS COMMAND
WRIGHT PATTERSON AIR FORCE BASE, OHIO 45433

NOTICE

When Government drawings, specifications, or other data are used for any purpose other than in connection with a definitely related Government procurement operation, the United States Government thereby incurs no responsibility nor any obligation whatsoever; and the fact that the government may have formulated, furnished, or in any way supplied the said drawings, specifications, or other data, is not to be regarded by implication or otherwise as in any manner licensing the holder or any other person or corporation, or conveying any rights or permission to manufacture use, or sell any patented invention that may in any way be related thereto.

This report has been reviewed by the Office of Public Affairs (ASD/PA) and is releasable to the National Technical Information Service (NTIS). At NTIS, it will be available to the general public, including foreign nations.

This technical report has been reviewed and is approved for publication.

ARTHUR J. WENNERSTROM
Chief, Compressor Research Group
Technology Branch

WALKER H. MITCHELL
Chief, Technology Branch
Turbine Engine Divivsion

FOR THE COMMANDER

H. IVAN BUSH
Director, Turbine Engine Division
Aero Propulsion Laboratory

If your address has changed, if you wish to be removed from our mailing list, or if the addressee is no longer employed by your organization please notify AFWAL/POTX, *W-PAFB, OH 45433 to help us maintain a current mailing list.*

Copies of this report should not be returned unless return is required by security considerations, contractual obligations, or notice on a specific document.

UNCLASSIFIED

SECURITY CLASSIFICATION OF THIS PAGE

A159 312

REPORT DOCUMENTATION PAGE

1a. REPORT SECURITY CLASSIFICATION UNCLASSIFIED	1b. RESTRICTIVE MARKINGS
2a. SECURITY CLASSIFICATION AUTHORITY	3. DISTRIBUTION/AVAILABILITY OF REPORT Approved for Public Release; Distribution Unlimited
2b. DECLASSIFICATION/DOWNGRADING SCHEDULE	
4. PERFORMING ORGANIZATION REPORT NUMBER(S) R84AEB460	5. MONITORING ORGANIZATION REPORT NUMBER(S) AFWAL-TR-84-2109
6a. NAME OF PERFORMING ORGANIZATION General Electric Aircraft Engine Business Group 6b. OFFICE SYMBOL (If applicable)	7a. NAME OF MONITORING ORGANIZATION Aero Propulsion Laboratory (AFWAL/POTX)
6c. ADDRESS (City, State and ZIP Code) General Electric Co. Advanced Technology Programs Department Cincinnati OH 45215	7b. ADDRESS (City, State and ZIP Code) Wright-Patterson AFB OH 45433
8a. NAME OF FUNDING/SPONSORING ORGANIZATION Aero Propulsion Laboratory 8b. OFFICE SYMBOL (If applicable) AFWAL/POTX	9. PROCUREMENT INSTRUMENT IDENTIFICATION NUMBER
8c. ADDRESS (City, State and ZIP Code) Wright-Patterson AFB OH 45433	10. SOURCE OF FUNDING NOS. PROGRAM ELEMENT NO.: 61102F PROJECT NO.: 2307 TASK NO.: 51 WORK UNIT NO.: 39
11. TITLE (Include Security Classification) Spanwise Redistribution of Energy and Loss in Axial Flow Compressor by Wake Centrifugation	
12. PERSONAL AUTHOR(S) C. E. Whitfield, J.S. Keith	
13a. TYPE OF REPORT Final 13b. TIME COVERED FROM 15SEP81 TO 15MAR84	14. DATE OF REPORT (Yr., Mo., Day) 85 05 15. PAGE COUNT 106
16. SUPPLEMENTARY NOTATION	

17. COSATI CODES			18. SUBJECT TERMS (Continue on reverse if necessary and identify by block number)
FIELD	GROUP	SUB. GR.	
21	05		Axial Compressor Analysis Secondary Flow Phenomena Spanwise Mixing
21	01		

19. ABSTRACT (Continue on reverse if necessary and identify by block number)

This report describes formulas derived for definition of the peak radial and streamwise velocity decrements/increments in a wake at a blade trailing edge and their decay with downstream distance. Comparisons with data show good agreement in most cases. In addition, the thickness, displacement thickness, and momentum thickness of the wake have been calculated and used in the prediction of changes in the circumferential average flow solution caused by the migration of wake fluid accross streamlines.

20. DISTRIBUTION/AVAILABILITY OF ABSTRACT UNCLASSIFIED/UNLIMITED ☒ SAME AS RPT. ☐ DTIC USERS ☐	21. ABSTRACT SECURITY CLASSIFICATION UNCLASSIFIED
22a. NAME OF RESPONSIBLE INDIVIDUAL Steven L. Puterbaugh	22b. TELEPHONE NUMBER (Include Area Code) 513-255-4738 22c. OFFICE SYMBOL AFWAL/POTX

DD FORM 1473, 83 APR EDITION OF 1 JAN 73 IS OBSOLETE.

Unclassified

SECURITY CLASSIFICATION OF THIS PAGE

Preface

This Final Technical Report was Prepared by the Advanced Engineering Technologies Department, Aircraft Engine Business Group, General Electric Company, Evendale, Ohio for the United States Air Force Systems Command, Air Force Wright Aeronautical Laboratories Wright-Patterson Air Force Base, Ohio under Contract F33615-81-C-2090. The work was performed over a period of two and one-half years starting in September 1981. Lucien L. Debruge was the Air Force Project Engineer for this program.

The objective of this program was to develop and codify a method for predicting the spanwise redistribution of energy and loss associated with rotor/stator wakes in an axial-flow compressor. The mechanisms considered were: (1) spanwise transport of wake fluid due to imbalance of the radial pressure gradient; and (2) accumulation/dilution of wake fluid at the inner and outer casing. The work consisted of developing computer modules that perform the above defined objective.

For the General Electric Company Mr. J.S. Keith was the Technical Program Manager for this program. Dr. C.E. Whitfield was the principal investigator. Mr. A.J. Bilhardt was the overall Program Manager.

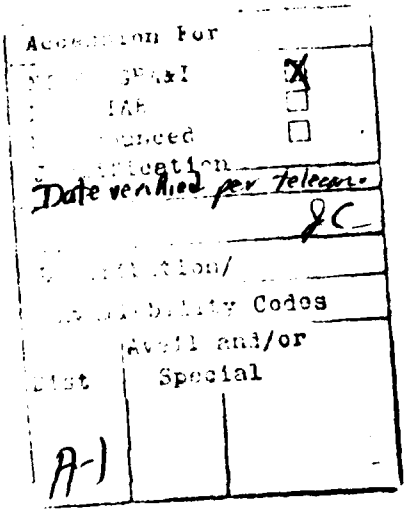

TABLE OF CONTENTS

TABLE OF CONTENTS

LIST OF ILLUSTRATIONS

LIST OF ILLUSTRATIONS (Continued)

LIST OF ILLUSTRATIONS (Concluded)

SYMBOLS

Symbol	Definition
a	Blade Spacing
C	Absolute air velocity (free stream)
c	Absolute air velocity (wake)
C_p	Specific heat at constant pressure
D	Substantial derivative
D	Normalized maximum streamwise velocity defect in the wake $\frac{W - W_{xp}}{W}$
D^*_{eq}	Equivalent diffusion ratio
E	Energy increment
F	Wake profile function
G	Normalized maximum radial velocity increment in the wake, u_{r_p}/W
G_{I1}, G_{I2}, G_{I3}	Gaussian Integrals
H	Form factor $\frac{\delta^*}{\theta}$ or total enthalpy
h	Static enthalpy
H	Total enthalpy
h_m	Lamina thickness
I	Total rothalpy
M	Mass or Mach number
m	Distance along streamline in nonorthogonal coordinate system

SYMBOLS (Continued)

Symbol	Definition
N_B	Number of blades in the row
n	Power law index or distance normal to streamline
η	Distance normal to streamlines in the cross-annulus direction
P	Property-stagnation enthalpy, stagnation rothalpy, angular momentum or entropy
p	Static pressure
q	Distance along nonorthogonal coordinate
R	Gas constant
r	Radius
S	Entropy
T	Static temperature
Δt	Arbitrary time interval
t_{max}/c	Maximum thickness/chord ratio
U	Rotational speed
u	Wake incremental velocity, (w - W)
u_p	Peak streamwise velocity decrement at the center of the wake, $W-w_p$. Note sign convention difference between u and u_p.
u_g	Streamwise wake mass-energy-weighted velocity decrement. Sign convention is the same as for u_p.
V_o	Free-stream velocity before wake mixing
V_1	Inlet velocity
V_{max}	Maximum velocity on the suction surface
V_p	Mean passage velocity in the throat region
W_{tf}	Total flow rate in the annulus
W	Free-stream relative velocity

SYMBOLS (Continued)

Symbol	Definition
w	Wake relative velocity
x	Streamwise coordinate
y	Cross-wake coordinate
z	Axial coordinate
α	Absolute air angle
β	Relative air angle of the primary flow (that is, before secondary flow effects are added)
δ	Boundary layer thickness or wake half thickness
δ^*	Boundary layer or wake total displacement thickness
ΔP	Passage-mass-weighted increment of property P
$\Delta P'$	Passage-mass-weighted increment of property P which results from the redistribution due to wake centrifugation
ε	Eddy viscosity or mixing coefficient
η	$\frac{y}{\delta}$, normalized wake coordinate
θ	Boundary layer or wake total momentum thickness or factor used in mixing equation discretization
λ	Circumferential (blade or boundary layer) blockage factor
ψ	Stream function
ξ	$x-x_o$, downstream distance from origin of wake decay
ρ	Density
σ	Solidity or angle between q-direction and radial direction
ϕ	Angle between axisymmetric stream surface and z-direction in meridional plane
Ω	Angular velocity

Equation (18) can be simplified further. Writing

$$\frac{\partial u_r}{\partial t} + \vec{w} \cdot \nabla u_r = \frac{Du_r}{Dt} \simeq W \frac{Du_r}{Dx} \qquad \text{(x is streamwise)}$$

$$w_\theta + W_\theta + 2\Omega r = C_\theta + c_\theta$$

where C_θ is the absolute tangential velocity in the freestream, c_θ is the absolute tangential velocity in the wake and

$$\begin{aligned} u_\theta &= w_\theta - W_\theta \\ &= (w_x - W) \sin \beta \\ &= D\ W\ F \sin \beta \text{ (from the previous section).} \end{aligned}$$

Neglecting the fourth and last terms in the left-hand side of Equation (18), in accordance with Equation (1) of Section 3.1.1, and introducing the concept of eddy viscosity, as was done in the previous section, gives the following "simplified radial momentum equation" for the wake fluid:

$$W \frac{Du_r}{Dx} = - \frac{C_\theta + c_\theta}{r} \ D\ W\ F \sin \beta + \varepsilon \frac{\partial^2 u_r}{\partial y^2} \tag{19}$$

The value of c_θ in Equation (19) can be calculated from the expression

$$c_\theta = W(1 - DF) \sin \beta + \Omega r$$

The results given in Reference 12 were obtained using the approximation

$$c_\theta \simeq C_\theta$$

which is felt to be reasonable in the far wake except when the absolute velocity is near axial.

Assume that the radial velocity profile of the wake can be represented by the same Gaussian function as the streamwise profile

$$\frac{u_r}{W} = \frac{w_r - W_r}{W} = G\ F = G\ e^{-\pi\eta^2}$$

Here $\vec{w}$ is the velocity of any wake particle and F_v represents the viscous forces in the wake. The wake incremental velocity, u, is defined by:

$$\vec{w} = \vec{u} + \vec{W}$$

where $\vec{W}$ is the freestream velocity, and ρ_e will denote the freestream fluid density.

Substituting for $\vec{w}$ in Equation (16) gives

$$\frac{\partial \vec{u}}{\partial t} + \vec{w}\cdot\nabla\vec{u} + \vec{u}\cdot\nabla\vec{W} + 2\vec{\Omega} \times \vec{u} + \left(\frac{1}{\rho_w} - \frac{1}{\rho_e}\right)\nabla p - F_v$$

$$= -\left\{\frac{\partial \vec{W}}{\partial t} + \vec{W}\cdot\nabla\vec{W} + 2\vec{\Omega} \times \vec{W} - \Omega^2\vec{r} + \frac{1}{\rho_e}\nabla p\right\} = 0 \qquad (17)$$

The right-hand side of the above equation is the equation of motion for the freestream fluid which is assumed to be satisfied.

Using cylindrical polar coordinates and making use of the vector relationships

$$\frac{\partial(\vec{i}_\theta)}{\partial\theta} = -\vec{i}_r$$

and

$$\frac{\partial(\vec{i}_r)}{\partial\theta} = \vec{i}_\theta$$

gives, for the radial component of Equation (17)

$$\frac{\partial u_r}{\partial t} + \vec{w}\cdot\nabla u_r - \frac{w_\theta u_\theta}{r} + \vec{u}\cdot\nabla W_r - \frac{u_\theta W_\theta}{r} - 2\Omega u_r + \left(\frac{1}{\rho_w} - \frac{1}{\rho_e}\right)\frac{\partial p}{\partial r} = F_{v_r} \qquad (18)$$

Substituting this into Equation (12) gives the results

$$\frac{d\delta^2}{dx} = \frac{4\pi\epsilon}{W} \tag{13}$$

and

$$\frac{dD}{dx} = -\frac{D}{W}\frac{dW}{dx} - \frac{2\pi\epsilon D}{\delta^2 W} \tag{14}$$

Therefore, if the eddy viscosity, ϵ, and the freestream velocity, W, are constant with distance downstream, the wake thickness and velocity deficit will vary as

$$\delta \propto (x - x_o)^{\frac{1}{2}} \tag{15a}$$

and

$$D \propto (x - x_o)^{-\frac{1}{2}} \tag{15b}$$

The choice of x_o in the results presented in References 11 and 12 was determined empirically from experimental data as a point 12% of chord upstream of the trailing edge.

3.2.2 Radial Wake Decay

A similar approach is used to calculate the decay of the peak radial velocity in the wake with distance downstream. The equation of motion for flow in rotating coordinates is

$$\frac{\partial \vec{w}}{\partial t} + (\vec{w}\cdot\nabla)\vec{w} + 2\vec{\Omega}\times\vec{w} - \Omega^2\vec{r} + \frac{1}{\rho}\nabla p = F_v \tag{16}$$

Knowing the form factor at the trailing edge, H_{TE}, and using the above, the maximum streamwise deficit at the trailing edge, D_{TE}, is given by

$$D_{TE} = \sqrt{2}\left(1 - \frac{1}{H_{TE}}\right) \tag{10}$$

3.2 WAKE DEVELOPMENT

3.2.1 Streamwise Wake Decay

In order to follow the path of the wake fluid, it is necessary to predict the decay of the wake velocity defect. This is accomplished by considering the streamwise momentum equation for the wake which can be written

$$w_x \frac{\partial w_x}{\partial x} + w_y \frac{\partial w_x}{\partial y} + \frac{1}{\rho}\frac{dp}{dx} = \epsilon \frac{\partial^2 w_x}{\partial y 2} \tag{11}$$

In the "far wake" (greater than some fractional blade chord distance downstream), $w_x \simeq W$. Also, from the freestream momentum equation

$$W \frac{\partial W}{\partial x} = -\frac{1}{\rho}\frac{dp}{dx}$$

Neglecting the second term in Equation (11) and assuming that the pressure and density in the wake are equal to the freestream values, Equation (11) becomes

$$W \frac{\partial w_x}{\partial x} - W \frac{\partial W}{\partial x} = \epsilon \frac{\partial w_x}{\partial y^2} \tag{12}$$

where ϵ is an eddy viscosity.

In Section 3.1.2 the wake profile was described by a universal function:

$$\frac{W - w_x}{W} = D\,F(\eta) = D\,e^{-\pi\eta^2}$$

and its momentum thickness, likewise

$$\frac{\theta}{\delta} = \int_{-\infty}^{\infty} \left(1 - \frac{w_x}{W}\right) \frac{w_x}{W} \frac{dy}{\delta} = D\int_{-\infty}^{\infty} F\, d\eta - D^2\int_{-\infty}^{\infty} F^2 d\eta \tag{8}$$

Integrals of the Gaussian profile function are found to be:

$$G_{I1} = \int_{-\infty}^{\infty} F\, d\eta = 1 \tag{9a}$$

$$G_{I2} = \int_{-\infty}^{\infty} F^2 d\eta = \frac{1}{\sqrt{2}} \tag{9b}$$

$$G_{I3} = \int_{-\infty}^{\infty} F^3 d\eta = \frac{1}{\sqrt{3}} \tag{9c}$$

Thus, the wake form factor is

$$H = \frac{\delta^*}{\Theta} = \frac{DG_{I1}}{DG_{I1} - D^2 G_{I2}} = \frac{1}{1 - D\,\dfrac{G_{I2}}{G_{I1}}}$$

$$H = \frac{1}{1 - \frac{1}{\sqrt{2}} D}$$

Formulas for calculating these velocity ratios may be found in Appendix 1 of Reference 7.

Given the value of H_{TE}, Equations (4) and (3) are substituted into Equation (2) which is integrated from midchord to the trailing edge of the blade. It is assumed that at midchord the blade boundary layer is collateral. It is further assumed that the result of the integration of Equation (2) is a radial velocity increment at the trailing edge, which is to be added to the free-stream radial velocity. Note that the value 0.05 was selected so Equation (2) would yield the peak wake radial velocity observed experimentally.

3.1.2 Streamwise Wake Velocity Defect

The streamwise wake velocity defect is based on the assumption that all wake profiles can be represented by a single function

$$\frac{W-w_x}{W} = D\,F(\eta) \tag{6}$$

where

W = freestream relative velocity

w_x = streamwise velocity in the wake

D = maximum velocity defect, $\frac{W-w_{xp}}{W} = \frac{u_p}{W}$

$F(\eta)$ = Gaussian profile function = $e^{-\pi\eta^2}$

$\eta = \frac{y}{\delta}$

δ = wake thickness parameter, approximately equal to the wake half width

x, y = streamwise and cross-stream coordinates.

The displacement thickness of the wake is

$$\frac{\delta^*}{\delta} = \int_{-\infty}^{\infty}\left(1 - \frac{w_x}{W}\right)\frac{dy}{\delta} = D\int_{-\infty}^{\infty} F(\eta)\,d\eta \tag{7}$$

$$k_w = (0.05)^{\frac{1}{n}} = (0.05)^{\frac{H-1}{2}} \tag{3}$$

In order to integrate Equation (2) along the blade chord we must find an expression for H, the form factor of the streamwise boundary layer. Assume that boundary layer growth is most pronounced over the trailing half of the blade. Let the streamwise boundary layer be represented by

$$\frac{w_z}{W_z} = \left(\frac{y}{\delta}\right)^{\frac{1}{8}}$$

at the midchord of the blade. Then $H = H_o = 1.25$ at this point and, if the chordwise distribution of H is given by a parabola, we have

$$H(z) = H_o + 4\,(H_{TE} - H_o)\,(z - z_o)^2\,/(z_{te} - z_1)^2 \tag{4}$$

where z_o is at midchord and H_{TE} has yet to be determined.

The loss correlations of Koch and Smith (Reference 7) show the variation of trailing edge form factor and momentum thickness with equivalent diffusion ratio. In this work we are interested in the value of trailing edge form factor resulting from the suction surface only; the Koch and Smith curves have been modified to reflect this. Since only leading and trailing edge information is assumed known, the calculation of equivalent diffusion ratio is related to the following three velocity ratios:

$$D^*_{eq} = \frac{V_{max}}{V_{oTE}} = \frac{V_p}{V_1}\,\frac{V_{max}}{V_p}\,\frac{V_1}{V_{oTE}} \tag{5}$$

where

V_p = mean passage velocity in the throat region,
V_{max} = maximum velocity on the suction surface,
V_o = free stream velocity before wake mixing
V_1 = inlet velocity.

3.0 ANALYSIS AND COMPUTATIONAL TECHNIQUES

3.1 TRAILING EDGE WAKE DEFINITION

3.1.1 Wake Peak Radial Velocity

The wake radial velocity calculation is based on Equation (32) of Adkins and Smith (Reference 1).

$$\frac{Dw_r}{W_z} = \frac{1}{k_w}\left\{\frac{DW_r}{W_z} - \frac{Dz}{r}\left[\tan^2\beta_z\,(1 - k_w^2) + 2\,\tan\beta_z\,\frac{\Omega r}{W_z}\,(1 - k_w)\right]\right\} \quad (1)$$

where

$$k_w = \frac{w_z}{W_z}$$

If it is assumed that $DW_r = 0$ (no free-stream radial acceleration), Equation (1) becomes

$$\frac{Dw_r}{W_z} = \frac{-Dz\,\tan\beta_z}{r}\left[\tan\beta_z\left(\frac{1}{k_w} - k_w\right) + \frac{2\Omega r}{W_z}\left(\frac{1}{k_w} - 1\right)\right] \quad (2)$$

The boundary layer streamwise velocity profile can be approximated by a power law distribution:

$$\frac{w_z}{W_z} = \left(\frac{y}{\delta}\right)^{\frac{1}{n}}$$

which yields

$$H = \frac{\delta^*}{\theta} = \frac{n+2}{n}$$

It is reasonable to assume that conditions in the boundary layer are typified by those occurring at some point relatively deep in it, say at $y/\delta = 0.05$. It can be seen (for example, Johnston in Reference 14) that this is sufficiently far away from the wall for inviscid theory to be used in estimating the radial crossflow. Thus,

2.3 CONTENTS

This report describes the techniques used to predict the wake peak radial velocity, the peak streamwise velocity decrement, and the momentum thickness and displacement thickness at the trailing edge of a blade. Also defined are the "mass-energy-average" velocity decrements of the wake and the decay of these various velocity decrements with distance downstream. The radial velocity of the wake fluid will also be affected by its proximity to the annulus walls. Taking these factors into account, the tracking of wakes is described. Finally, the insertion of the wake source terms into the mixing equation and the subsequent effects on the circumferential average flow solution are shown.

The results obtained during the course of this investigation show the agreement between theory and experimental data obtained for peak radial and streamwise velocity increments/decrements in the wakes of four machines, together with differences in peak radial velocities calculated by the Adkins and Smith method and by the method described here. Comparisons of circumferential average flow solutions obtained with the Adkins and Smith scheme, and with the new scheme showing both the effect of the new wake definition on the mixing results and the effect of the inclusion of wake fluid migration in addition to this, have been made for the Air Force 1500 ft/s, Transonic, High-Through-Flow, Single-Stage Axial-Flow Compressor.

Not presented in this final report is the effect of the wake impinging on the pressure side of downstream blade rows in altering the radial velocity of the wake. This effect was studied and then omitted because it was found inconsequential.

that at the midchord of the blade the boundary layer is collateral and the form factor grows parabolically from midchord to the value predicted by the modified Koch and Smith curves at the trailing edge of the blade.

These assumptions enable the Adkins and Smith equation for the peak radial velocity of a representative particle in the blade suction surface boundary layer to be integrated from the midchord to the trailing edge of a blade. When combined with the wake radial velocity increment decay laws formulated in the course of this work and described here, encouraging agreement is found between theory and experimental data for most test cases studied.

2.2 MIXING CALCULATION

The objective behind a better calculation of the peak radial velocity in the wake is to include the effects of wake migration in the movement of fluid properties across streamlines - the mixing process. In the original work of Adkins and Smith, wake radial velocity and thickness were used to modify the spanwise secondary flow profile resulting from the various Trefftz-plane solutions of Poisson's equation for the secondary flow stream function.

In the work described here, the definition of the wake radial velocity and width have been improved. In addition, the effect of wake fluid property migration, as opposed to mixing of circumferential average properties, has been modeled.

Consider a wake shed from a rotor blade. The fluid in the wake will have a lower relative streamwise velocity than the surrounding fluid. Because of this, the wake fluid will have a higher absolute swirl velocity and hence, assuming the total rothalpy in the wake is equal to that in the free stream, a higher total enthalpy and angular momentum. The entropy of the wake fluid will also be higher than that of the surrounding fluid. As the wake fluid progresses downstream it will carry these property increments with it; thus, as the fluid migrates radially, there will be a redistribution of properties.

In order to calculate the effect of wake fluid migration on the radial distribution of circumferential average properties, it is necessary to define the "property carrying capacity" of the wake, the streamwise and radial velocities at which the properties will be carried, and the radial location of the wake fluid at the various calculation stations downstream of the shedding row. To include this property migration in the circumferential average flow solution, it is necessary to modify the mixing equation of Adkins and Smith to include these wake "source" terms and use this new form of the equation in the through-flow computer analysis.

The calculations of Adkins and Smith demonstrate quite dramatically the effects of enabling and disabling the mixing process. Agreement obtained between calculations and test data with mixing enabled showed clearly the need for taking this process into account when calculating the circumferential average flow solution. However, at the outset of the work described here it was felt that the blade boundary layer/wake centrifugation model used by Adkins and Smith was considerably less sophisticated than their other work. First, it was felt that the trailing edge estimates of wake width and the spanwise component of velocity were unnecessarily crude. Second, their modeling of the "mixing" process through the use of the homogeneous diffusion equation precluded the possibility of predicting the tendency for the high temperature fluid in the rotor wake to migrate outward, accumulate near the casing, and increase the circumferential average temperature there.

Thus, the work described here and in References 8 through 13 falls into two categories: improvement of the blade boundary layer/wake centrifugation model of Adkins and Smith to bring it to the same level of sophistication as the other four secondary flow models, and reformulation of their mixing model in order to present a more realistic picture of the flow properties as they are convected downstream.

2.1 WAKE RADIAL VELOCITY DEFINITION

The method used by Adkins and Smith to determine the maximum radial velocity in the wake shed from a rotating or stationary blade in an axial-flow turbomachine is believed to be deficient in that no account was taken of the effects of blade loading. The approach taken here is intended to rectify this situation.

In order to derive an expression for spanwise velocity in the boundary layer on an axial-flow turbomachine blade, Adkins and Smith considered the spanwise acceleration of a representative small mass of fluid in the blade boundary layer at a representative point along the chord. In the absence of viscous stresses, this acceleration was assumed to act over the time taken by the particle to travel a representative distance, resulting in a spanwise velocity. Comparison with available test data led to the selection of the value of a constant in the model.

For the present work, the equation derived by Adkins and Smith has been retained. Application of this equation requires an integration along the chord of the blade and it is the underlying assumptions behind this integration that have been changed. In particular, blade loading effects have been included by means of the loss correlations of Koch and Smith (Reference 7) which have been modified for this purpose to reflect boundary layer growth on the blade suction surface only. It has been assumed that the streamwise velocity profile of the boundary layer on the blade suction surface can be represented by a power law distribution, and also that conditions in the boundary layer are typified by those occurring at a point relatively deep in it whose location can be chosen to approximate the peak radial velocity. It is assumed further

2.0 INTRODUCTION

In the study of the complex flow that occurs within the compressor and turbine of today's axial flow turbomachines it is usual for simplifying assumptions to be made. For instance, virtually all analytical methods used at present in the design of compressor and turbine blade rows contain the assumption that the flow remains on axisymmetric stream surfaces as it passes through the blade row; an assumption that, as designers are aware, is not really valid.

The causes of blade-to-blade stream surface distortion are many and various. For instance, if the incoming flow to a blade row contains vorticity or if the blade circulation varies along the span, secondary flows are generated that cause blade-to-blade (or S1) stream surface twists. Likewise, if a sweep condition is present, the tendency of the flow to maintain its spanwise velocity component while other velocity components are changed by the turning action of the blades will lead to S1 surface distortions. Another physical reason why some portion of the fluid passing through a blade row may depart substantially from otherwise axisymmetric or slightly twisted S1 surfaces involves three dimensional flow in the blade boundary layers and wakes. It is this last phenomenon with which the present work is concerned.

In a recent paper, Adkins and Smith (Reference 1) describe a method whereby the secondary flows generated within the blade passages of an axial-flow turbomachine can be quantified and used in an analysis of the meridional flow field. In the course of this work, they considered that the secondary flow field was the resultant of five effects: (1) mainstream nonfree-vortex flow, (2) end wall boundary layers, (3) blade end clearances, (4) blade end shrouding, and (5) blade boundary layer and wake centrifugation. The techniques used were based on earlier work of Smith (References 2 through 5) and Lakshiminarayana and Horlock (Reference 6). In particular, models were developed to predict:

a. The overturning/underturning swirl angle deviation that must be added to the primary (two-dimensional blade-to-blade) flow to arrive at the full three-dimensional flow swirl angles

b. Spanwise redistribution of (circumferential average) total temperature and total pressure

c. End wall losses that may be applied on a blade-row by blade-row basis and used with the profile loss model of Koch and Smith (Reference 7).

The present effort is directed toward improvement of Part (b) of the Adkins and Smith (Reference 1) work. Parts (a) and (c) are left essentially intact.

1.0 SUMMARY

This report describes work accomplished under Air Force Contract F33615-81-C-2090 between September 1981 and March 1984. During this time, formulae have been derived and encoded for definition of the peak radial and streamwise velocity decrements/increments in a wake at a blade trailing edge and their decay with downstream distance. Comparisons with data show good agreement in most cases. In addition, the thickness, displacement thickness, and momentum thickness of the wake have been calculated and used in the prediction of changes in the circumferential average flow solution caused by the migration of wake fluid across streamlines. Wake fluid has been tracked from its shedding blade row through the downstream row with the effects of fluid buildup on hub and casing walls taken into account. Final results compare circumferential average flow results obtained using the new wake definition model with earlier analysis.

SYMBOLS (Concluded)

Symbol	Definition
Subscripts	
e	Free stream
g	Wake aggregate
m	Meridional
p	Peak or centerline value within the wake
r	Radial
s	Spanwise
TE	Trailing edge
θ	Tangential
w	Wake
x	Streamwise
z	Axial
o	Origin
1	Inlet to cascade
2	Outlet from cascade

where G is the maximum value of $\frac{u_r}{W}$

Substitution in Equation (19) leads to the result

$$\frac{dG}{dx} = - \frac{2D\ C\theta}{rW} \sin \beta - \frac{G}{2(x - x_o)}$$

if W is constant with distance downstream and $C_\theta = c_\theta$. In integral form this equation is

$$G_2 = G_1 - \int_1^2 \left[\frac{2C_\theta \sin \beta}{rW} D + \frac{G}{2(x - x_o)} \right] dx \qquad (20)$$

where 1 and 2 are adjacent points in the streamwise direction. Equation (20) is integrated numerically, no analytic result having been found.

3.3 WAKE PARTICLE TRACKING

3.3.1 Calculation of Wake Fluid Trajectories

Consider a blade row in an axial-flow turbomachine. There is flow relative to this row; thus, a wake is shed from the trailing edge of each blade in the row. At each radial streamline position, the initial deficits in the wake in both streamwise and radial directions can be calculated by the formulae of Section 3.1. As the wake passes downstream we can calculate the decay of these deficits by the application of formulae from Section 3.2. Primarily we are concerned with the radial movement of the wake fluid relative to the circumferential average flow streamlines. This is accomplished by integrating

$$\int_{TE} d\psi_g = \frac{1}{W_{tf}} \int_{TE} 2\pi r \lambda \rho C_m u_{rg} \cos \phi \, Dt,$$

where ψ_g is the stream function value of the wake aggregate, u_{rg} is the radial velocity increment of the wake fluid ($u_{rg} = w_{rg} - W_r$), W_{tf} is the total mass flow rate and λ, ρ, C_m, and ϕ are the circumferential average through-flow values of blockage, density, meridional velocity, and meridional angle.

The radial velocity increment, u_{rg}, may take into account not only the radial velocity in the wake but any effects of secondary flow in downstream blade rows and any modification to the wake radial velocity caused by contact with downstream blade surfaces. Such effects were considered in some detail in the early part of this study, and the results were reported in References 9, 10, and 11. However, because these effects are small (in terms of the overall mixing process), it was felt that the additional complexity needed to include the impingement and secondary flow modification to radial wake velocities in the product code was not justified and, hence, has been omitted.

3.4 TRANSPORT OF WAKE PROPERTIES

3.4.1 General

Let P be any property. Further, let $\bar{P}$ be the circumferential average of P and ΔP the (mass-averaged) increment of P associated with a spanwise migrating "hot" wake. Specifically,

$$\Delta P = \frac{\int_{-\delta}^{\delta} (P - \bar{P}) \rho w_x \, dy}{\frac{2\pi r \lambda}{N_B} \bar{\rho} \bar{C}_m}$$

Consider the spanwise transport of P when:

1. There exists a blade-to-blade variation of the spanwise velocity and a radial variation of $\bar{P}$, but $\Delta P = 0$ everywhere, or

2. There is a radial migration of the "hot" wake, for which ΔP is nonzero, but $\bar{P}(r)$ is radially constant.

These two cases are schematically depicted in Figure 1.

Conceptually, both of these cases can be treated by the inviscid convection equations. First, identify a large number of fluid elements at, say, the trailing edge plane, and then use a (presumed) knowledge of the three-dimensional flow field velocities (especially the spanwise velocity components) to compute the relative position of these fluid elements at a downstream plane. From the conserved convected properties, stagnation enthalpy (rothalpy) or entropy, of each fluid element a determination of the downstream circumferential average property is possible.

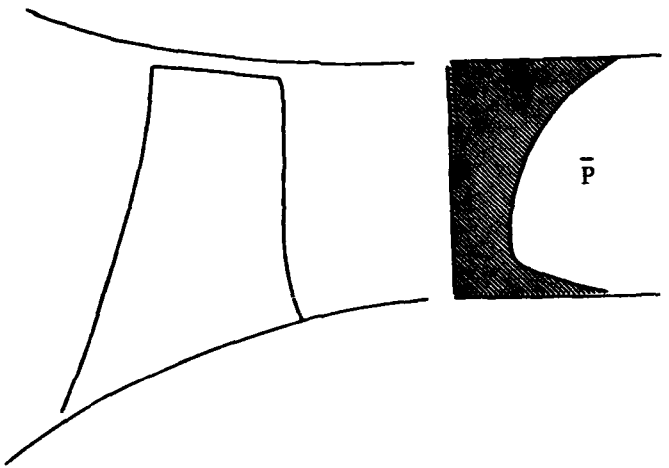

(1) Radial Variation of $\bar{P}$ with $\Delta P = 0$

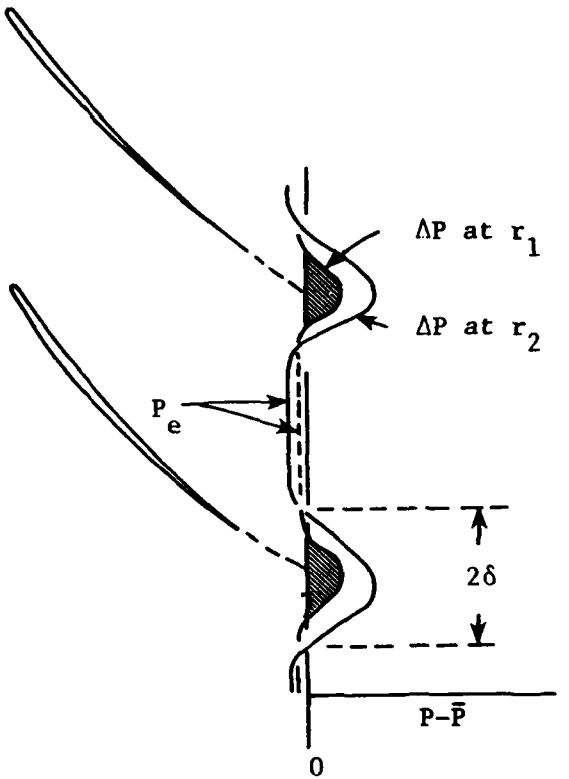

(2) Radial Variation of Nonzero ΔP with Constant $\bar{P}$

Figure 1. Two Cases for Which Radial Transport of P Is Considered.

In practice, Adkins and Smith, in Section 4.1 of Reference 1, found that the spanwise transport of $\bar{P}$ (Case 1) is modeled simply and accurately by the diffusion equation*:

$$\rho C_m \frac{D\bar{P}}{Dm} - \frac{1}{r}\frac{\partial}{\partial n}\left(r\epsilon \frac{\partial \bar{P}}{\partial n}\right) = 0 \qquad (21)$$

where

$$\epsilon = \frac{\rho m}{aC_m}\int_o^a V_s^2\, dt$$

Unfortunately, this equation does not model a convection process in which there exists a correlated cross-passage variation of property P and radial velocity w_r; that is, when the cross-passage P and w_r profiles have roughly the same shape (Case 2).

A method for treating this second type of spanwise transport is the subject of the present section. The method for combining the two cases is subsequently described in Section 3.5.

Before proceeding, a point of clarification: As illustrated in Figure 2, one can define two values of ΔP

$$\Delta P_w = \frac{N_B\int_o^a \max\,(0,\ P-\bar{P})\ \rho w_x\, dy}{2\pi r\lambda\ \bar{\rho}\,\bar{C}_m}$$

$$\Delta P_{fs} = \frac{N_B\int_o^a \min\,(0,\ P-\bar{P})\ \rho w_x\, dy}{2\pi r\lambda\ \bar{\rho}\,\bar{C}_m}$$

*Equation (21) was derived by considering only spanwise secondary flow. The equation is not strictly valid in a region with a large cross-passage component of secondary velocity, as occurs near the end wall.

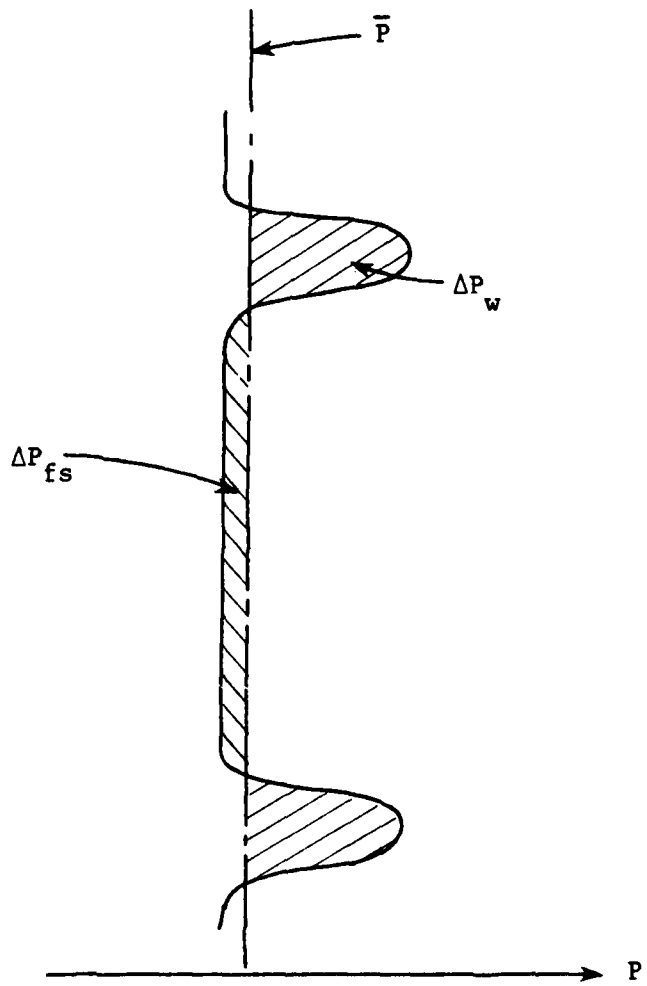

Figure 2. Illustration of Wake and Free-Stream Property Increments.

where the integrals are carried out over one blade spacing and

max (A, B) ≡ larger of A and B

min (A, B) ≡ smaller of A and B

From the above it follows that:

$$\Delta P_w + \Delta P_{fs} = 0$$

So, ΔP_{fs}, the property (or energy) increment associated with the freestream fluid, is the same magnitude as that of the wake fluid (ΔP_w). However, the radial velocity of the freestream fluid, opposite in sign from that of the wake fluid to maintain continuity, is much smaller in magnitude. Hence, the spanwise displacement of energy ΔP_{fs} is smaller than that of ΔP_w and is neglected.

Furthermore, it is convenient to use the freestream, rather than the average value, as the reference level. Thus, in the following sections, the freestream value, P_e, will replace $\bar{P}$ in the equations that define ΔP.

3.4.2 Passage-Mass-Weighted Wake Property Increments

As described in Section 3.3, particles of wake fluid are generated at the trailing edge of a blade row and, as described in the same section, are tracked through the next downstream row. These particles of fluid are carrying energy in the form of total enthalpy or total rothalpy, and they also have entropy associated with them. Therefore, they do not move downstream at the peak streamwise velocity decrement calculated earlier, but rather at a mass-energy-decrement-weighted average velocity obtained as follows. Consider an aggregate of wake fluid: this aggregate has mass

$$M_g = \Delta t \, h_m \int_{-\delta}^{+\delta} \rho w_x \, dy \qquad (22)$$

where

h_m = lamina thickness
Δt = arbitrary time interval

Assume the aggregate is carrying energy in the form of total enthalpy and is part of a wake shed from a rotor blade. Assume also that the total rothalpy across the wake is constant and equal to the freestream value.

Thus in the wake

$$H = I + U\, c_{\theta_w} = I + U(U + w_\theta)$$

$$H = I + U^2 + U w_x \sin \beta$$

and for the freestream

$$H_e = I + U^2 + UW \sin \beta$$

where β is generally negative for a rotor. The local energy increment of the wake fluid is, thus,

$$H - H_e = U(w_x - W) \sin \beta \tag{23}$$

and the integrated mass-energy-decrement is

$$M_g\, \delta H_g = \Delta t\, h_m \int_{-\delta}^{\delta} (H - H_e)\, \rho w_x\, dy$$

$$= -\Delta t\, h_m\, \rho_e\, UW^2 \sin \beta \int_{-\delta}^{\delta} \left(1 - \frac{w_x}{W}\right) \frac{\rho w_x}{\rho_e W}\, dy$$

$$M_g \delta H_g = -\Delta t\, h_m\, \rho_e\, UW^2 \sin \beta\, \Theta \tag{24}$$

where θ is the momentum thickness in the wake.

The total mass of fluid for a given lamina thickness, h_m, is given as

$$M_T = \Delta t\, \frac{2\pi r \lambda}{N_B}\, h_m\, \bar{\rho}\, \bar{C}_m \tag{25}$$

where $\bar{\rho}$ and $\bar{C}_m$ are circumferentially mass-averaged values used in the through-flow analysis program and N_B is the number of blades. From this it follows that the passage-mass-weighted-energy increment, for any spanwise position, is:

$$\Delta H = \frac{M_g \delta H_g}{M_T} = -\frac{UW^2 \sin \beta}{\lambda\, C_m}\, \frac{N_B \theta}{2\pi r} \tag{26}$$

The small difference between the freestream density, ρ_e, and the average density, $\bar{\rho}$, has been neglected.

In addition to the increment of energy, the wake fluid also convects an increment of entropy (loss). By definition,

$$S - S_e = C_p \ln \left(\frac{T}{T_e}\right) - R \ln \left(\frac{P}{P_e}\right)$$

where S is the entropy at any point in the wake and S_e is the entropy in the freestream. Since the pressure is uniform across the wake, the above immediately reduces to

$$S - S_e = C_p \ln \left(\frac{h}{h_e}\right)$$

$$= C_p \ln \left[\frac{I + \frac{1}{2} U^2 - \frac{1}{2} w_x^2}{I + \frac{1}{2} U^2 - \frac{1}{2} W^2}\right]$$

$$= C_p \ln (1+x)$$

where

$$x = \frac{(W-w_x)(W + w_x)/2}{I + \frac{1}{2} U^2 - \frac{1}{2} W^2}$$

The term x can be considered small. Therefore, the expansion

$$\ln(1+x) = x - \frac{1}{2} x^2 + \frac{1}{3} x^3 \ldots\ldots$$

is approximately equal to x and the expression for entropy becomes:

$$S-S_e = C_p \frac{W^2}{h_e} \left(1 - \frac{w_x}{W}\right) \qquad (27)$$

Here, the approximation that

$$\tfrac{1}{2}(W+w_x) = W$$

has already been made.

Now following the same steps as were made earlier for the stagnation enthalpy increment, it follows that:

$$M_g \delta S_g = \Delta t\, h_m \int_{-\delta}^{\delta} (S - S_e)\, \rho w_x \, dy$$

$$= \Delta t\, h_m \rho_e \frac{C_p W^3}{h_e} \int_{-\delta}^{\delta} \left(1 - \frac{w_x}{W}\right) \frac{\rho w_x}{\rho_e W} \, dy$$

$$M_g \delta S_g = \Delta t\, h_m \rho_e \frac{C_p W^3}{h_e} \Theta \tag{28}$$

Finally, the passage-mass-weighted entropy increment is

$$\frac{\Delta S}{R} = \frac{M_g \delta S_g}{M_T R} = \frac{\gamma}{\gamma - 1} \frac{W^3}{\lambda C_m h_e} \frac{N_B \Theta}{2\pi r} \tag{29}$$

where R is the gas constant and γ is the ratio of specific heats.

Equations (26) and (29) are expressions for the energy and entropy carried by the aggregate wake particle. The effective streamwise velocity at which it travels is now to be defined.

The mass-energy-weighted average streamwise-velocity-decrement of the wake, u_g, is given by

$$M_g \delta H_g u_g = \Delta t\, h_m \int_{-\delta}^{\delta} (W - w_x)(H - H_e)\, \rho w_x \, dy$$

which, using Equation (27) and the formula of Section 3.1.2, leads to

$$\frac{u_g}{u_p} = \frac{1}{\Theta D} \int_{-\delta}^{\delta} (DF)^2 (1 - DF)\, dy$$

or

$$\frac{u_g}{u_p} = \frac{G_{I2} - D\, G_{I3}}{G_{I1} - D\, G_{I2}} \tag{30}$$

Behind a rotor, the fluid in the wake is hotter than the free-stream fluid because more work has been done by accelerating it to a higher swirl velocity. Behind a stator, the argument is reversed. The wake is assumed to possess the same stagnation enthalpy as the free-stream fluid and the stagnation rothalpy increment is determined. Writing again the definition for total rothalpy, for any particle within the wake:

$$I = H - U\, c_\theta = H - U c_x \sin \alpha$$

and for the freestream

$$I_e = H - UC \sin \alpha$$

The energy increment is then

$$I - I_e = U(C - c_x) \sin \alpha$$

and the mass integrated energy increment is

$$\begin{aligned} M_g\, \delta I_g &= \Delta t\, h_m \int_{-\delta}^{\delta} (I - I_e)\, \rho\, c_x\, dy \\ &= \Delta t\, h_m\, \rho_e\, UC^2 \sin \alpha \int_{-\delta}^{\delta} \left(1 - \frac{c_x}{C}\right) \frac{\rho c_x}{\rho_e C}\, dy \\ &= \Delta t\, h_m\, \rho_e\, UC^2 \sin \alpha\, \Theta \end{aligned} \tag{31}$$

Finally, the passage mass-weighted energy increment is:

$$\Delta I = \frac{M_g \delta I_g}{M_T} = \frac{N_B \, UC^2 \sin \alpha \, \Theta}{2\pi r \, \lambda \, C_m} \tag{32}$$

Notice, that Equation (32), for the stator trailing edge, is very similar to Equation (26) which was derived for the rotor.

3.4.3 Radial Transport of Aggregate Wake Fluid

The radial movement of the aggregate wake fluid across the mean streamlines is simply the integral of:

$$Dr = \frac{u_{rg}}{w_g} Dx \tag{33}$$

where

Dx = differential distance in streamwise direction

w_g = velocity in the streamwise direction of the aggregate wake fluid (see Figure 3)

and the incremental radial velocity is reduced from the peak value by the same ratio as the streamwise aggregate to peak velocity ratio [see Equation (30) of Section 3.4.2].

$$u_{rg} \equiv w_{rg} - W_r = \frac{u_g}{u_p} u_{rp}$$

$$u_{rg} = \frac{u_g}{u_p} W \, G \tag{34}$$

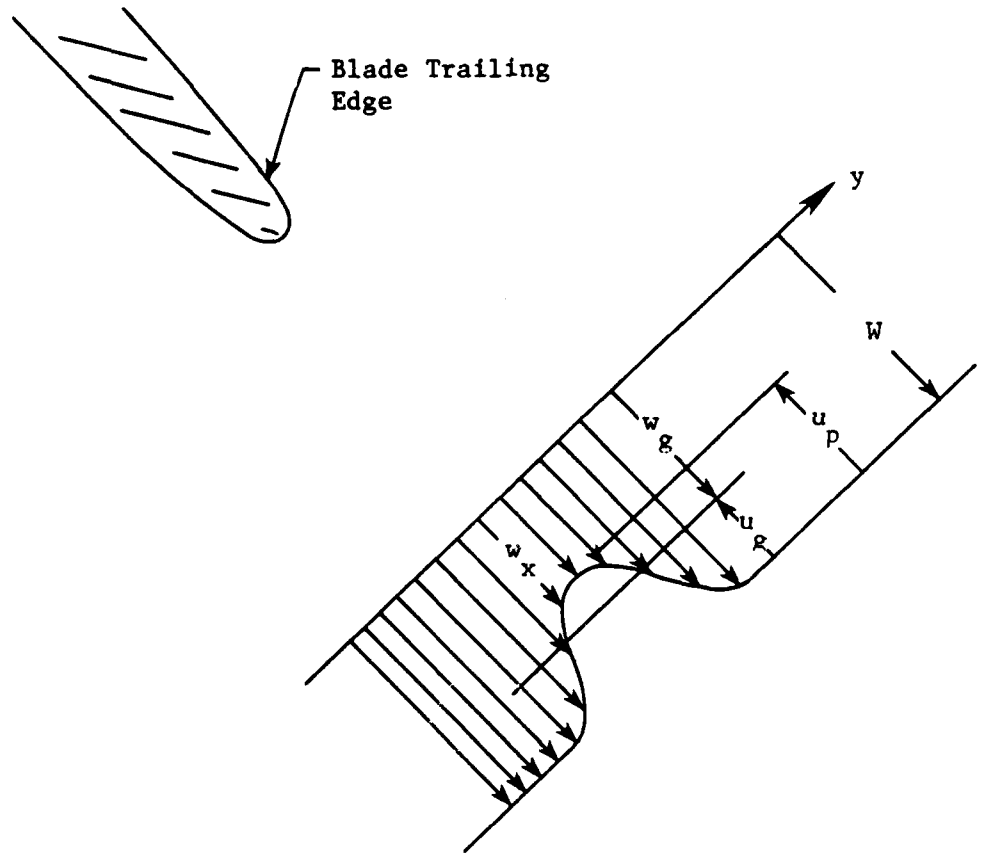

Figure 3. Illustration of Velocity and Velocity Decrement Terminology.

Instead of integrating Equation (33), a transformation is made to the stream function coordinates, ψ:

$$W_{tf}\, D\psi_g = 2\pi r\, \lambda\, \rho\, C_m \cos \phi\, Dr \tag{35}$$

where ψ_g is a dimensionless stream function and W_{tf} is the flow rate in the annulus. Substitution of Equation (34) into Equation (35) leads to:

$$\psi_g = \psi_{gte} + \frac{1}{W_{tf}} \int_{TE} 2\pi r\, \lambda\, \rho\, C_m\, u_{rg} \cos \phi\, Dt \tag{36}$$

with

$$Dt = Dx/w_g$$

The values of ψ_g at the trailing edge are taken as the calculation grid values at the trailing edge of the shedding blade row. At this station ψ_g varies between zero and unity.

The difficulty that now arises is that the integrated values of ψ_g quickly go out of the zero-to-unity bounds. The formulas for the radial velocity G take no account of the presence of the end walls, because of the omission of constraints imposed by a continuity equation and the local change in radial pressure gradient which must exist to retard the radial wake movement.

Instead, this problem is handled by (1) simply letting the ψ_g values go out of bounds and (2) defining a buffer zone adjacent to both end walls into which the wake fluid arriving outside the end walls is relocated. This process is illustrated in Figure 4. The adjustment is taken to be quadratic in form, allowing a smooth transition of particle displacement at the buffer boundary. The adjusted values of ψ_g are denoted as ψ_w.

3.4.4 Spanwise Redistribution

To illustrate the process by which energy and enthalpy are transported radially, the passage-mass-weighted property increment, ΔP, is plotted versus ψ_w in Figure 5 at the shedding blade row trailing edge and at some downstream station. For simplicity, ΔP will be taken as any of tne following:

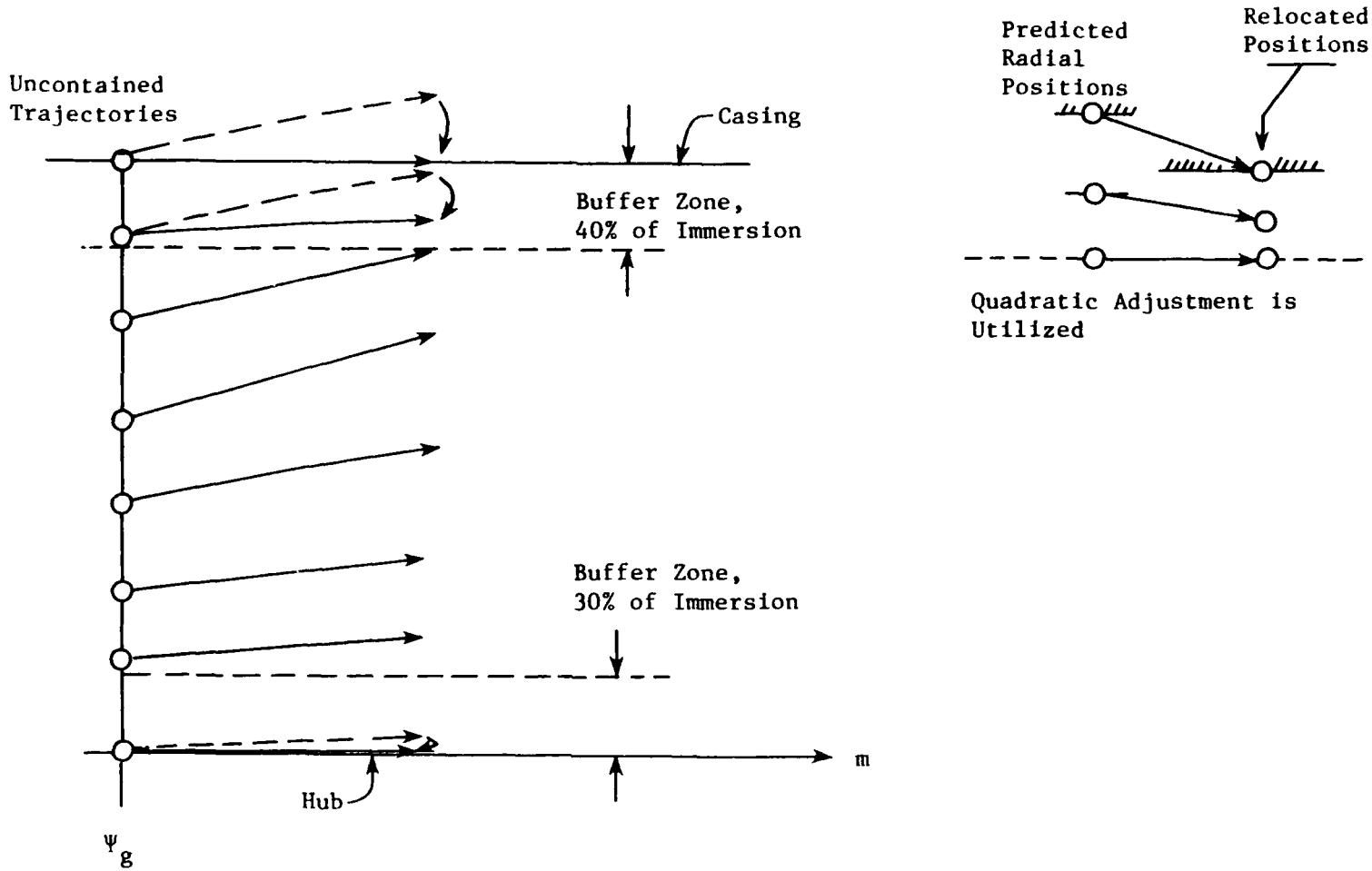

Figure 4. Predicted Movement of Wake Fluid Aggregates.

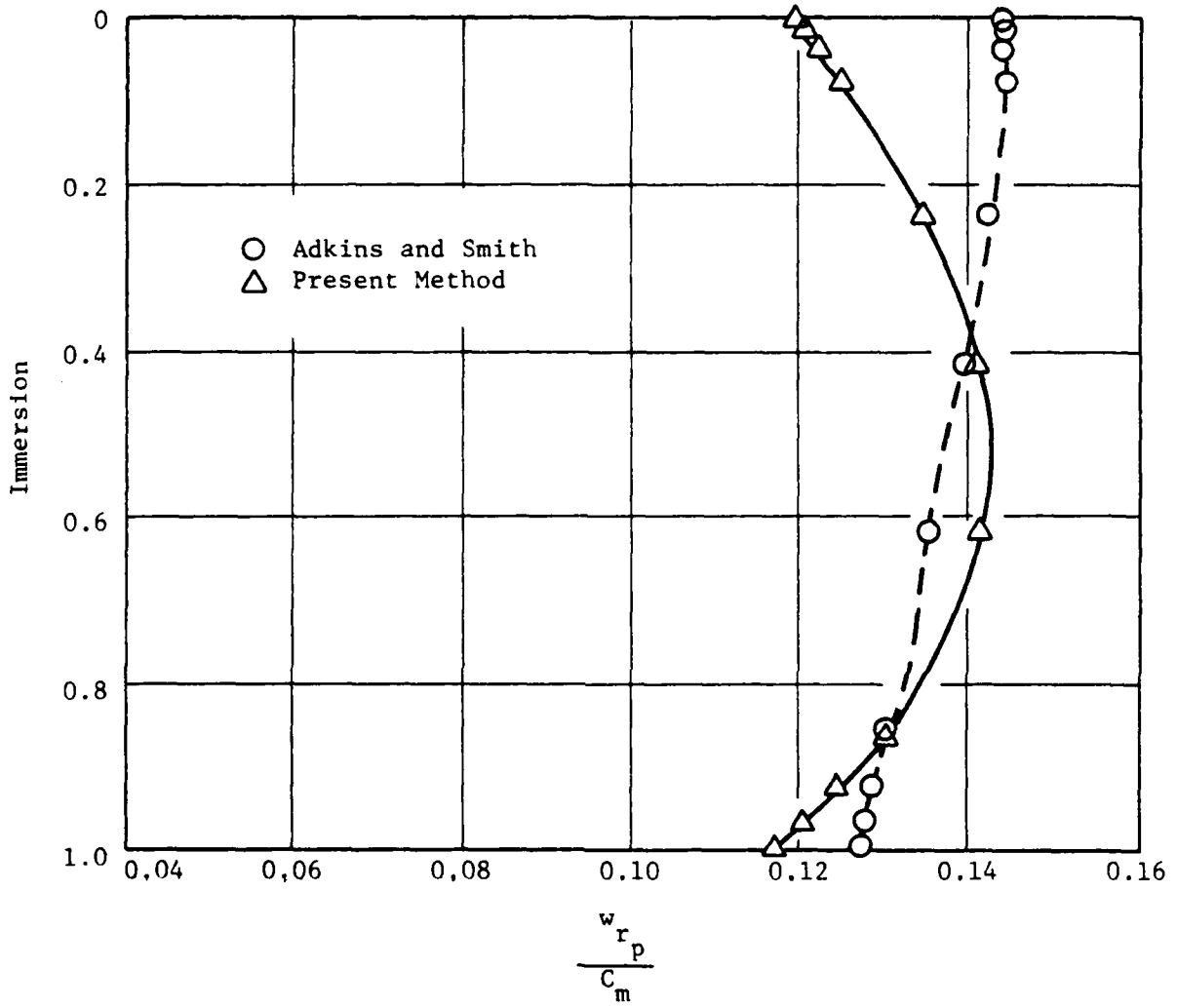

Figure 11. ONERA Rotor - Comparison of Methods of Calculating Peak Radial Velocity in the Wake.

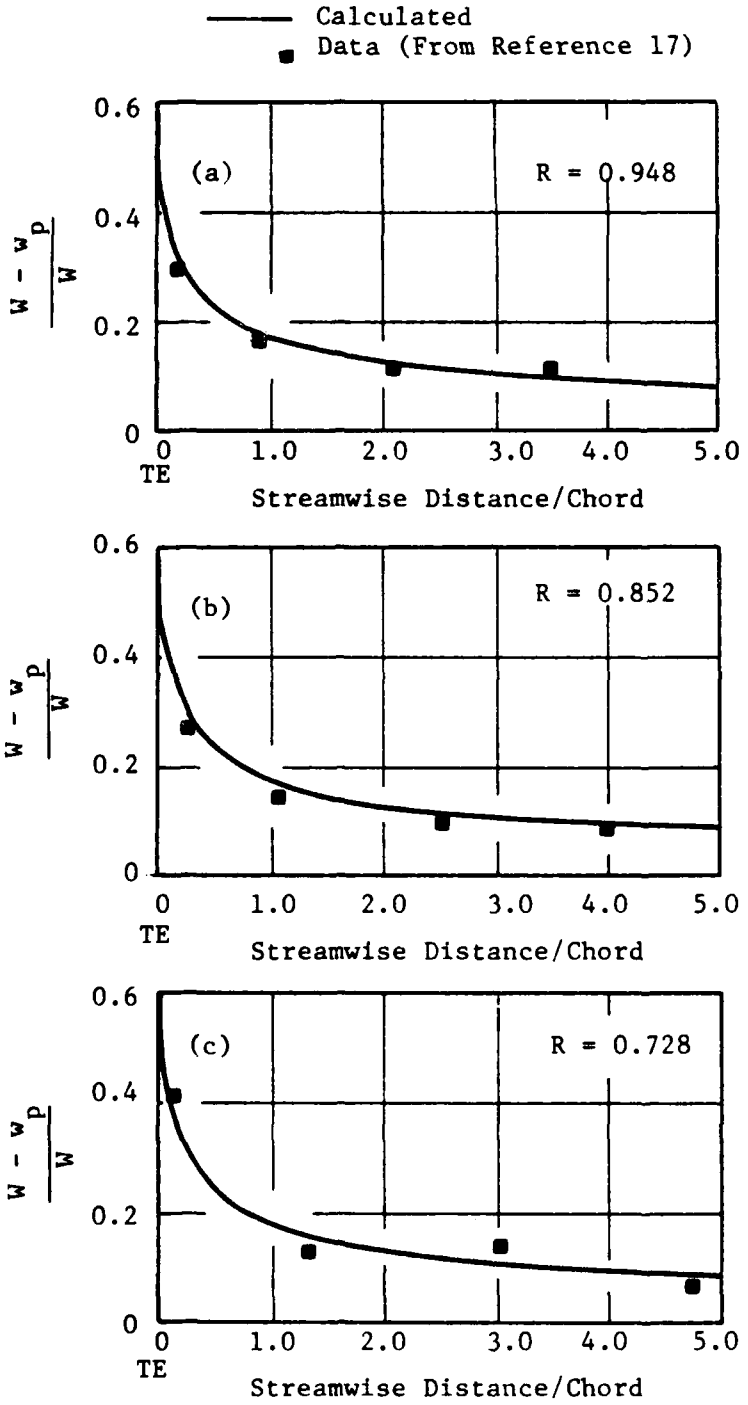

Figure 10. ONERA Rotor - Decay of the Streamwise Wake Velocity Defect.

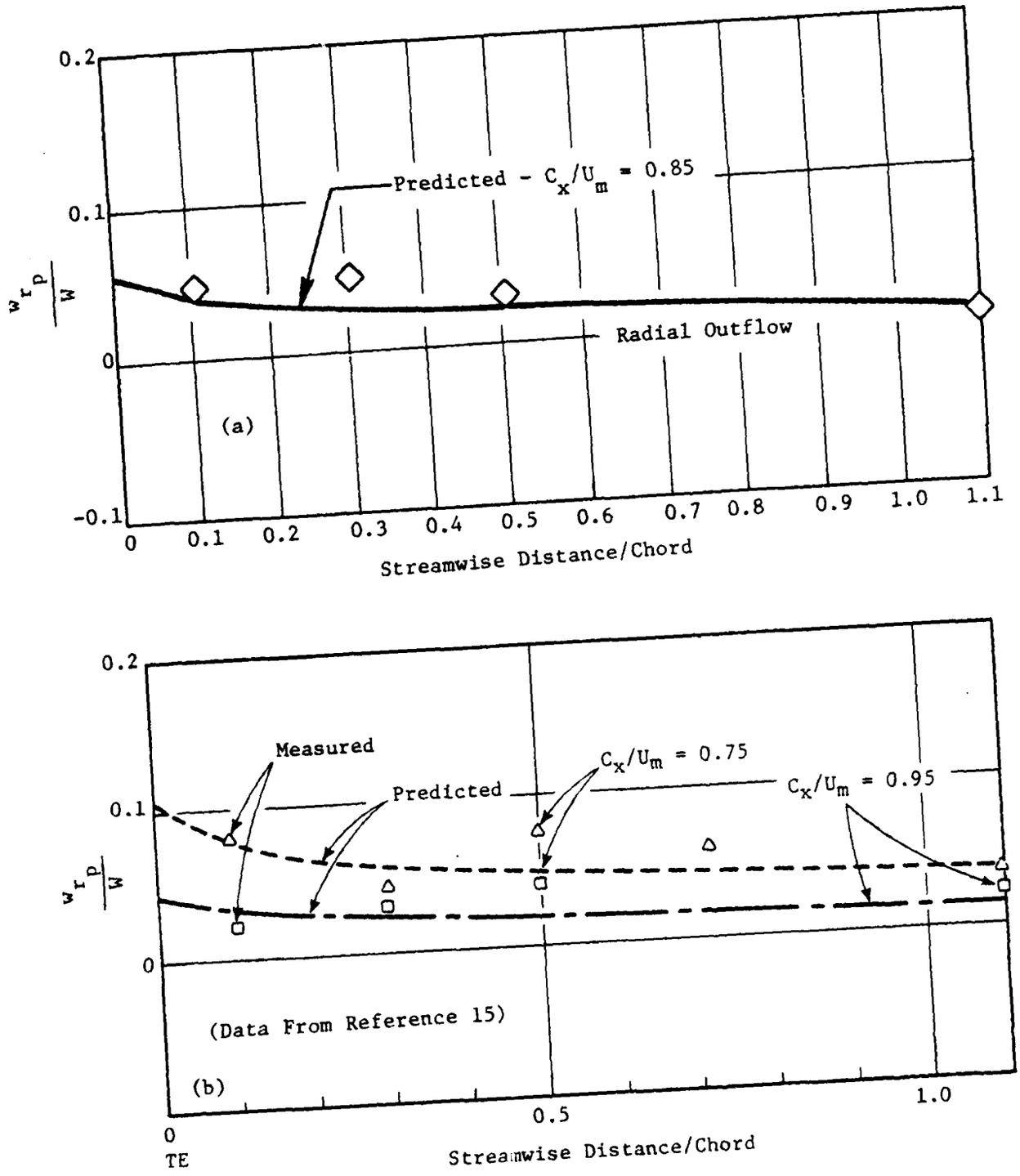

Figure 9. Dring Rotor - Decay of the Midspan Wake Radial Velocity.

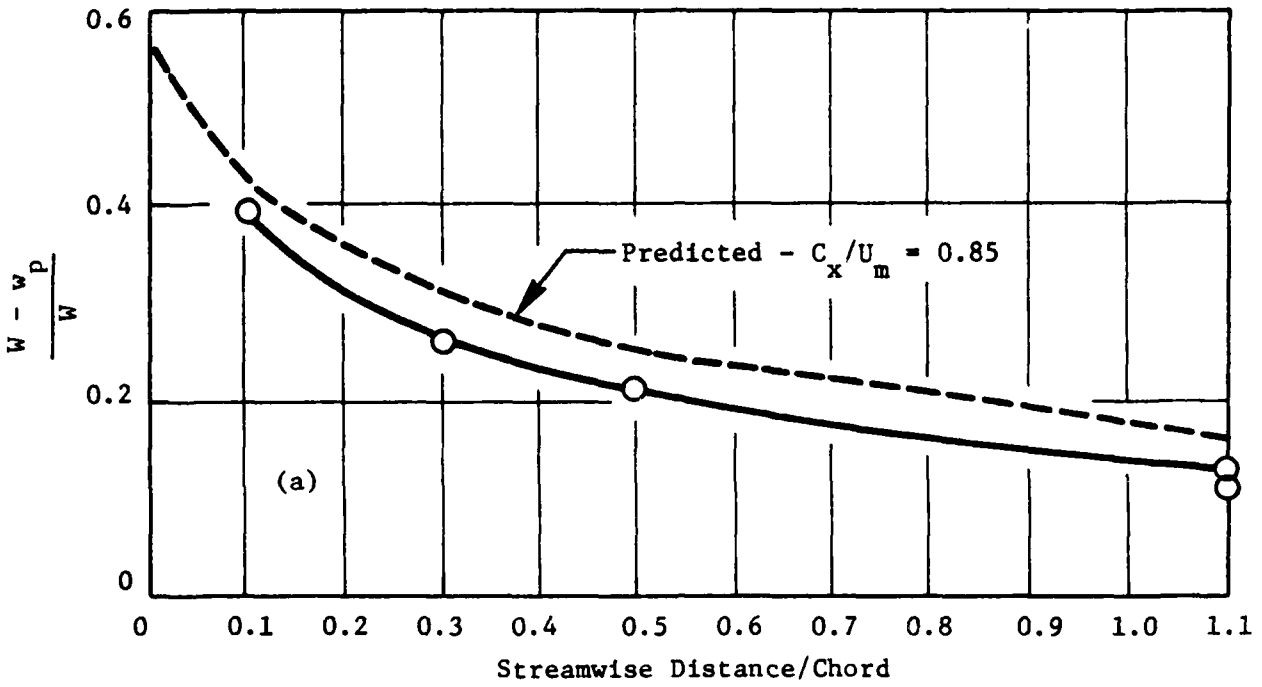

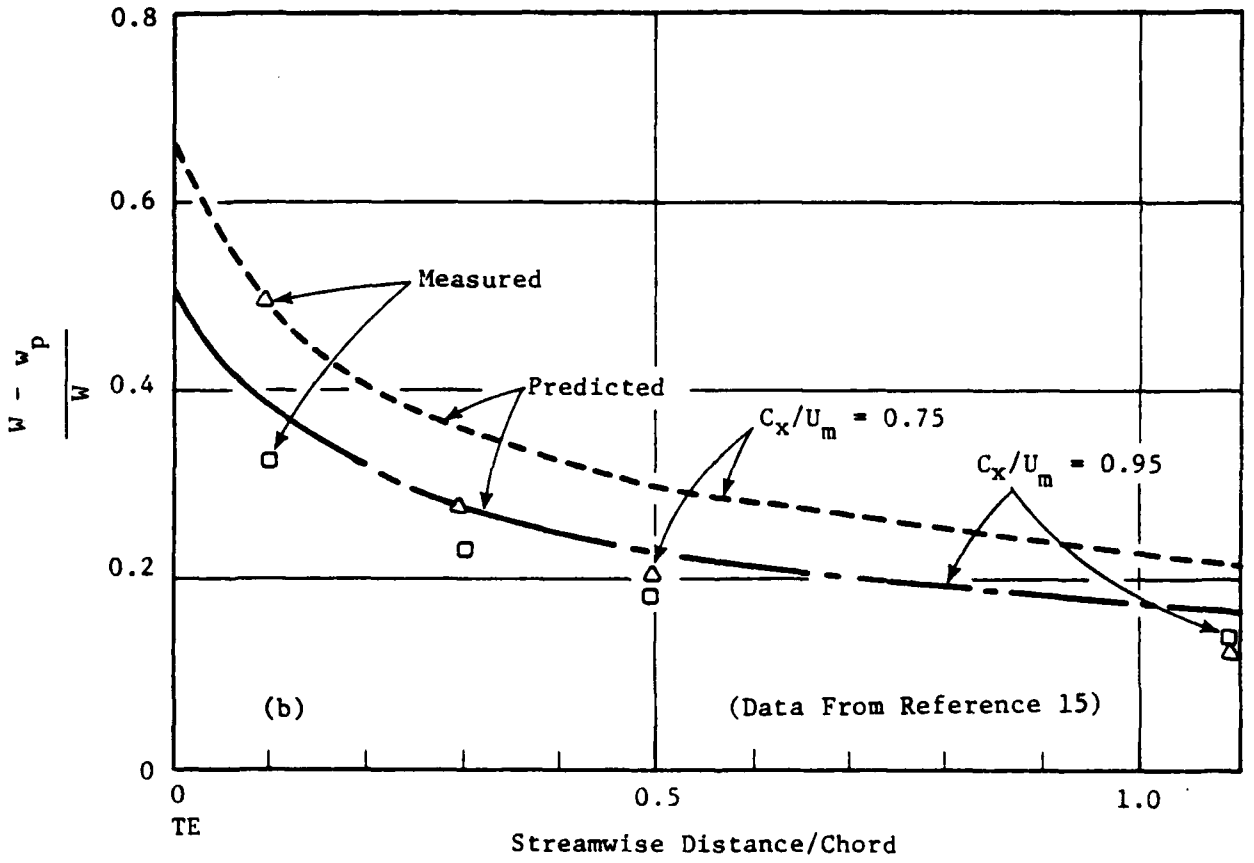

Figure 8. Dring Rotor - Decay of the Midspan Wake Velocity Defect.

Figures 8 and 9 compare measurements of streamwise and radial wake velocities as functions of downstream distance, with the values predicted by the formula of Section 3.0. One requirement needed before prediction can be made is the location of the virtual origin of the decay. (The virtual origin enters the expressions as a function of the wake width and thus should be the same for both streamwise and radial components.) The value selected, x_o = 0.12 x (chord), was chosen to be the best compromise for this machine at a C_x/U_m value of 0.85. At the time, it was felt that this value of x_o would be changed as experience was gained with other test vehicles, but in practice this has proved not to be the case and the value of 0.12x (chord) is built into the coding.

Agreement between measurement and theory is less favorable for the decay of the streamwise deficit at a C_x/U_m of 0.75. The measured decay of the deficit is considerably more rapid than the prediction suggesting that, perhaps, for this more highly loaded case the assumptions made in the development of the theory are not sufficiently stringent or that the blade boundary layer was separated. Agreement of the radial outward decay is good in all cases.

4.1.2 The ONERA Rotor (Larguier, References 16 and 17)

This rotor was used as a calibration case by Adkins and Smith (Reference 1) where the main item of interest was the peak radial velocity. In the current investigation, attention has been drawn to the decay of the streamwise velocity defect at three values of radius ratio.

These results are shown in Figure 12 of Reference 17. A comparison between theory and experiment for each radius is shown here in Figure 10. (The experimental values of the defect were obtained as described by Dring in Reference 15.) Again, the value of x_o was that used originally in the analysis of the Dring rotor; it can be seen that agreement between theory and experiment is good at each radius. One impressive feature of this rotor is the agreement obtained between measurements made with different forms of instrumentation (hot wire, pressure probe, and laser velocimeter). For this reason, it is felt that matching this data is a significant step in the validation of the wake model.

At first sight, the peak radial velocity calculated by the new technique at approximately midspan (Figure 11) appears to be in close agreement with that calculated by Adkins and Smith. It should be borne in mind, however, that the Adkins and Smith peak radial velocity is calculated a short distance (typically 20% axial chord projection) downstream of the trailing edge, whereas the new method calculates a trailing edge value. At the measurement station (not shown), it is found that the Adkins and Smith value is closest to that measured by a hot-wire probe, whereas the new technique is in best agreement with rotating pressure probe data.

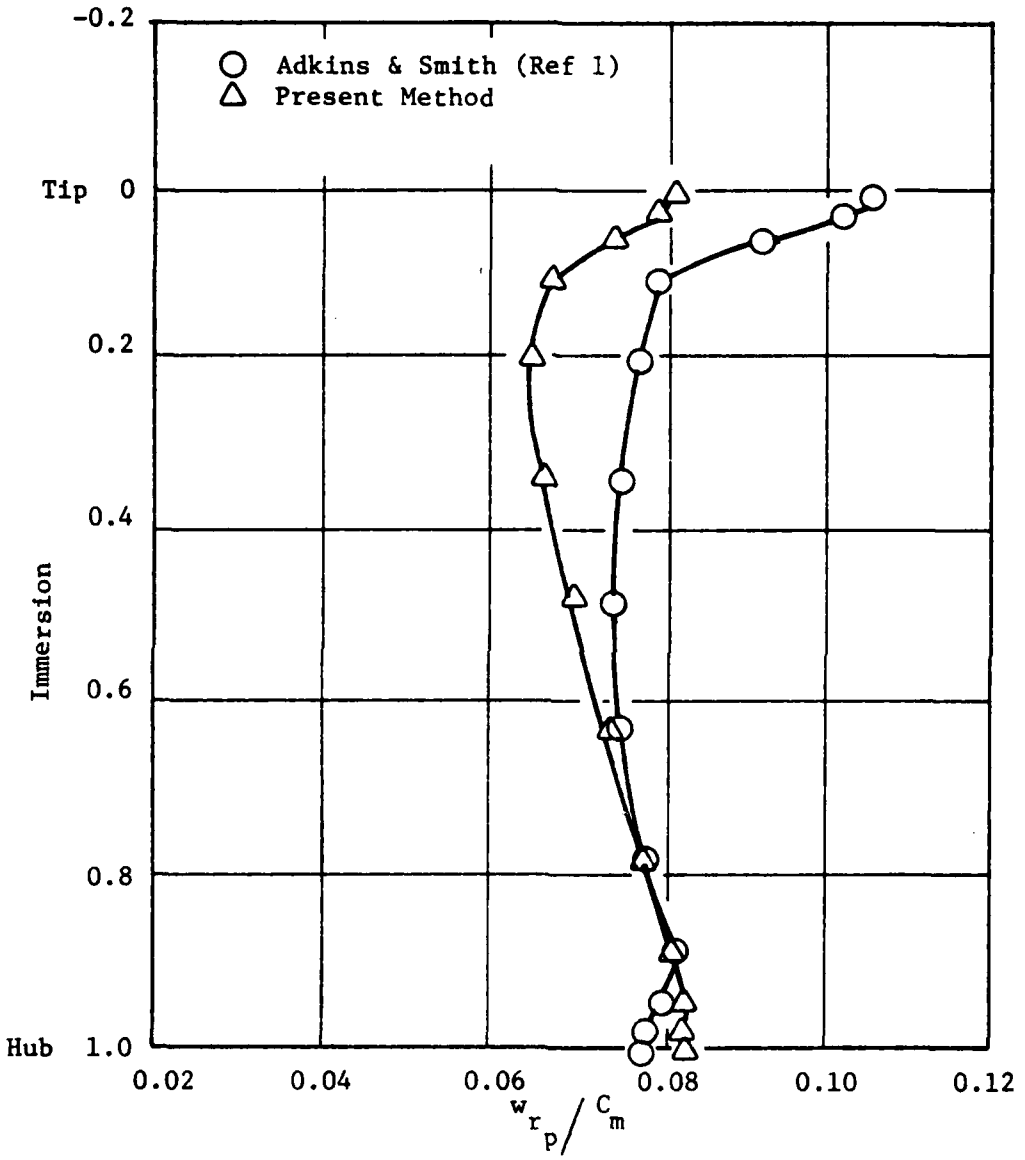

Figure 7. Comparison of Methods of Calculation of Peak Radial Velocity - Dring Rotor (Reference 12) $C_x/U_m = 0.85$.

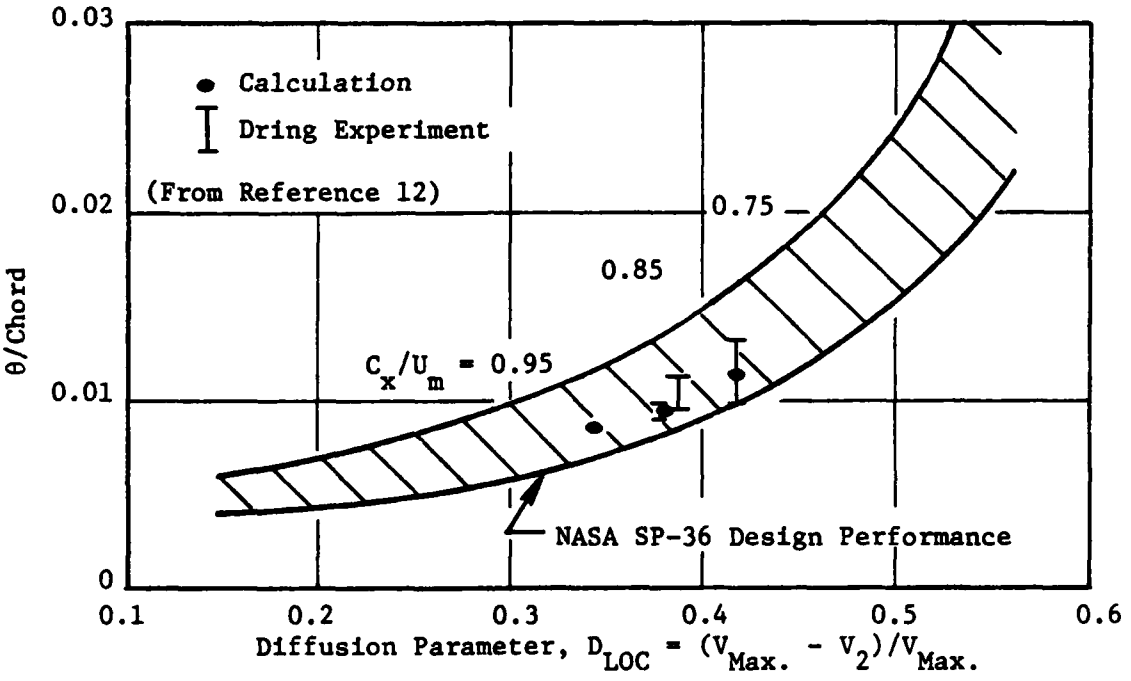

Figure 6. Dring Rotor - Comparison Between Calculated and Measured Trailing Edge Momentum Thicknesses.

4.0 RESULTS

The results obtained during the course of this program fall into two categories: those concerned with the development of the blade wake model as such, and those in which the inclusion of the wake properties into the mixing process are compared with the results obtained using the original method of Adkins and Smith (Reference 1).

4.1 WAKE DEVELOPMENT

We are concerned with (1) the successful prediction of wake properties (thickness, streamwise and radial velocity defects) at the trailing edge of the shedding blade row, and (2) the successful prediction of the variation of these properties with downstream distance.

The test cases that have been run to verify the wake model are discussed in References 15 through 19. In general, each consists of a low-speed rotor whose downstream flow characteristics have been measured with stationary and/or rotating hot wire anemometry and, in some instances (notably References 16 and 17), with stationary and rotating pressure probes as well. Data are presented at various locations downstream, thereby providing many checks on the model. Questions have been raised concerning the origin of the distance measurements for References 18 and 19.

4.1.1 The Dring Rotor

This rotor is described in Reference 15. It consists of an isolated rotor in a cylindrical duct. Predicted results have been compared with midspan data at four downstream locations under three different flow conditions defined by C_x/U_m, the ratio of the midspan axial velocity to the midspan wheel speed of the rotor.

Figure 6 has been included for interest. It shows a comparison between measured and calculated trailing edge momentum thickness versus diffusion parameters at C_x/U_m values of 0.75, 0.85, and 0.95. It can be seen that at C_x/U_m = 0.95 the calculated diffusion parameter is somewhat less than that measured, but at all three conditions the momentum thickness is very close to the error band of the measurements.

Figure 7 compares the results obtained from the different methods of calculating the peak radial velocity in the wake - those used by Adkins and Smith and the new technique described in Section 3.0. Again, these were for the Dring rotor at a C_x/U_m of 0.85. It can be seen that the Adkins and Smith model gives higher values than the other, especially at the tip. At the hub, the effect of blade loading becomes apparent with the new technique showing an increasing trend, while the Adkins and Smith results decrease with decreasing radius. It is felt that the new method should model the real flow more closely than the original method.

$$\frac{D\bar{H}}{Dm} = \frac{D\ \Delta H'}{Dm}$$

which is in agreement with Equation (39.1) of the previous section.

Conversely, if the radial migation term $\Delta H'$, is zero - either because (1) the wake radial velocity is zero or (2) both the energy increments, ΔH, and the radial velocities are radially uniform - then the right-hand side is zero and the mixing equation reverts to the Adkins and Smith form.

The formulation of the numerical solution to Equations (40), (41), and (42) is quite complex, partly because the calculation stations in the through-flow analysis program may not be orthogonal. The details of the exact algorithm are presented in Sections 7.0 and 8.0.

$$\rho C_m \frac{D\bar{H}}{Dm} - \frac{1}{r}\frac{\partial}{\partial n}\left(r\epsilon \frac{\partial \bar{H}}{\partial n}\right) = \rho C_m \frac{D\ \Delta H'}{Dm} \tag{40}$$

$$\rho C_m \frac{D\bar{I}}{Dm} - \frac{1}{r}\frac{\partial}{\partial n}\left(r\epsilon \frac{\partial \bar{I}}{\partial n}\right) = \rho C_m \frac{D\ \Delta I'}{Dm} \tag{41}$$

$$\rho C_m \frac{D\bar{S}}{Dm} - \frac{1}{r}\frac{\partial}{\partial n}\left(r\epsilon \frac{\partial \bar{S}}{\partial n}\right) = \rho C_m \frac{D\ \Delta S'}{Dm} \tag{42}$$

The computational procedure is as follows: values of ϵ, $\Delta H'$, $\Delta I'$, $\Delta S'$, $\delta\beta$, and $\bar{\omega}$ are computed by the formulas of Sections 3.1 to 3.4 of this report and Sections 3 and 4 of Reference 1. These calculations are uncoupled from the through-flow program.

The values of these six parameters (or their equivalents) at each streamline-calculation station node point are then input to the through-flow program. This program combines the numerical solution to Equations (40), (41), and (42) with the continuity and radial equilibrium equations to obtain the circumferential average flow field. Current practice is to specify the blade work distributions through the specification of (the best estimate of primary flow blade-to-blade spouting angles which are in turn, modified by the $\delta\beta$ secondary flow under/over turning angles mentioned above. During the convergence of the through-flow solution these six parameters are held constant. After convergence, the six parameters are recomputed and the process repeated. The total solution is obtained by an iteration between the through-flow analysis module and the secondary flow/wake centrifugation/loss prediction module.

It should be pointed out that in the through-flow module, Equation (41) is ignored within rotors (that is, the first station aft of the leading edge through the trailing edge) and Equation (42) is ignored within stators. At these stations the swirl is obtained from the prescribed swirl angle. Then either $\bar{H}$ or $\bar{I}$ is found by the relation

$$\Omega\ \overline{rC_u} = \bar{H} - \bar{I} \tag{43}$$

Notice that in the event that $\epsilon = 0$, the above equations reduce to, for example,

where, as discussed in Section 3.4.1, the two values of ΔP_w and ΔP_g are equal and opposite and therefore do not contribute to the equation. At some downstream station, however, the wake and freestream increments of P have redistributed themselves and, for this same streamline, are denoted by $\Delta P'_w$ and $\Delta P'_{fs}$. So

$$\bar{P} = \bar{P}_{te} + \Delta P'_w + \Delta P'_{fs}$$

The streamwise change in $\bar{P}$, then, is:

$$\frac{D\bar{P}}{Dm} = \frac{D\ \Delta P_w}{Dm} + \frac{D\ \Delta P'_{fs}}{Dm}$$

But again, as indicated in Section 3.4.1, the change in the freestream ΔP is presumed to be much smaller than the wake ΔP and is neglected. Additionally, subscript w is dropped. The result:

$$\frac{D\bar{P}}{Dm} = \frac{D\ \Delta P'}{Dm} \qquad (39.1)$$

3.5 NEW MIXING SCHEME

3.5.1 Inclusion of Wake Transport Terms in the Adkins and Smith Mixing Calculation

Mixing models have now been developed for complementary cases:

1. Radial diffusion of property $\bar{P}(r)$ with no allowances made for circumferential variations of P (that is, $\Delta P = 0$)

2. Radial migration of local "hot" wake fluid elements characterized by an increment $\Delta P'(r)$ referenced to a radially uniform free-stream value, $P_e \simeq \bar{P}$.

The general case of radially varying $\bar{P}(r)$ and $\Delta P'(r)$ is handled by "adding" the two procedures together. There is assumed to be no significant mutual interaction. On this basis, the following three equations are written:

Then by substitution of Equation (38) into Equation (39) and by using

$$d\psi = 2\pi r \lambda \bar{\rho} \bar{C}_m dn$$

we have, for either side of Equation (39):

$$N_B \int_{n_{j-1/2}}^{n_{j+1/2}} \left[\frac{1}{2\pi r \lambda \bar{\rho} \bar{C}_m} \int_{-\delta}^{\delta} (P - P_e) \rho w_x dy \right] 2\pi r \lambda \bar{\rho} \bar{C}_m dn$$

$$= N_B \int_{n_{j-1/2}}^{n_{j+1/2}} \int_{-\delta}^{\delta} (P - P_e) \rho w_x dy dn$$

Hence, the mass-weighted value of $(P-P_e)$ is held invariant. This is the desired result.

The numerical method for forcing these integrals to be invariant is:

1. Fit a staggered parabolic spline to the curve of ΔP_j versus ψ_{gj} at the shedding blade row trailing edge, then integrate the spline to determine each individual area, SDP_j.

2. At downstream stations, find the staggered spline coefficients which yield the prescribed values of SDP_j versus ψ_{wj}.

3. From the coefficients determined by (2), interpolate for the $\Delta P'_j$ values at the through-flow analysis stream functions, ψ_j.

These $\Delta P'$ values represent the redistributed passage-mass-weighted wake property increments for each through-flow streamline and station downstream of the shedding row.

The change in circumferential average values can be computed as follows: before the mixing process starts, at the blade t[illegible]ing edge, the average value of P on some given streamline is:

$$\bar{P} = \bar{P}_{TE} + \Delta P_w + \Delta P_{fs}$$

$$\Delta P \begin{cases} \equiv \dfrac{M_g \delta H_g}{M_T} \\ \equiv \dfrac{M_g \delta I_g}{M_T} \\ \equiv \dfrac{M_g \delta S_g}{M_T} \end{cases} \tag{37}$$

or in general:

$$\Delta P = \frac{\Delta t\ h_m \int_{\delta}^{\delta} (P - P_e)\ \rho w_x\ dy}{\Delta t\ h_m \dfrac{2\pi r \lambda}{N_B}\ \bar{\rho}\ \bar{C}_m} \tag{38}$$

where P is stagnation enthalpy, stagnation rothalpy, entropy, or $\Omega r C_u$.

The point of Figure 5 is that, as the fluid moves downstream and the wake moves radially, the individual areas under the curves, marked 1, 2, 3, and 4 are held invariant. By assumption, the dotted line boundaries, $\psi_{w_{j-1/2}}$ and $\psi_{w_{j+1/2}}$, are taken as halfway between the node points, ψ_{w_j}.

The justification for this is as follows: if we require that

$$\int_{\psi_{w_{j-1/2}}}^{\psi_{w_{j+1/2}}} \Delta P\ d\psi = \int_{\psi_{g_{j-1/2}}}^{\psi_{g_{j+1/2}}} \Delta P\ d\psi \tag{39}$$

(Downstream) (Upstream)

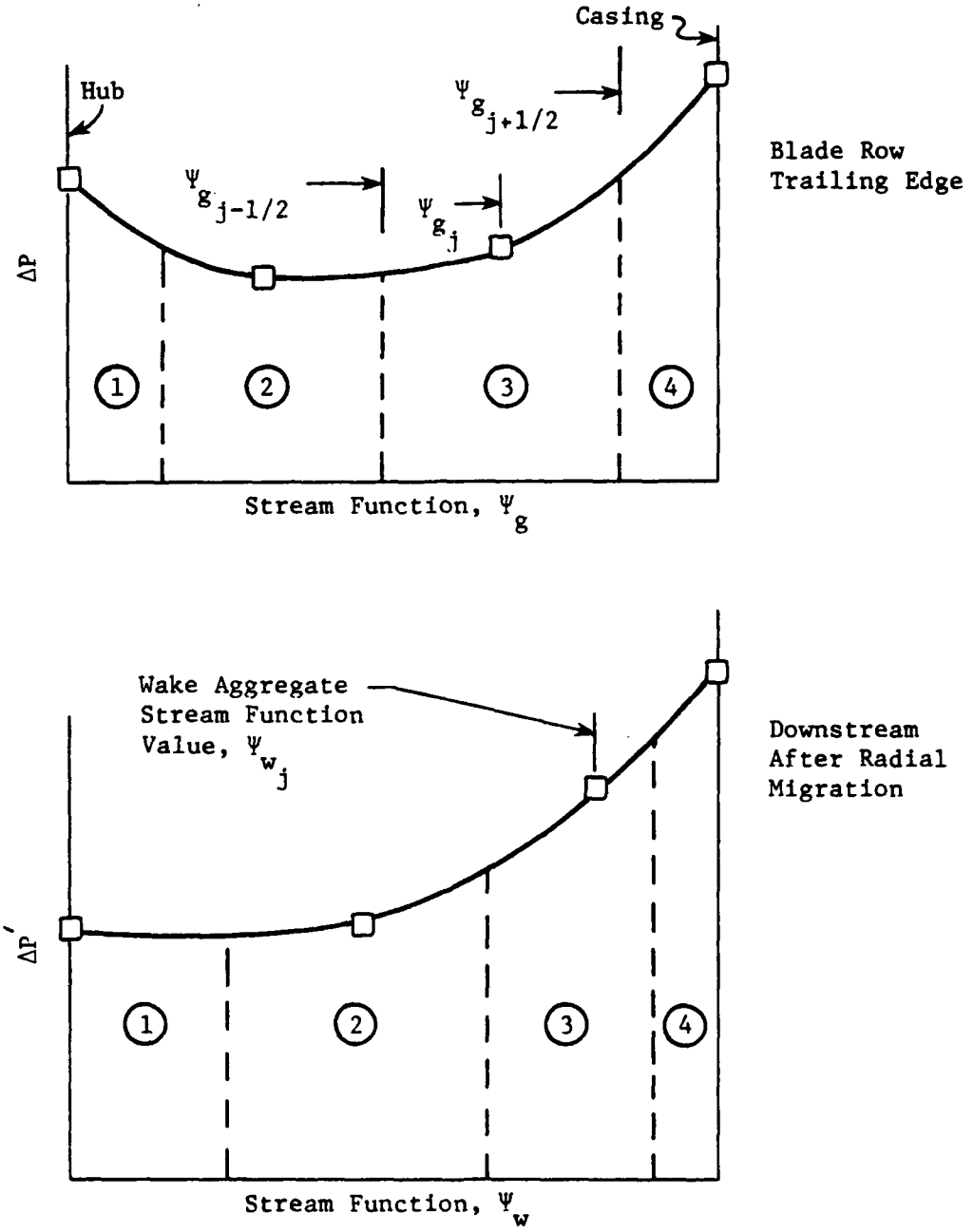

Figure 5. Conservation of Wake Increment Property, P.

4.1.3 Penn State Compressor (Reference 18)

The Penn State University (PSU) compressor consists of an inlet guide vane (IGV) row followed by a rotor with a stator row a significant distance downstream. The stage was originally designed (with more traditional spacing) by Smith in the early 1950's. Since its migration to Penn State, a great deal of data have been taken behind the rotor using both stationary and rotating instrumentation. For the purposes of calibrating the constants in the wake model, it is felt that data from stationary probes could be misleading because of the presence of IGV wakes which have been convected through the rotor. Consequently, as far as possible, only data from rotating instrumentation have been considered.

The results obtained are shown in Figures 12 through 15. Figures 12 and 13 respectively show the radial variations in peak spanwise velocity and maximum streamwise velocity defect. Also shown are experimental data from Reference 18 taken at 12% true chord axially downstream. Figure 12 shows that, in this case, both available methods for calculating peak radial velocity show the same trend with radius (in contrast with, for example, Figure 11).

Figure 14 shows the variation in streamwise velocity defect with downstream distance at three values of radius ratio. The hub/tip ratio of the machine is 0.5, so these represent immersions of 40.5%, 54.1%, and 68.4% of annulus height, respectively. It appears that in all cases the trailing edge defect is underestimated. At the outer two radii, the calculated and measured defects are in good agreement at streamwise distances greater than approximately 20% chord. At the innermost radius (R = 0.6581), agreement is not so good.

Figure 15 shows the streamwise decay of wake radial velocity at the same three radii. The calculated trailing edge values have been obtained using the new technique, while the data are taken from Reference 18. It can be seen that the calculation seriously underestimates the reported results. It was for this particular test case that Adkins and Smith (Reference 1) reported the greatest discrepancy between measurement and calculation. One possible explanation may lie in the unconventional shape of the blades, that is, the "hooked" trailing edge of the NACA A10 meanline tending to encourage centrifugation. One other point raised by Adkins and Smith concerns the efficiency at which the rotor was running. This was originally reported as around 82% and later revised to about 86%, both of which are low for the condition of "good efficiency" applied to the calculation procedure, and much lower than measured by Smith in the 1950's.

4.1.4 Penn State Fan (Reference 19)

Another test vehicle from the PSU stable, this fan consists of 12 blades of zero camber running some distance downstream of a row of support fins in a

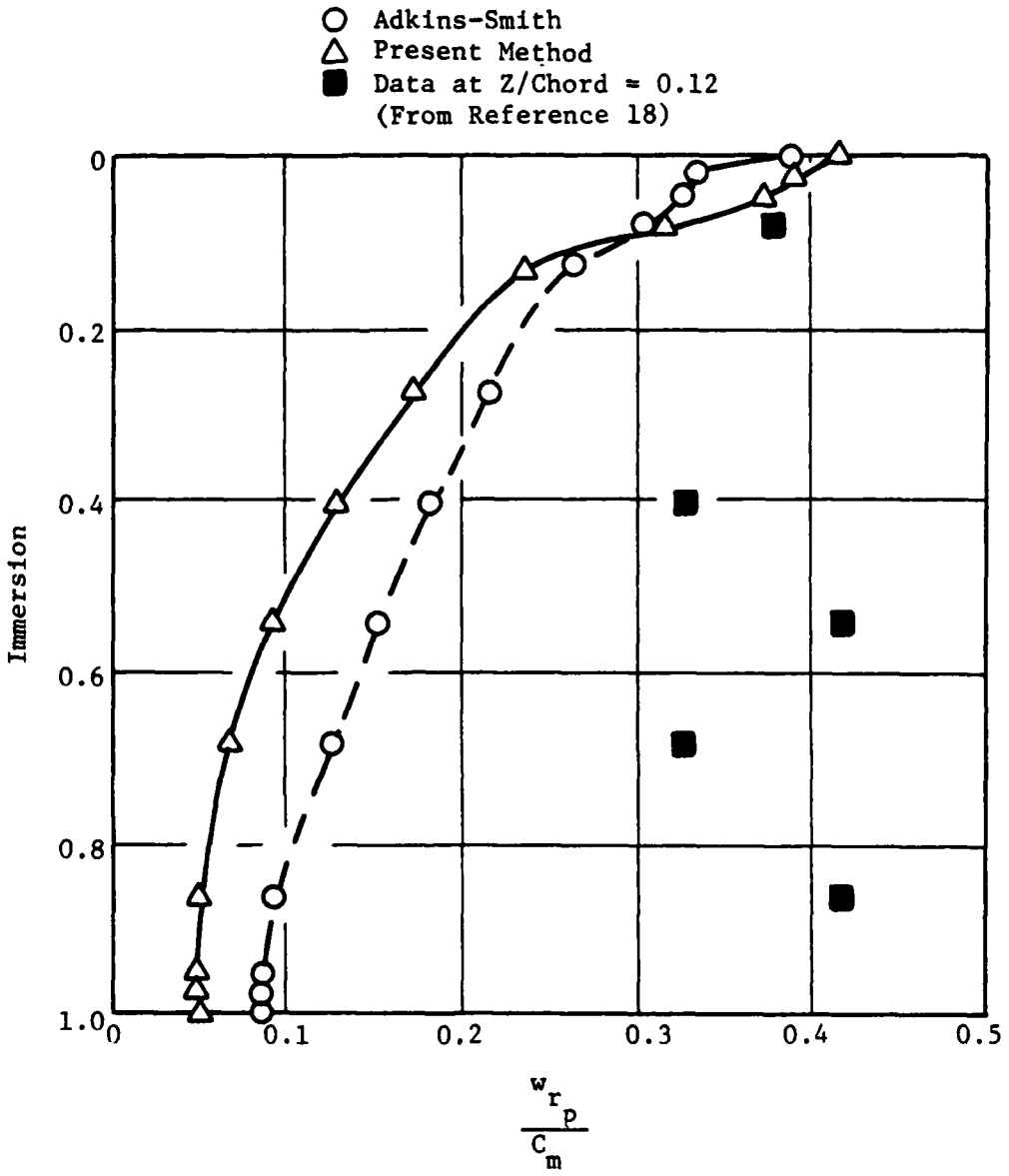

Figure 12. PSU Rotor - Comparison of Methods of Calculating Peak Radial Velocity in the Wake.

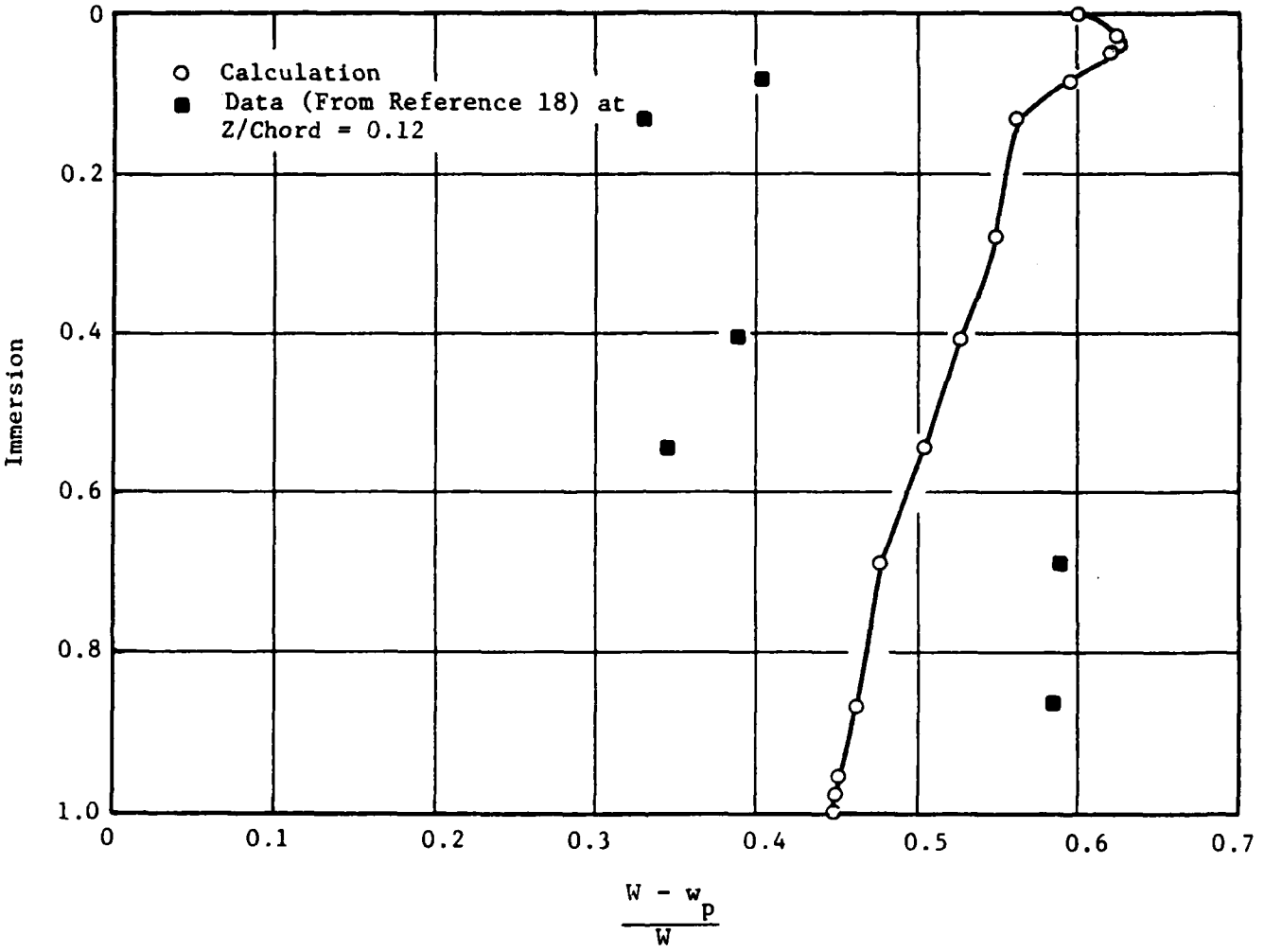

Figure 13. PSU Rotor - Radial Variation of Trailing Edge Streamwise Velocity Defect.

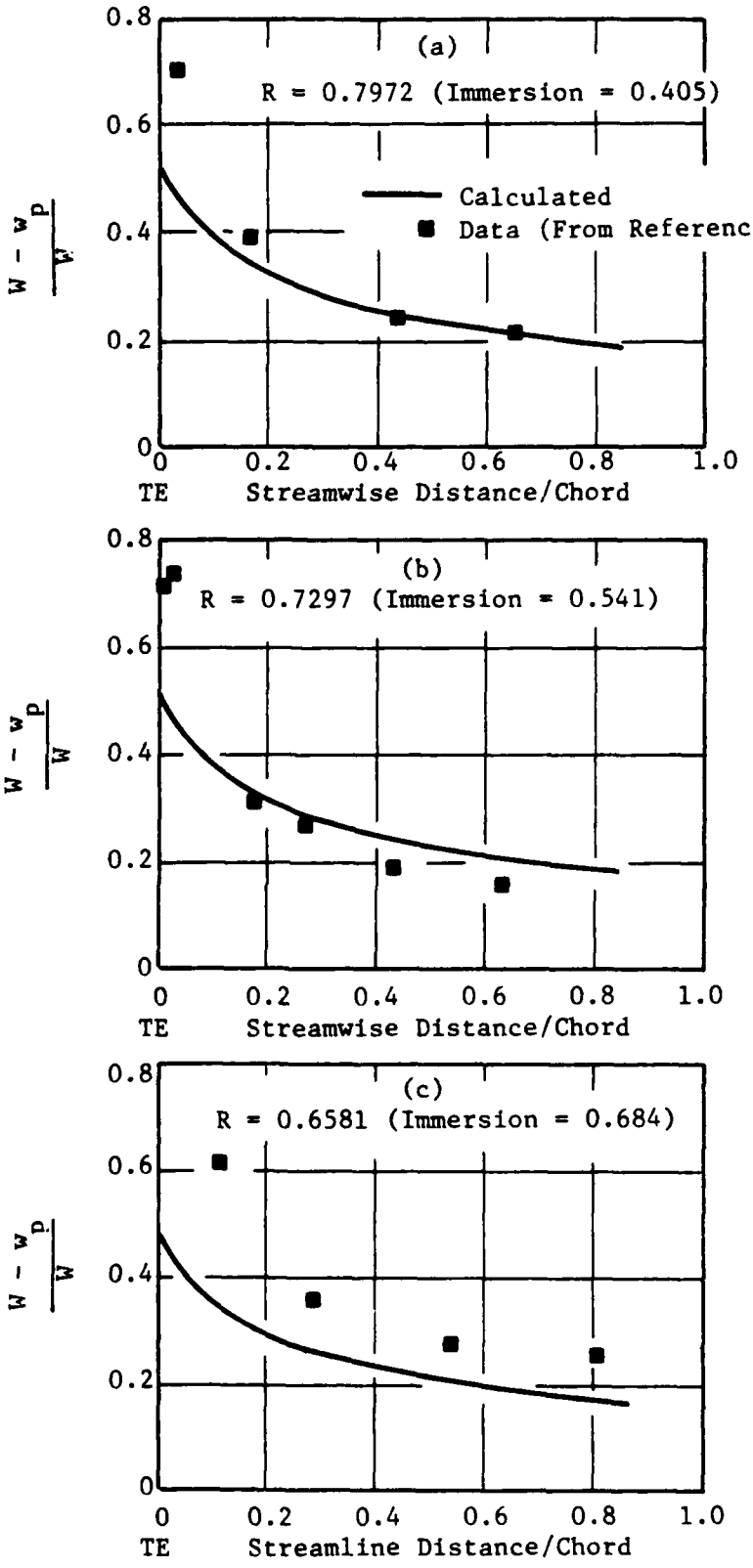

Figure 14. PSU Rotor - Decay of the Streamwise Wake Velocity Defect.

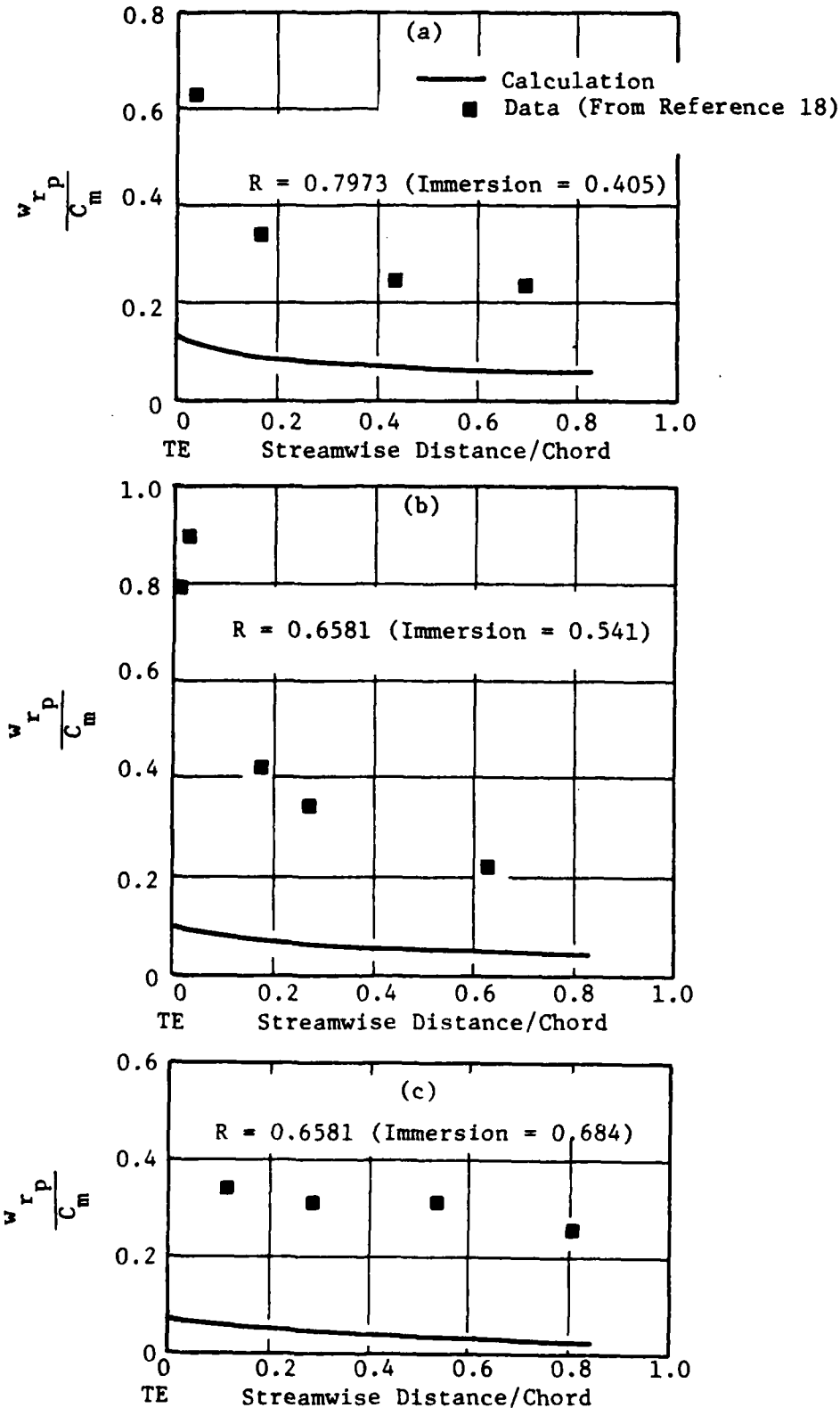

Figure 15. PSU Rotor - Decay of the Peak Radial Velocity in the Wake.

cylindrical duct. Data have been taken with rotating instrumentation at various blade incidences; Figures 16 and 17 compare measurements and calculation at a midspan incidence angle of 10° and a radius ratio R = 0.721 (which is the midspan position). Once again, agreement between calculation and measured data appears good for both peak radial velocity and streamwise velocity defect. Because of the normalization used in the measured data, the radial velocities shown in Figure 17 have been plotted against normalized axial distance. Also, it is worth noting that the two furthest downstream data points in this figure were taken with a stationary probe.

4.1.5 General Comments on Wake Prediction and Decay

The value of 0.12 x (chord) upstream of the trailing edge for the virtual origin of the wake decay was chosen originally (Reference 11) as a compromise between those values that fitted the wake defect decay data and peak radial velocity decay data of the Dring rotor when it was run at a C_x/U_m (axial velocity/midspan rotational speed) of 0.85. It was anticipated that this value would be changed when other data were available for comparison with the calculated results, but this appears to be a reasonable compromise for both radial and streamwise decay of the wakes in the low-speed machines reported on here. It would be interesting to obtain data from more realistic test vehicles in the future in order to verify this choice.

Areas that may require calibration in the peak radial velocity analysis of Section 3.0 are: (1) the selection of the immersion of the representative point in the blade boundary layer (currently 5% of the boundary layer thickness away from the surface) and (2) the fashion in which the boundary layer form factor changes from a selected value (currently the flat plate value) at mid-chord to the value given by the Koch and Smith correlations (Reference 14) at the trailing edge (currently parabolic). Again, for the results presented here, no changes have been made to the original scheme.

With the notable exception of the radial velocity in the wake of the Penn State rotor (Section 4.1.3 above), it appears that the experimental results and the calculations are in excellent agreement. With the same exception, this agreement seems least good for the wake speed defect of the Dring rotor at C_x/U_m = 0.75, followed by the streamwise decay of the velocity defect of the Penn State rotor at a radius ratio R = 0.6581. These cases are not consistent, however. For each flow rate examined for the Dring rotor, the calculated defect is higher than that measured; the converse is true of the Penn State data. It would be tempting to suggest that the calculation of the trailing edge value of the velocity defect needs re-thinking were it not for the excellent agreement obtained with the ONERA rotor and Penn State fan data (References 17 and 19, respectively).

Overall, it is felt that the new approach to the calculation of the trailing edge values of the wake velocity defects in both streamwise and radial directions and their decay with distance downstream represents a significant improvement over the Adkins and Smith technique.

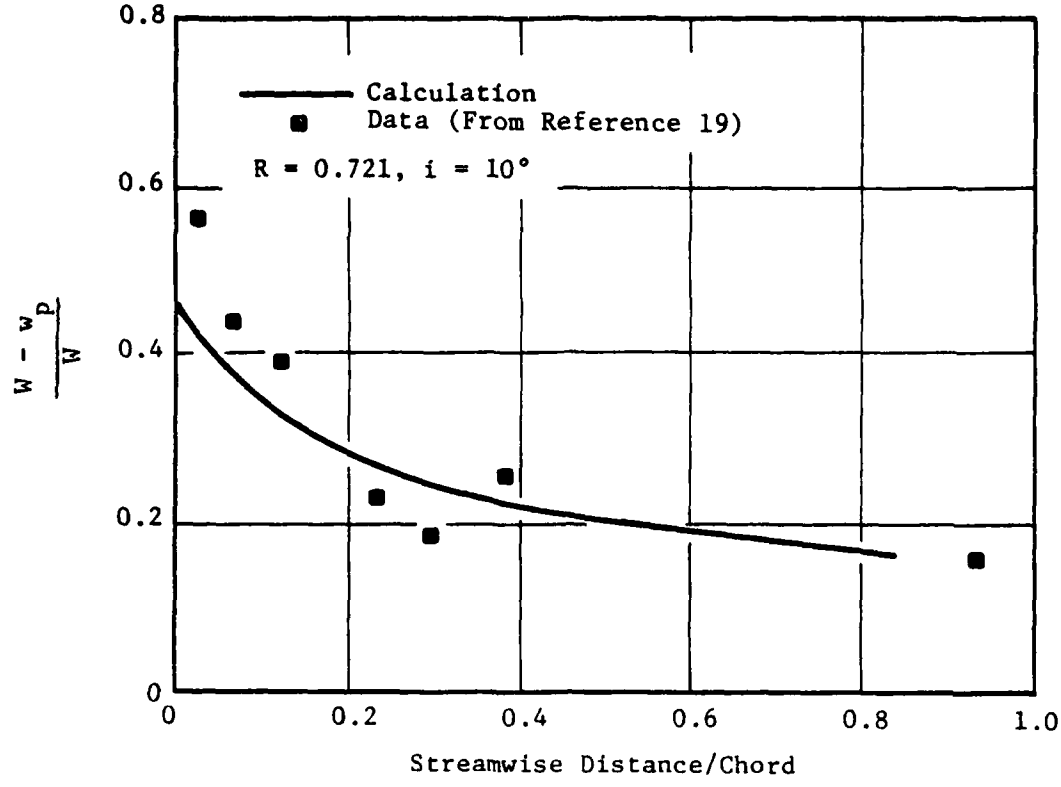

Figure 16. PSU Fan - Decay of the Streamwise Wake Velocity Defect.

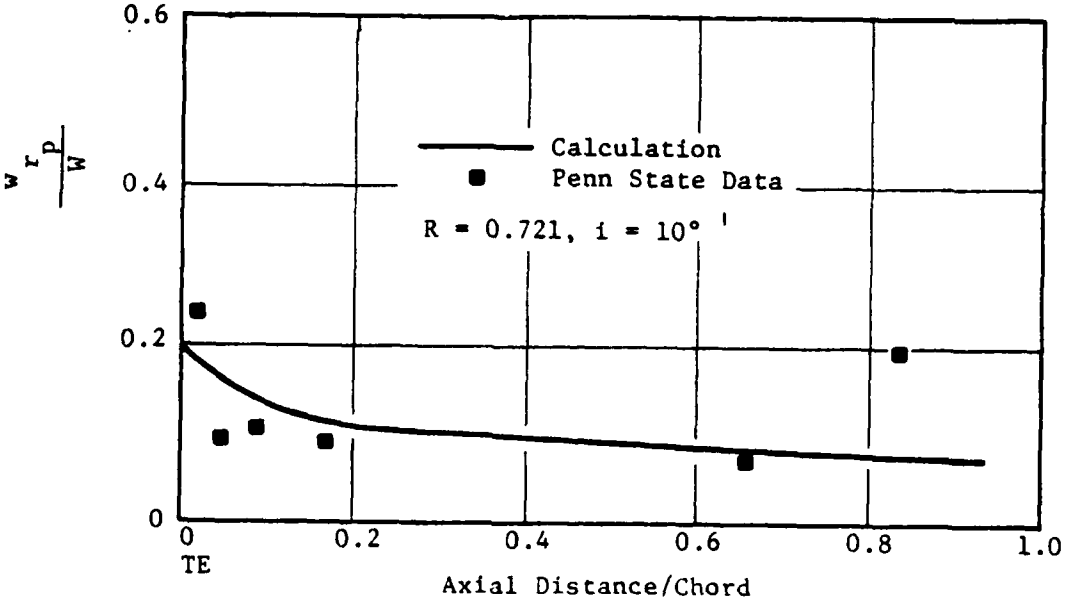

Figure 17. PSU Fan - Decay of the Peak Radial Velocity in the Wake.

4.2 MIXING CALCULATION RESULTS

In this section results are presented for the total mixing model as it is incorporated in the General Electric Circumferential Average Flow analysis with MIXing (CAFMIX) program. Comparisons are made with the Adkins and Smith model and with the case of no spanwise mixing. The vehicle for this presentation is the Air Force 1500 ft/s, Transonic, High-Through-Flow, Single-Stage Axial Flow Compressor, test data for which are reported in Reference 20. Figure 18 illustrates the flowpath and denotes the test data point. Also shown is the numerical streamline/station grid used in the calculation.

A data match analysis for this machine was first performed by Simonson (Reference 21) in 1977. The current results extend this original work to include the effects of the spanwise redistribution of stagnation properties and secondary flow turning.

The principal new finding is a more reasonable spanwise distribution of the rotor loss coefficient. Near the hub, Simonson found that a very small loss coefficient value of 0.003 was necessary to match the experimental measurements. With spanwise redistribution of entropy by the method of Section 3.0, this minimum loss coefficient is a more reasonable 0.04.

With the inclusion of spanwise diffusion, it is impossible to exactly match the experimental distributions of total temperature and total pressure reported in Reference 20. This is because the diffusion of these quantities by Equations (40), (41), (42) inherently smooths the rotor discharge values during their transport from Station 16 to Station 25. The objective, then, is to "match" the experimental data in some smooth-sense. Figures 19 and 20 show how closely the data-match-predicted total temperatures and pressures agree with measurements at Station 25, where the experimental results are believed to be reliable.

Losses used in the present effort are based on the Koch and Smith (Reference 7) and Smith (Reference 22) models. The profile loss for both the rotor and stator are computed by the formulation of Koch and Smith. The end wall losses are computed by the method described in the Appendix of Reference 1, except that the end wall boundary layer thickness in Equation (47) of Reference 1 is reduced by using the De Ruyck and Hirsch formulas (Equations 50, 51, and 52b of Reference 1). This modification to the Smith repeating-stage formula was made because recent experience for "first stages" now suggests that the end wall losses are indeed less than for the embedded repeating stage and because the full repeating stage value of boundary layer thickness also appeared to overpredict the losses measured in this application.

The rotor shock losses were initially based on the Koch and Smith (Reference 7) formulation. However, it was felt that this model may be underpredicting the shock losses. Consequently, the losses for the outer portion of the rotor have been increased, as shown in Figure 21, to yield a better match with the measurements. Figures 21 and 22 compare the present loss coefficient distribution (labeled by W.K) with those found by Simonson, which included no spanwise mixing.

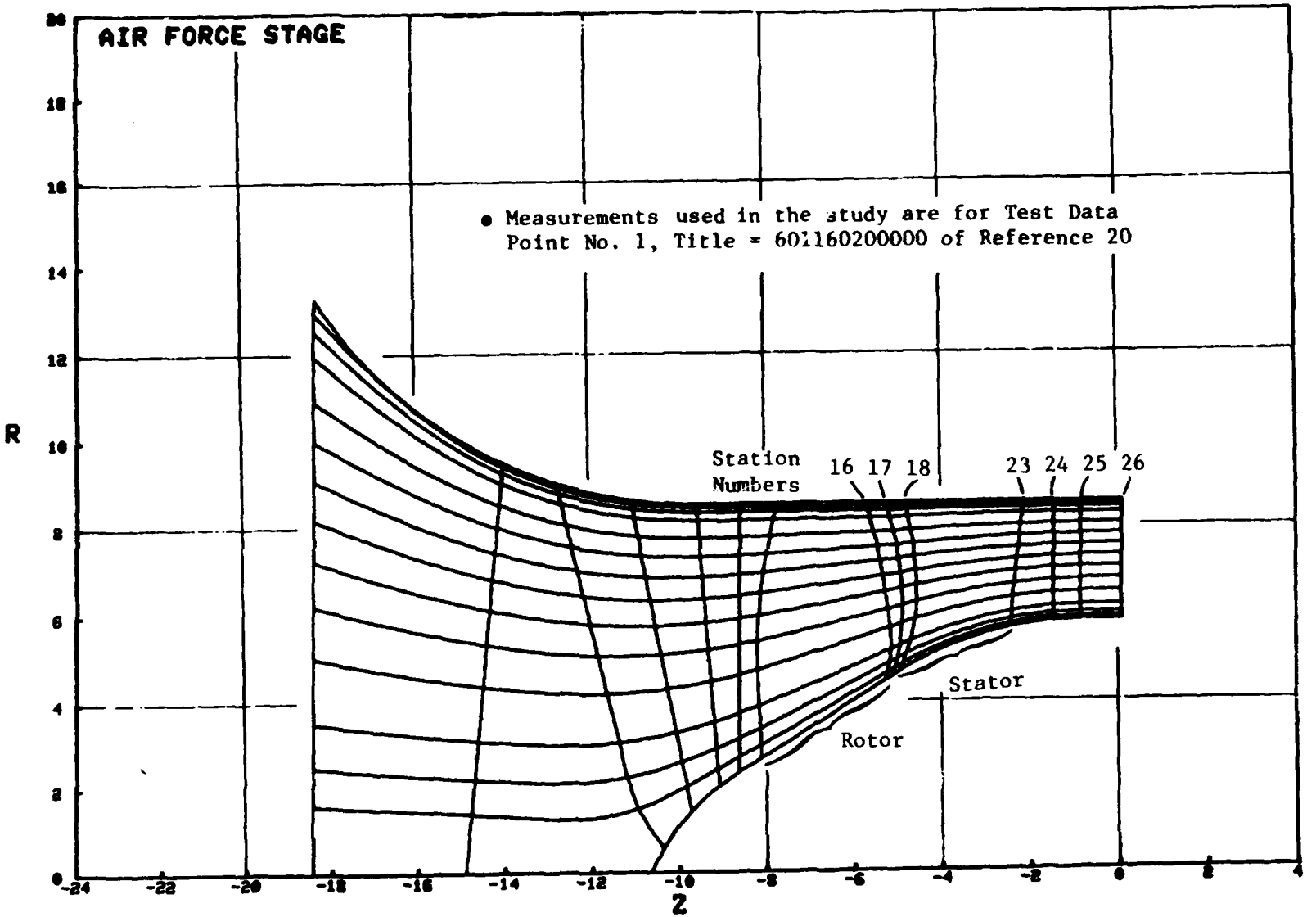

Figure 18. Streamlines and Calculation Stations for the Air Force High-Through-Flow Stage.

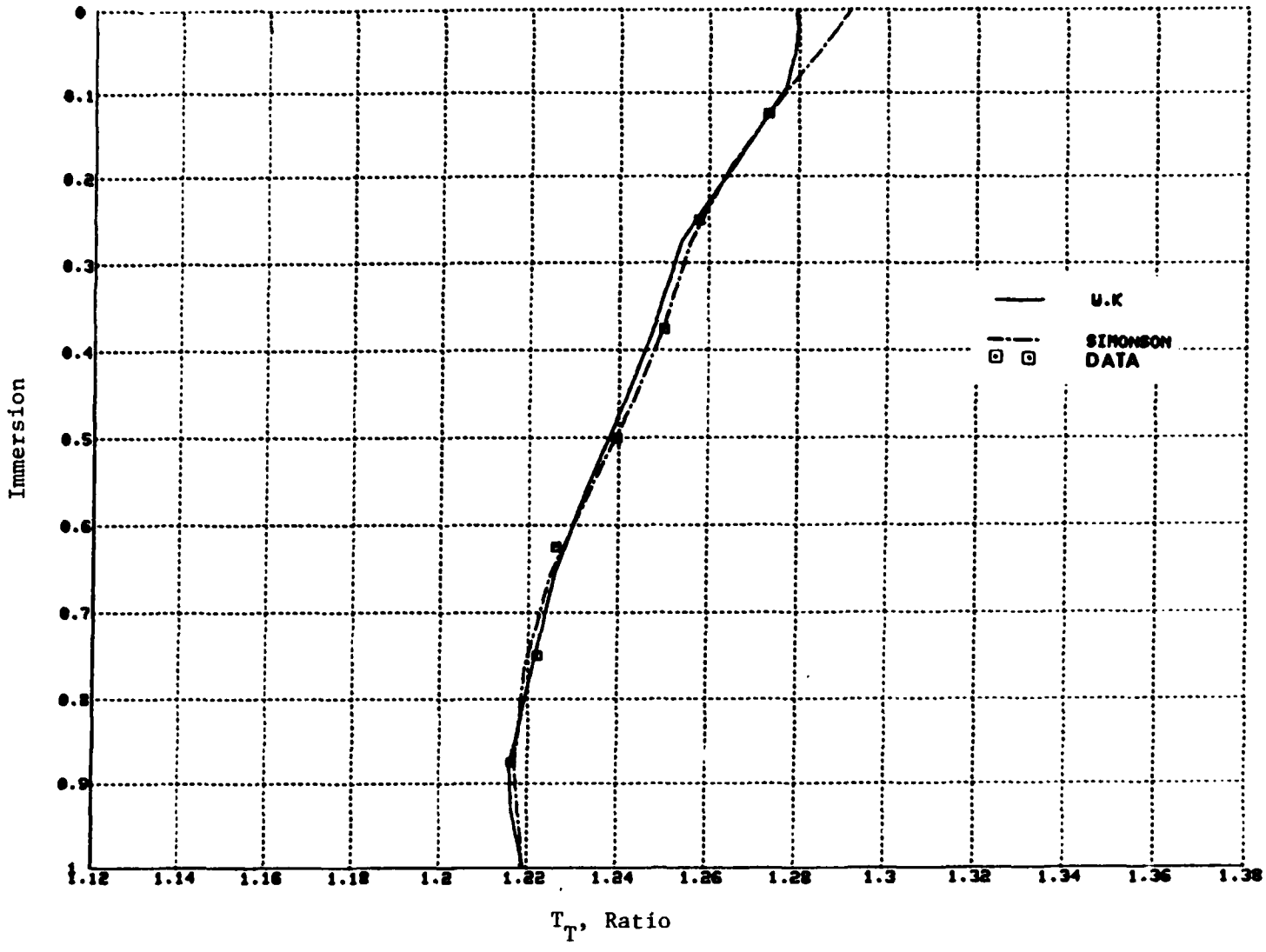

Figure 19. Total Temperature Data Match at Station 25 Achieved with Mixing (W.K) and with No Mixing (Simonson).

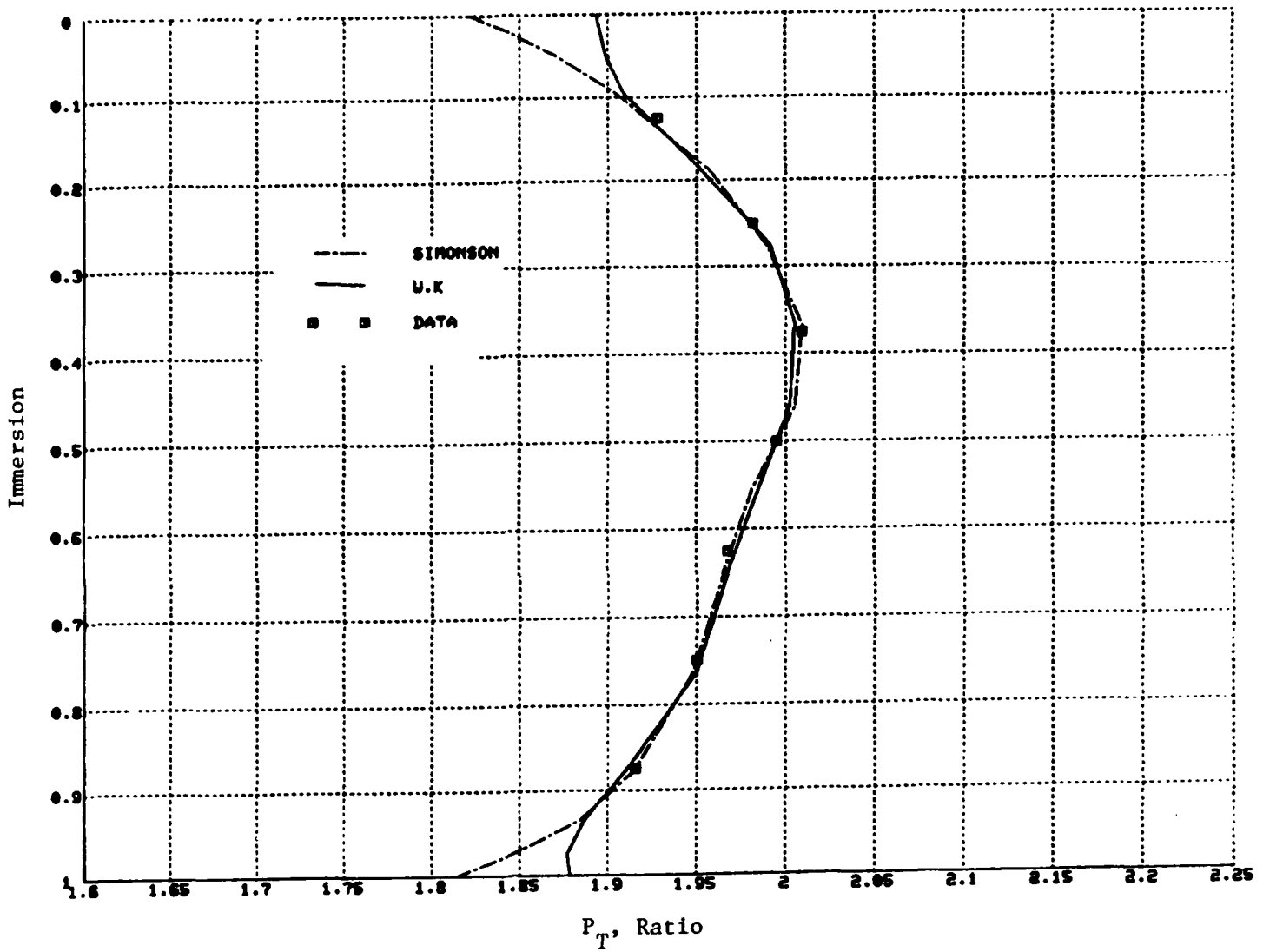

Figure 20. Total Pressure Data Match at Station 25 Achieved With Mixing (W.K) and With No Mixing (Simonson).

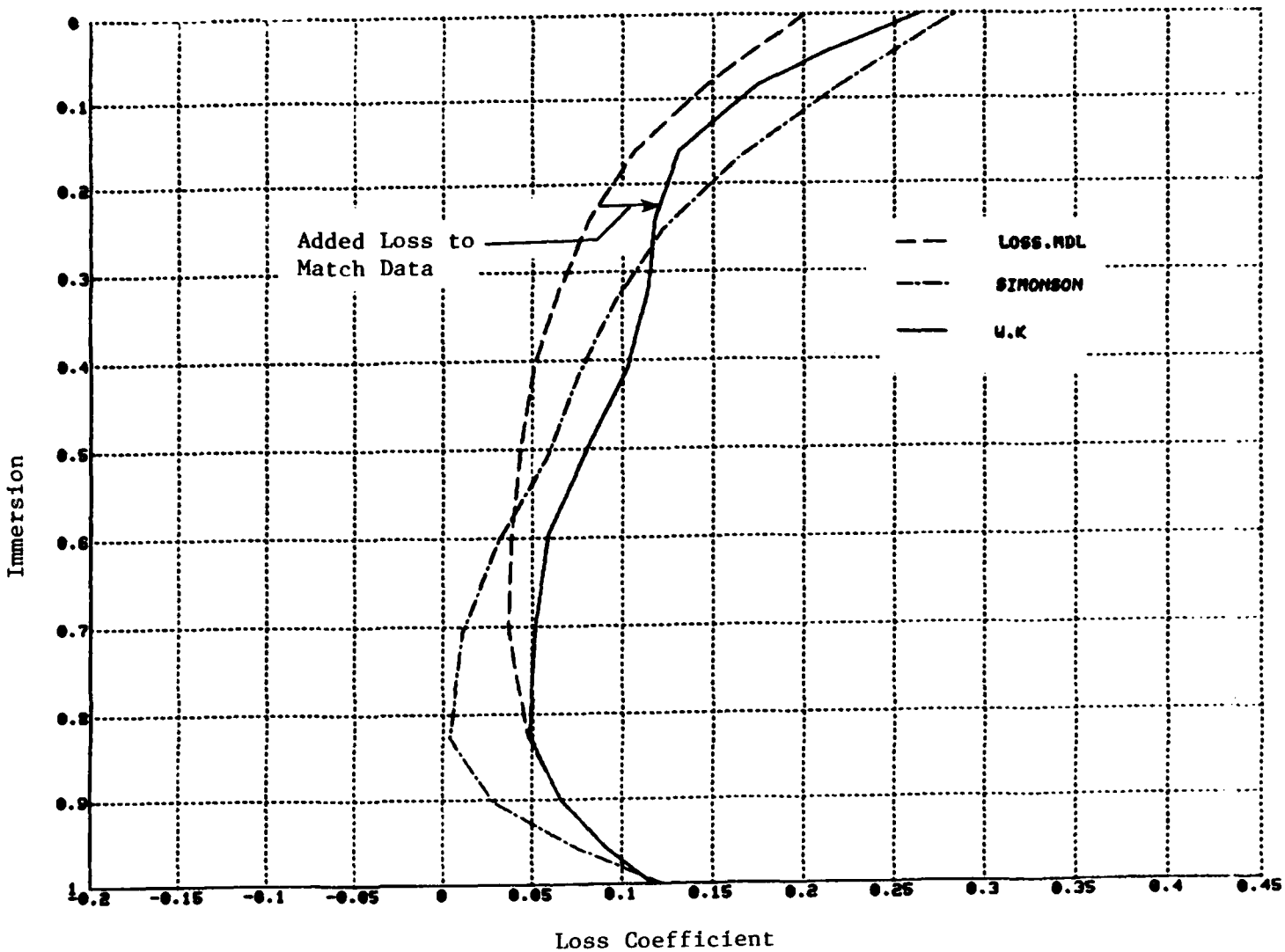

Figure 21. Rotor Loss Coefficients as Determined in the Present Study (labeled W.K.) and by Simonson.

Also shown is the modified loss model of Koch & Smith and Adkins & Smith (labeled LOSS.MDL).

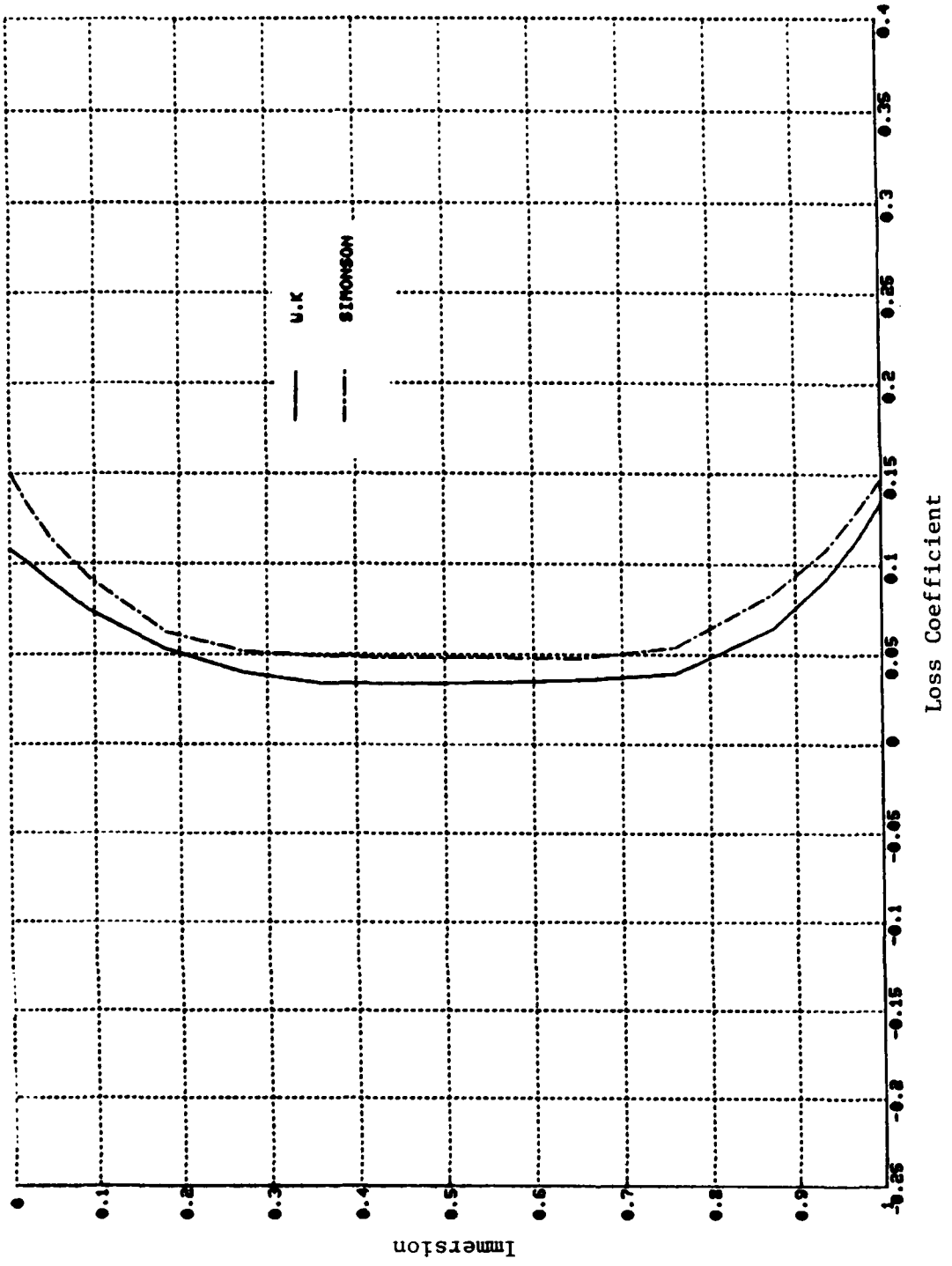

Figure 22. Stator Loss Coefficient Used in the Present Study (W.K) and in the No-Mixing Data Analysis (Simonson).

The stator losses used in the present method (labeled W.K in Figure 22) are somewhat less than those ascertained by Simonson from examination of the stator wake data, but the shape of the curve is very similar.

The mixing phenomenon upsets the normal method for emprically determining losses. Usually, the loss coefficient is determined from the measured total pressure just in front of and behind the blade row at immersions with the same stream function. The loss coefficient computed by CAFMIX in this way leads to the pseudovalues shown in Figure 23.

Figure 24 compares the data match values of the (primary flow) rotor discharge swirl angles with the design angles reported in Reference 20. Also shown are two values calculated by a coupled-boundary layer/inviscid blade-to-blade solution. These latter values are in rather good agreement with the present analysis. The predicted full three-dimensional circumferential flow angles (primary and secondary) are illustrated in Figure 25. There is little secondary flow under/overturning except at the end walls.

The remaining curves in this section illustrate the intermediate values of various parameters of the wake centrifugation model as applied to the Air Force stage; they compare these parameters, where appropriate, with the Adkins and Smith model. Figure 26 shows the predicted rotor wake width as defined in Figure 27. Note that the two models use very different wake widths. Adkins and Smith base their wake width on total losses (including shock losses but not end wall losses); they back-calculate a momentum thickness and wake thickness as described in Section 4.2 of Reference 1. In the current model, denoted as Whitfield and Keith, the wake width is consistent with the profile boundary-layer-growth correlations used by Koch and Smith to evaluate profile loss. The boundary layer is then thickened to account for one-third of the profile shock loss.

The model for the radial velocity in the wake has been discussed in some detail in Section 3.1.1. Results for several machines were presented in Section 4.1. The improved model, as shown in Figure 28, yields higher values for the rotor wake radial velocity than does the Adkins and Smith formulation. The radial velocities are small near the hub, but become quite large (approximately 70% of the meridional through-flow velocity) near the tip. Conversely, the stator wake radial velocities (not shown) are small across the span (about negative 1% of the meridional velocity).

The radial secondary flow velocities behind the rotor are shown in Figure 29. They are identical for the two models.

The wake width, wake radial velocity, and radial secondary velocity constitute the elements of the blade-to-blade trailing edge spanwise velocity field illustrated in Figure 27. This curve is integrated, and the mixing coefficient is calculated by the formulation presented in Section 4.0 of Reference 1. The resulting mixing coefficients are presented in Figures 30 and 31. The Whitfield and Keith coefficients (Figure 30) are initially higher at the rotor trailing edge) than the Adkins and Smith values,

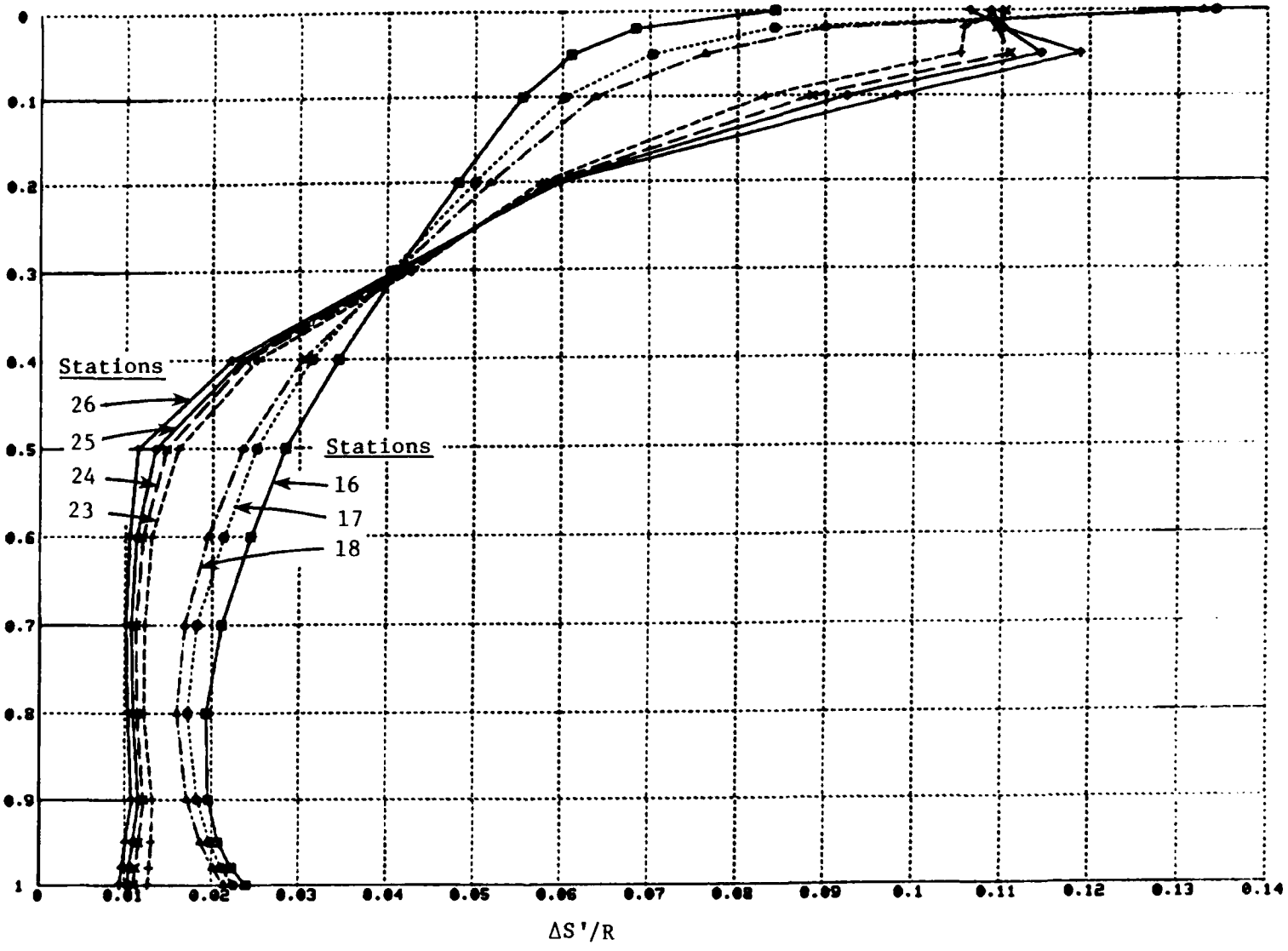

Figure 35. Spanwise and Streamwise Variation of Entropy Increment Generated by the Rotor Wake, Whitfield and Keith.

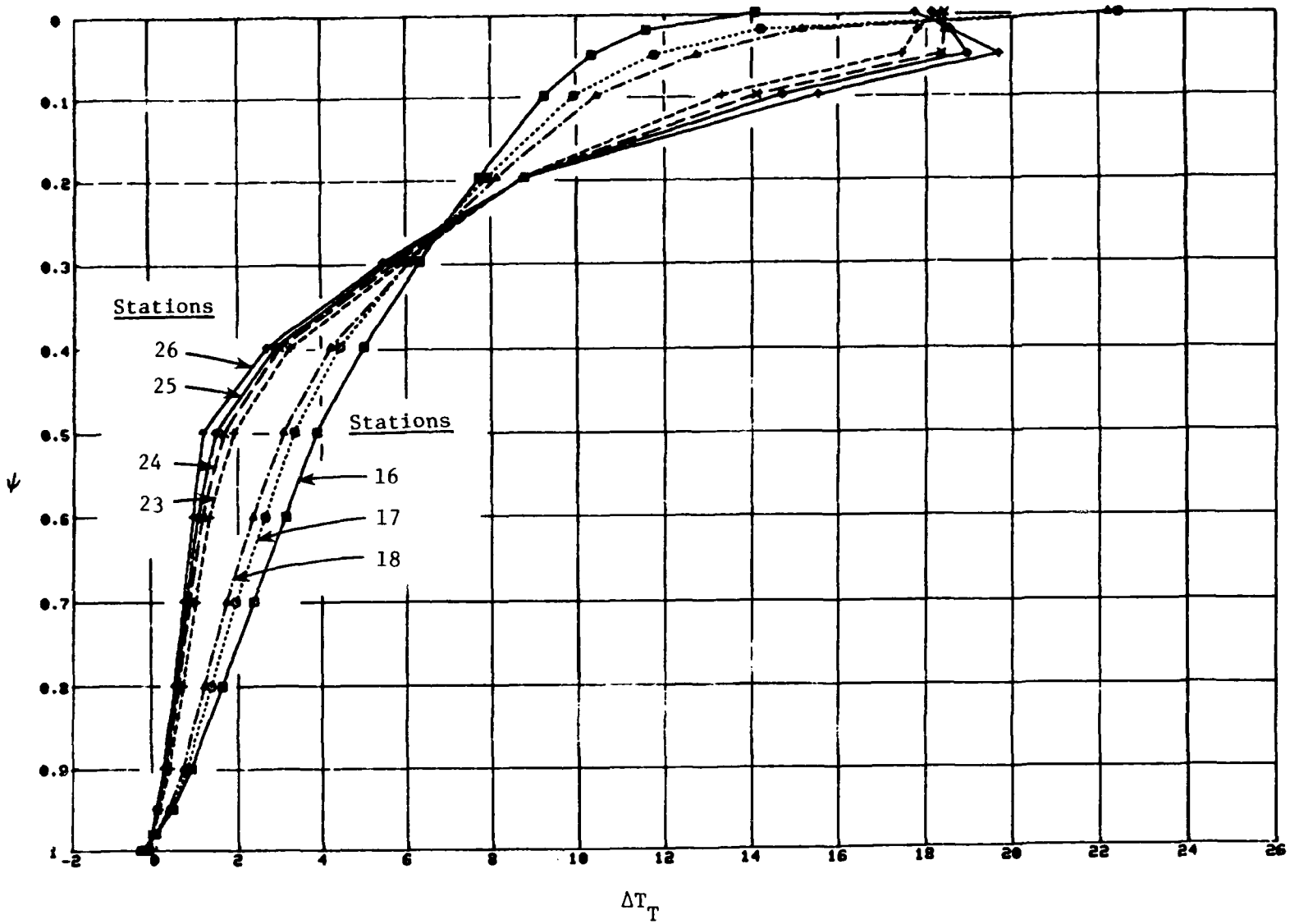

Figure 34. Spanwise and Streamwise Variation of Stagnation Temperature Increment Generated by the Rotor Wake, Whitfield and Keith.

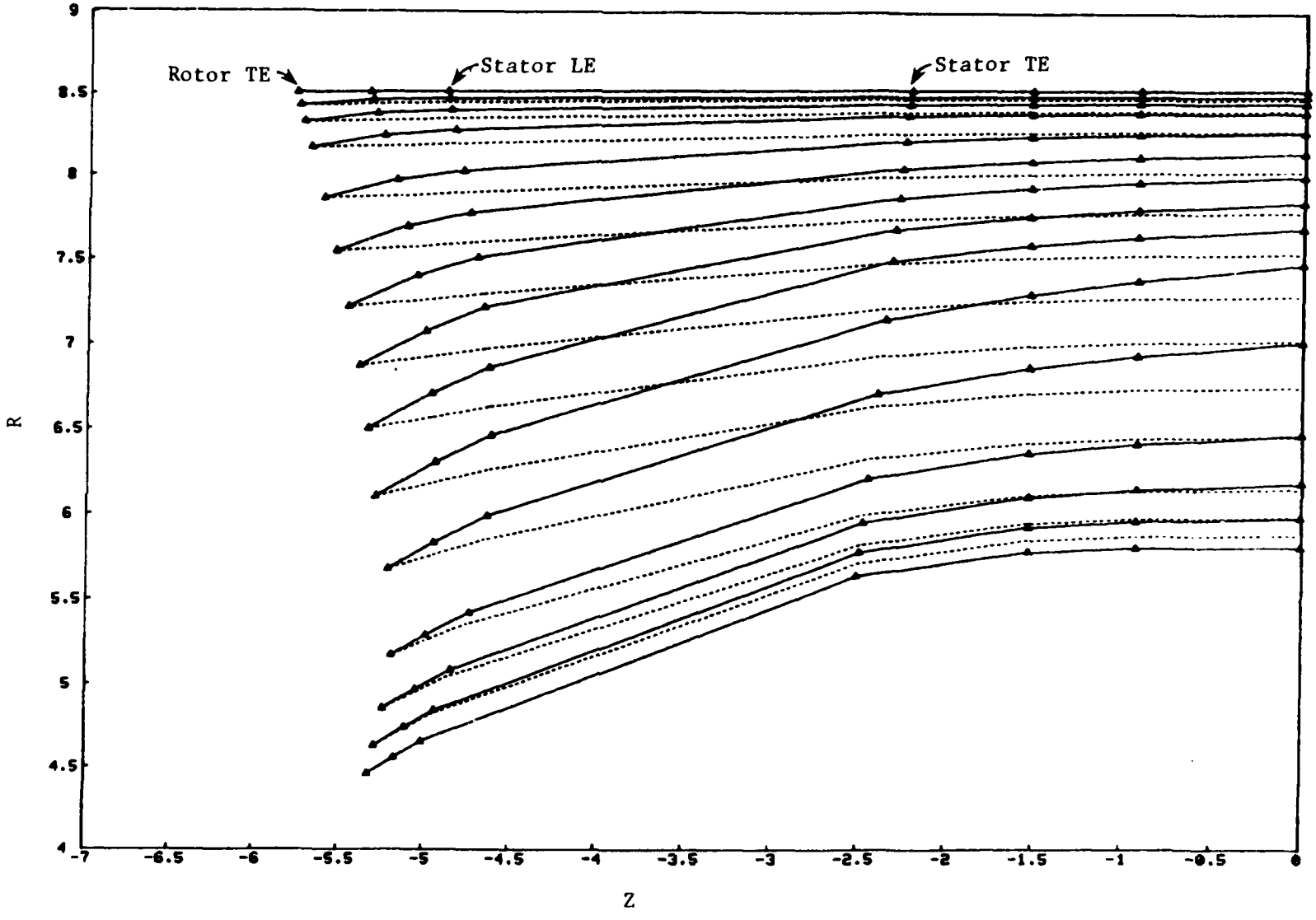

Figure 33. Aggregate Rotor Wake Fluid Trajectories, Whitfield and Keith.

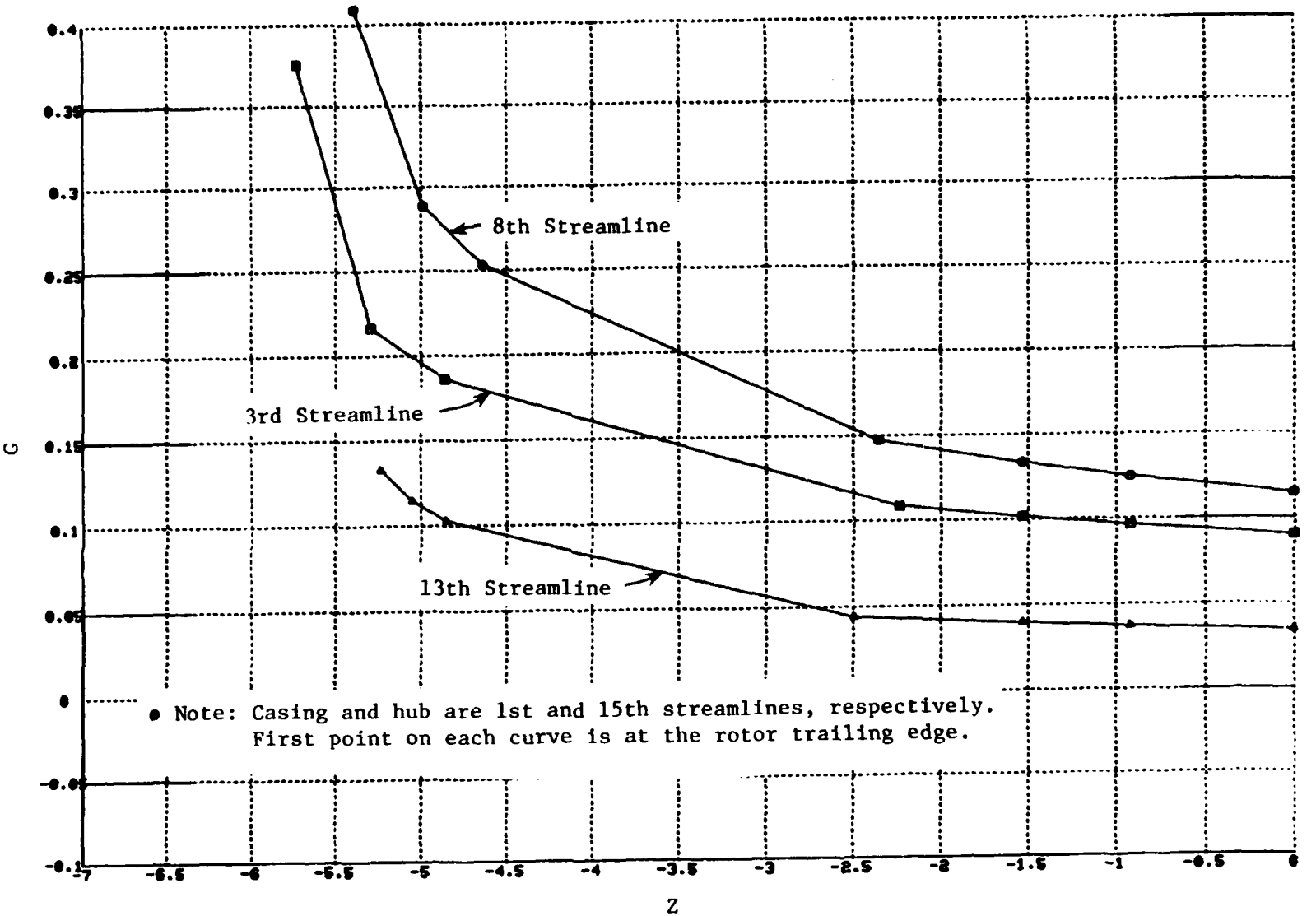

Figure 32. Decay of Radial Velocity, G, with Downstream Distance, Whitfield and Keith.

but then fall off. This is due to the use of the local decayed value of radial wake velocity, as predicted by the formulation of Section 3.2, rather than the invariant (trailing edge) velocities used by Adkins and Smith.

The decay of the wake radial velocities for three representative streamlines is shown in Figure 32. In Figure 33, trajectories of aggregate wake fluid particles, moving outward by velocities related to those shown in Figure 32, are plotted against a background of mean flow streamlines. Notice the large outward movement of the wake fluid. (These effects are computed by Equation (20) of Section 3.2.2 and Equation (36) of Section 3.4.3, respectively.)

In the midspan region of the annulus, the radial distance between the wake particles is increased as the wake moves downstream. This thins the wake and causes the mass-averaged $\Delta T_T'$ (Figure 34) and $\Delta S'$ (Figure 35) to decrease. Conversely, near the casing the wake fluid tends to pile up and $\Delta T_T'$ and $\Delta S'$ increase. However, the hub-to-tip integrated levels of both $\Delta T_T'$ and $\Delta S'$ remain constant. The effects shown in Figures 33, 34, and 35 are related to the rotor wake. Interaction of the rotor wake with the stator blade flow field is ignored, as is impingement of the wake on the pressure side of the stator blade.

The radial migration of the stator wake is small. Consequently, the plot of $\Delta S'$ for the sequence of stations behind the stator trailing edge all fall one upon the other (Figure 36). The methods for predicting $\Delta T_T'$ and $\Delta S'$ are given in Section 3.4.3.

Finally, for reference, the source terms in the spanwise mixing equations (Equations 40 and 42) are plotted in Figures 37 and 38. Again, it may be seen that these source terms must integrate (with respect to mean flow stream function) to zero.

An overall comparison between the present study and Adkins and Smith is provided in Figures 39 and 40. The two predictions use the same loss coefficients and rotor and stator (primary flow) exit angles. The differences shown indicate the differences that result from (1) the revised mixing coefficient and (2) the inclusion of "hot" wake radial migration effects. The differences are not large, but they are significant for this case.

This significance is further illustrated in Figure 41. This is a plot of the entropy distribution at a number of stations within the Air Force compressor. Both the jump in entropy across each blade row and the redistribution of entropy at subsequent downstream stations can be observed. The final distribution at Station 25 is shown to be in reasonable agreement with the experimental data. It is through the wake centrifugation process that the rotor losses (near the 80% immersion point) are "thinned" and the combined rotor and stator losses then agree with the Plane 25 measurements.

The calculations reported in this section have been carried out with an invariant radial equilibrium concept. The radial variation of streamline curvature and flow angle, together with certain streamwise derivatives, was determined by Simonson (Reference 21). His calculations included six stations in

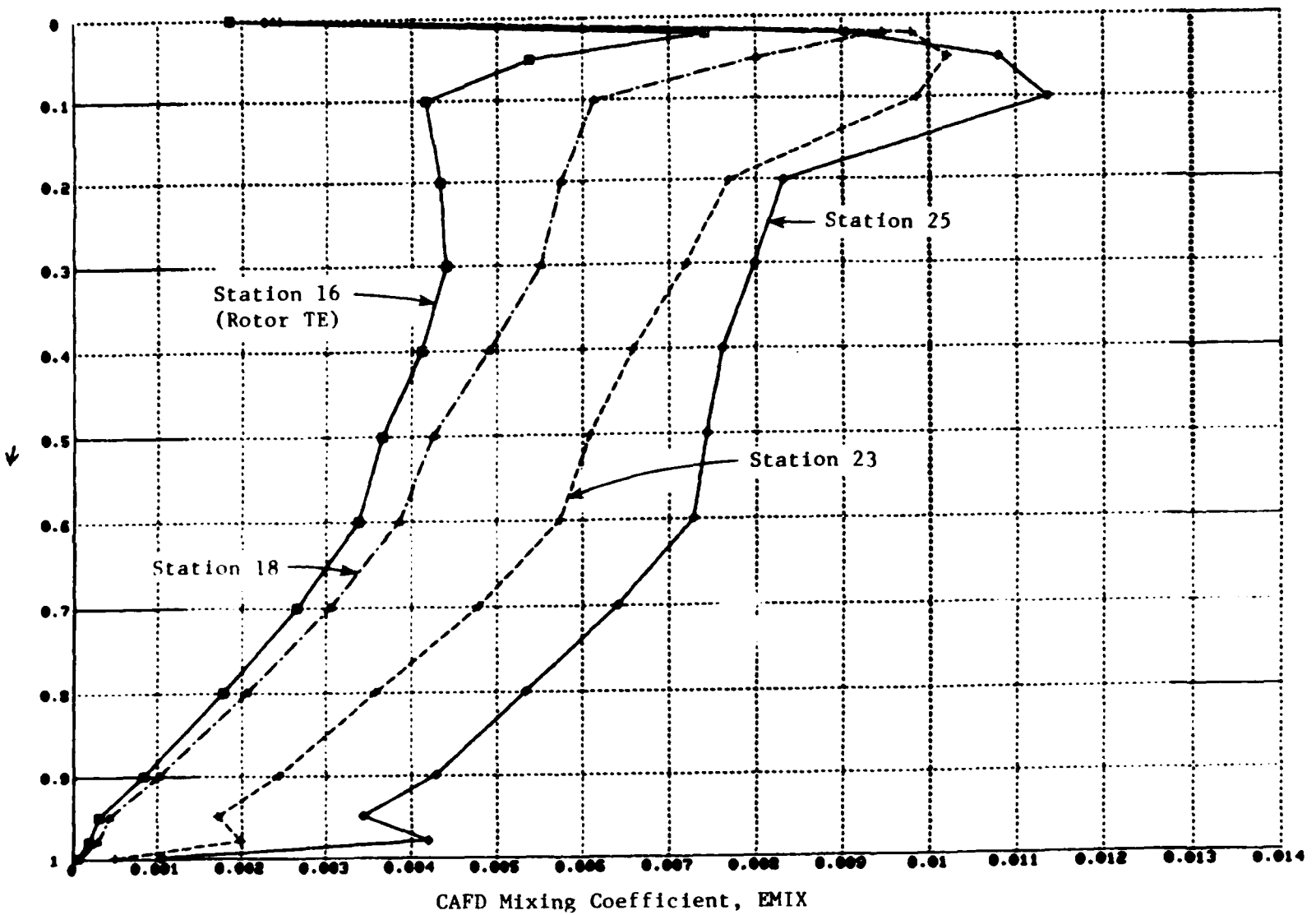

Figure 31. Predicted Diffusion Equation Mixing Coefficient, Adkins and Smith.

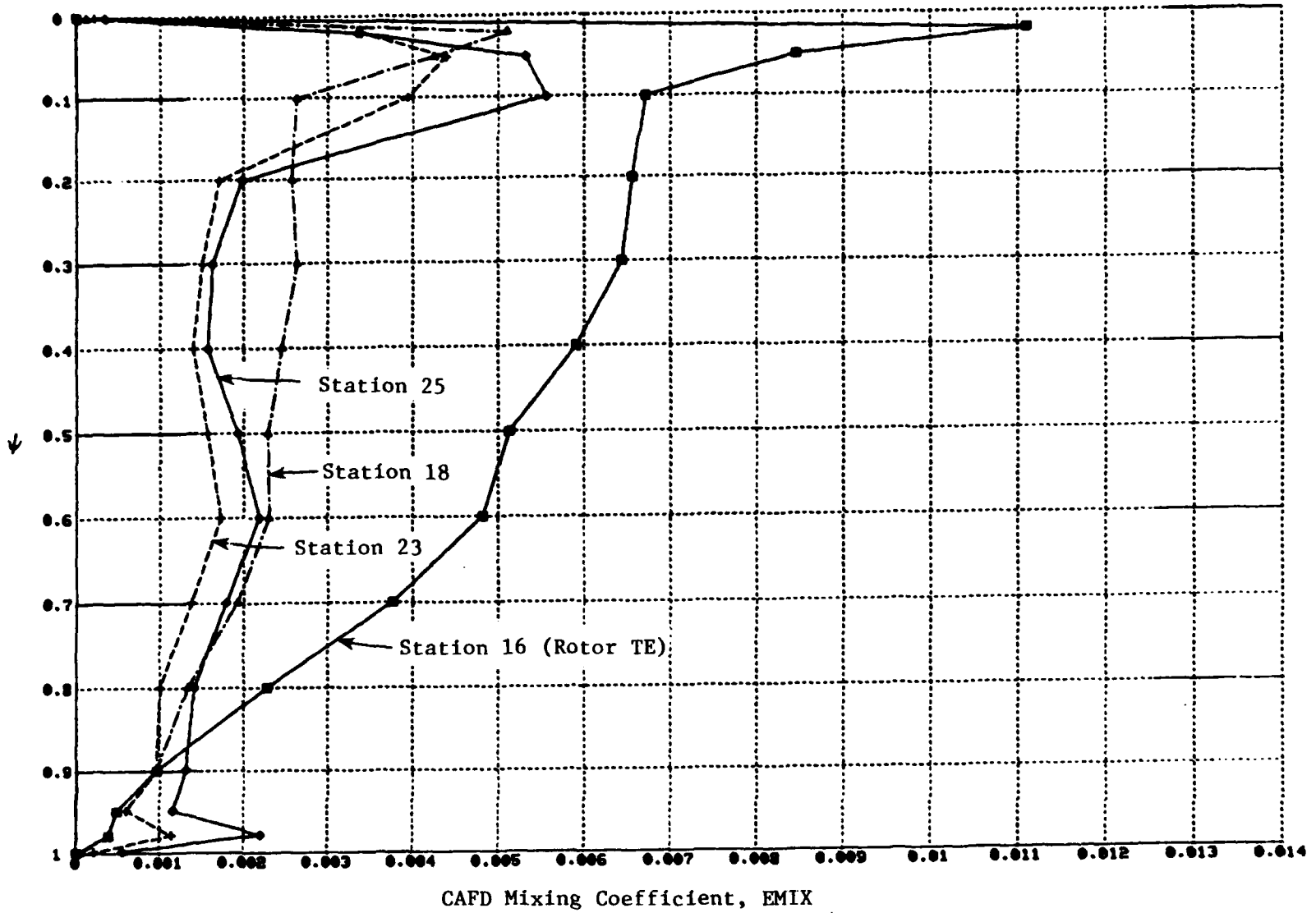

Figure 30. Predicted Diffusion Equation Mixing Coefficient, Whitfield and Keith.

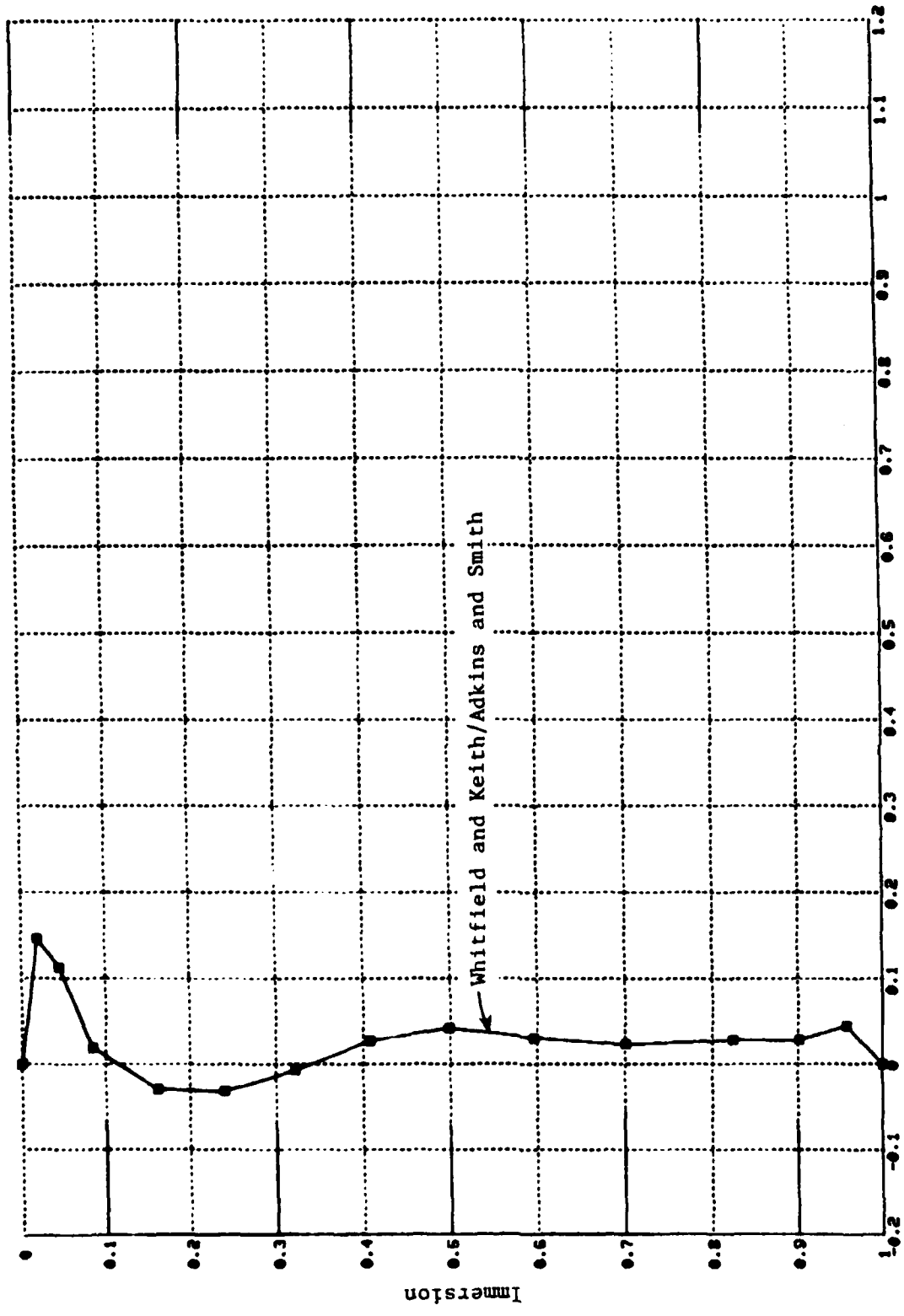

Figure 29. Predicted Spanwise Secondary Flow Velocity.

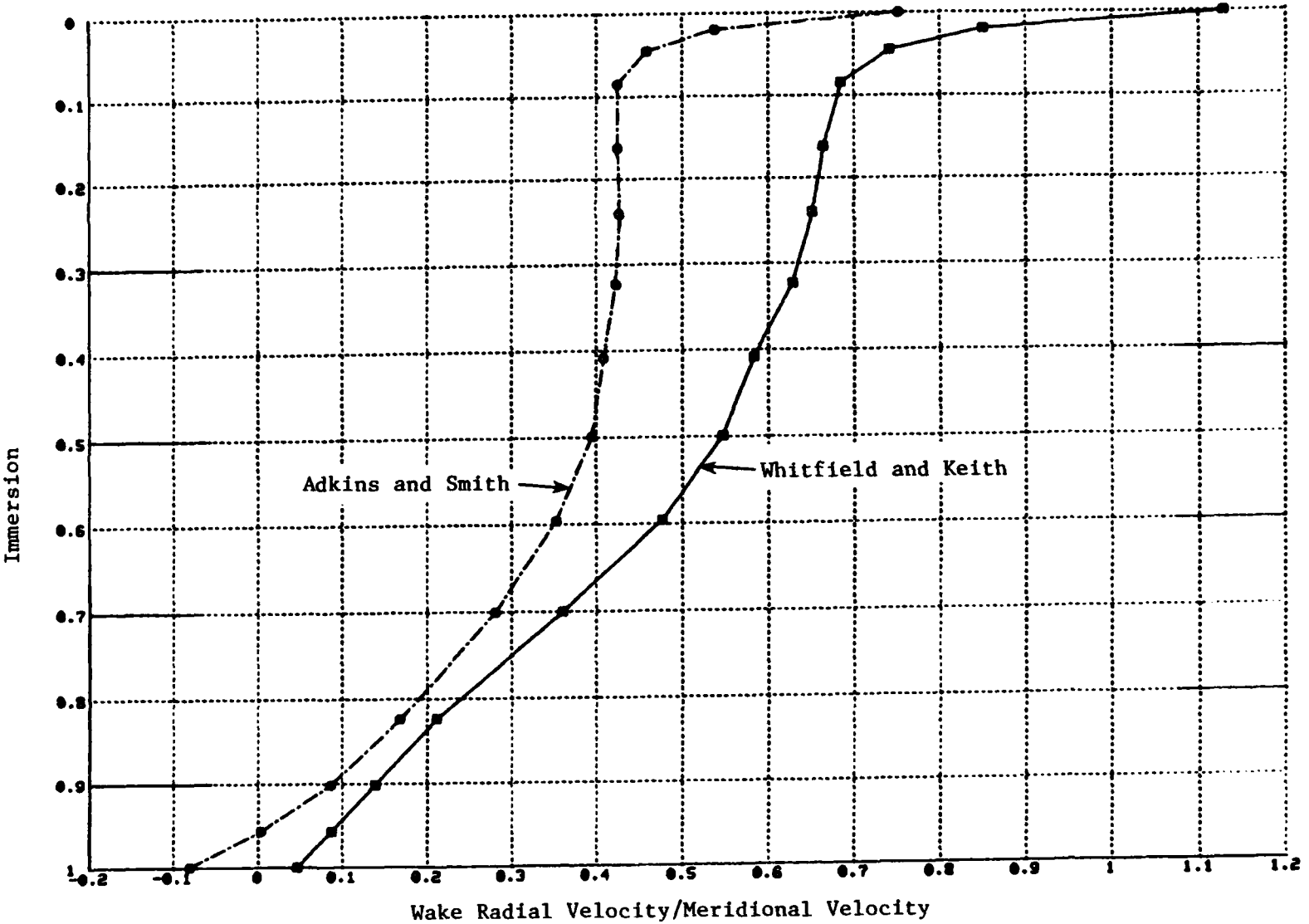

Figure 28. Predicted Rotor Wake Peak Radial Velocity.

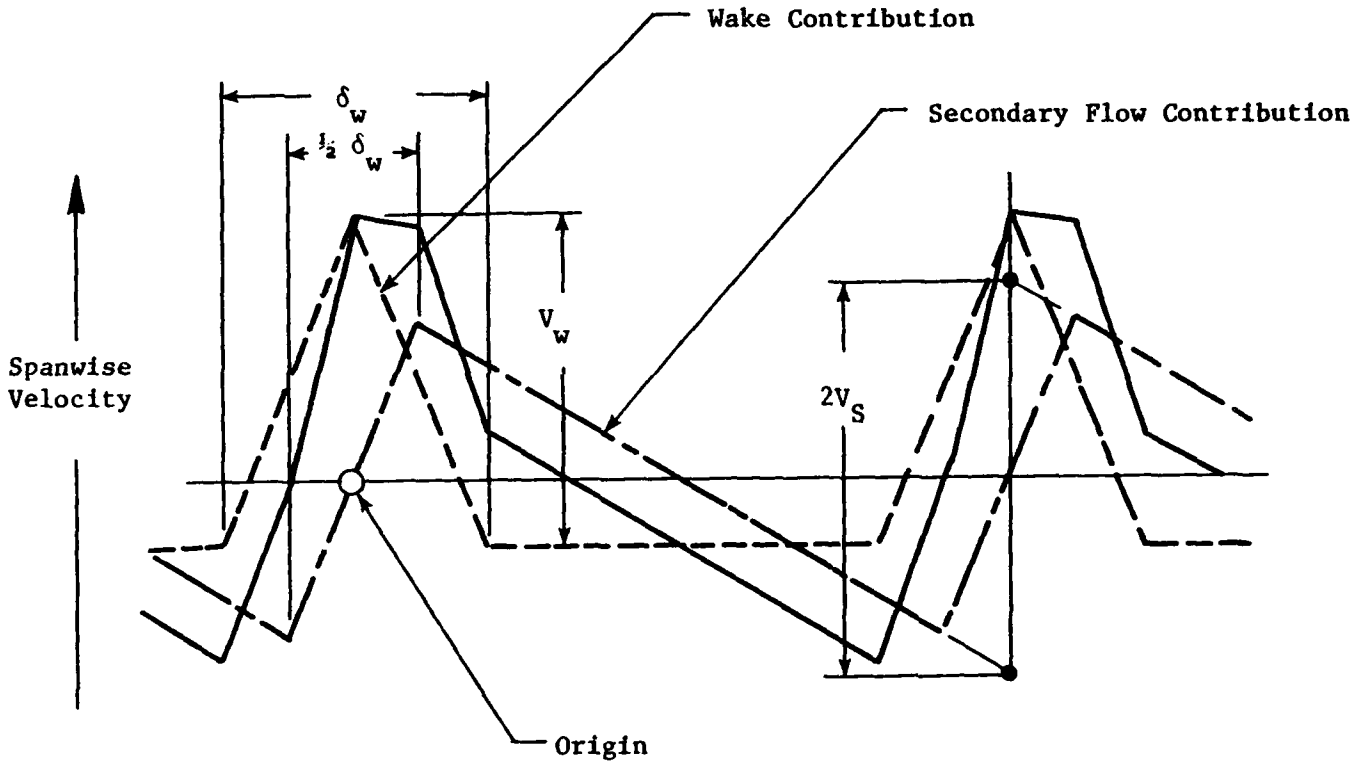

Figure 27. Construction of Spanwise Velocity Field From Secondary Flow and Wake Contributions.

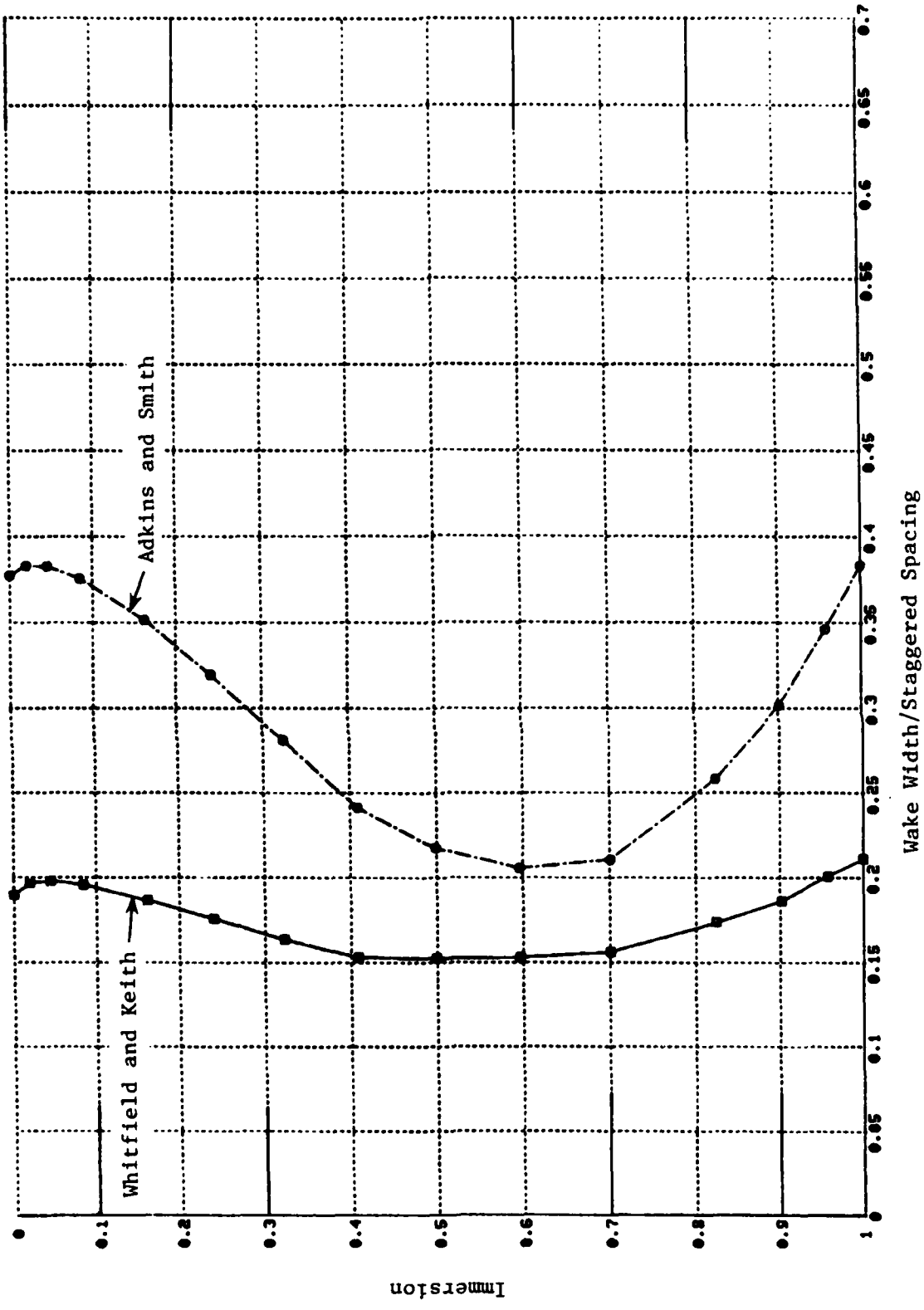

Figure 26. Predicted Rotor Wake Width.

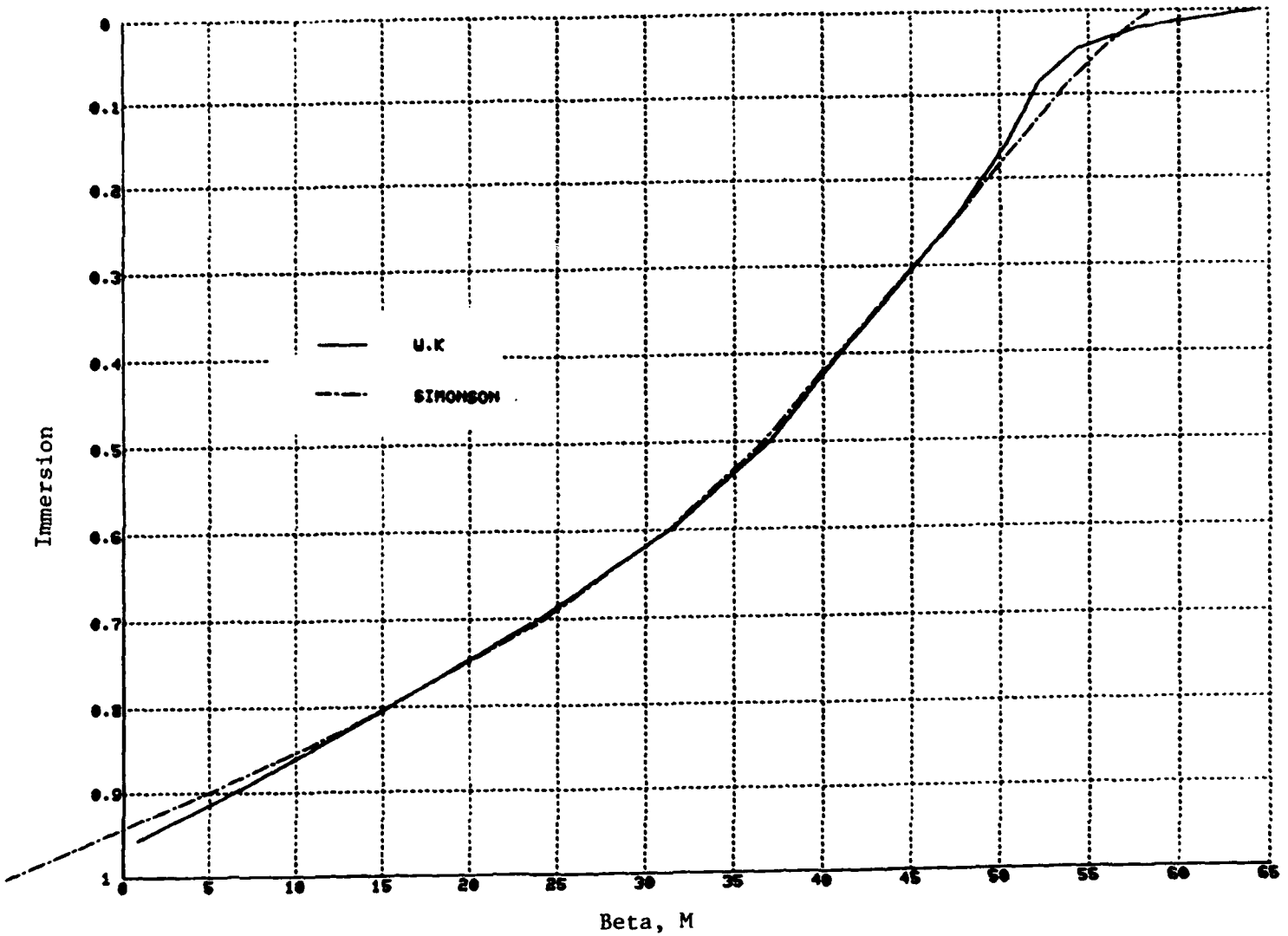

Figure 25. Actual Circumferential Angles (Primary + Secondary) at Rotor Trailing Edge.

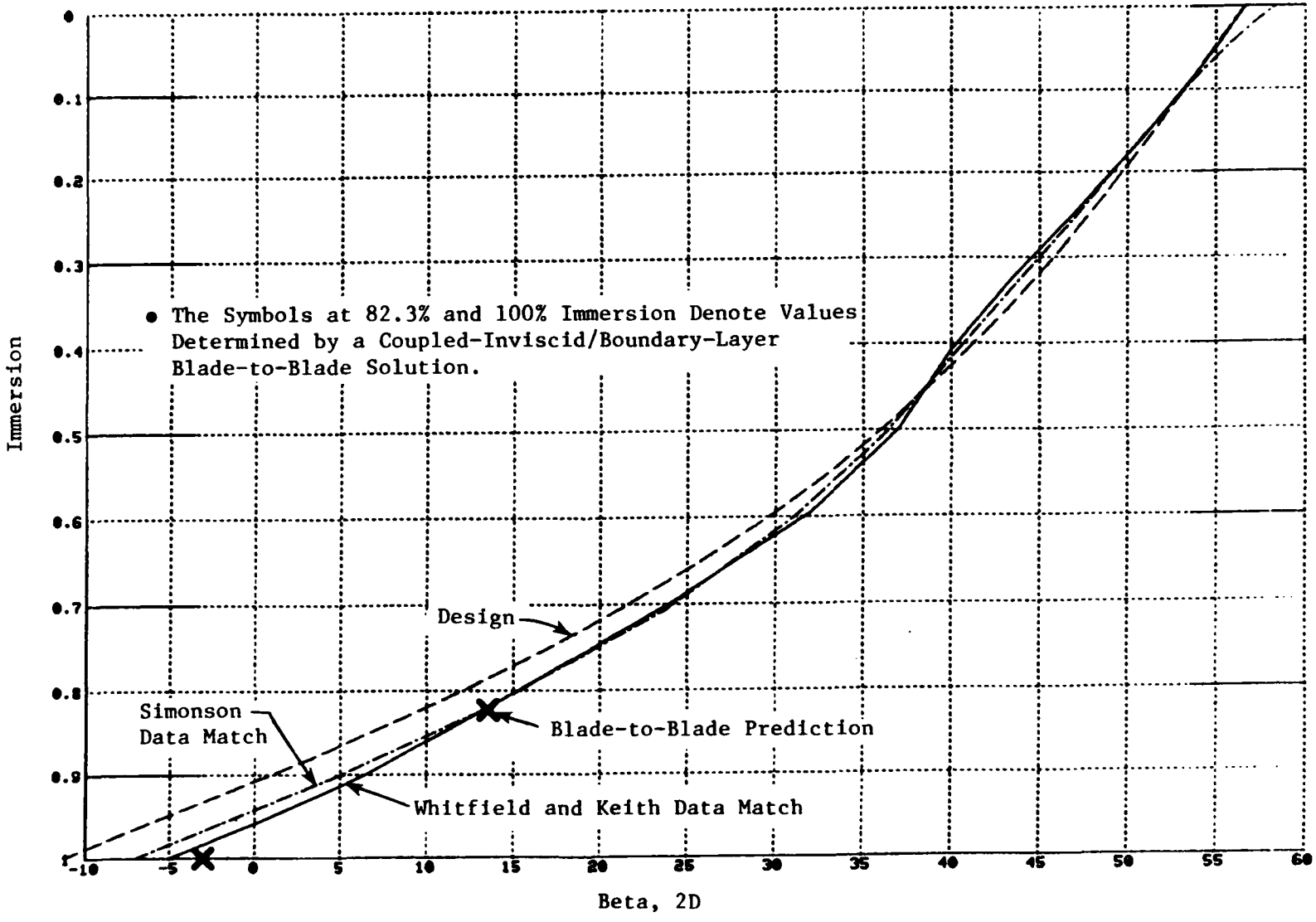

Figure 24. Data Match (Primary Flow) Rotor Spouting Angles Compared to the Design Flow Angles.

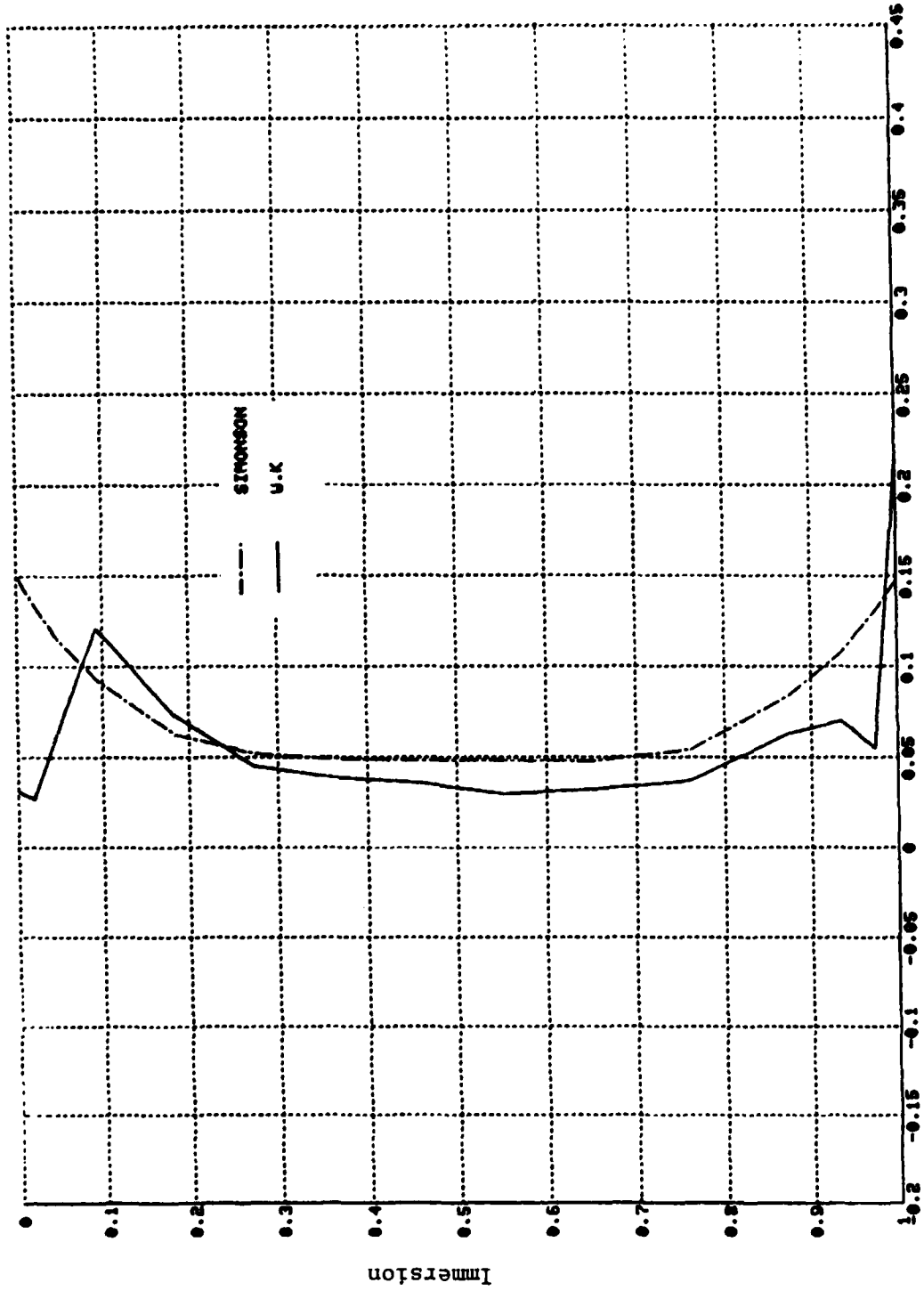

Figure 23. Stator Pseudo Loss Coefficient.

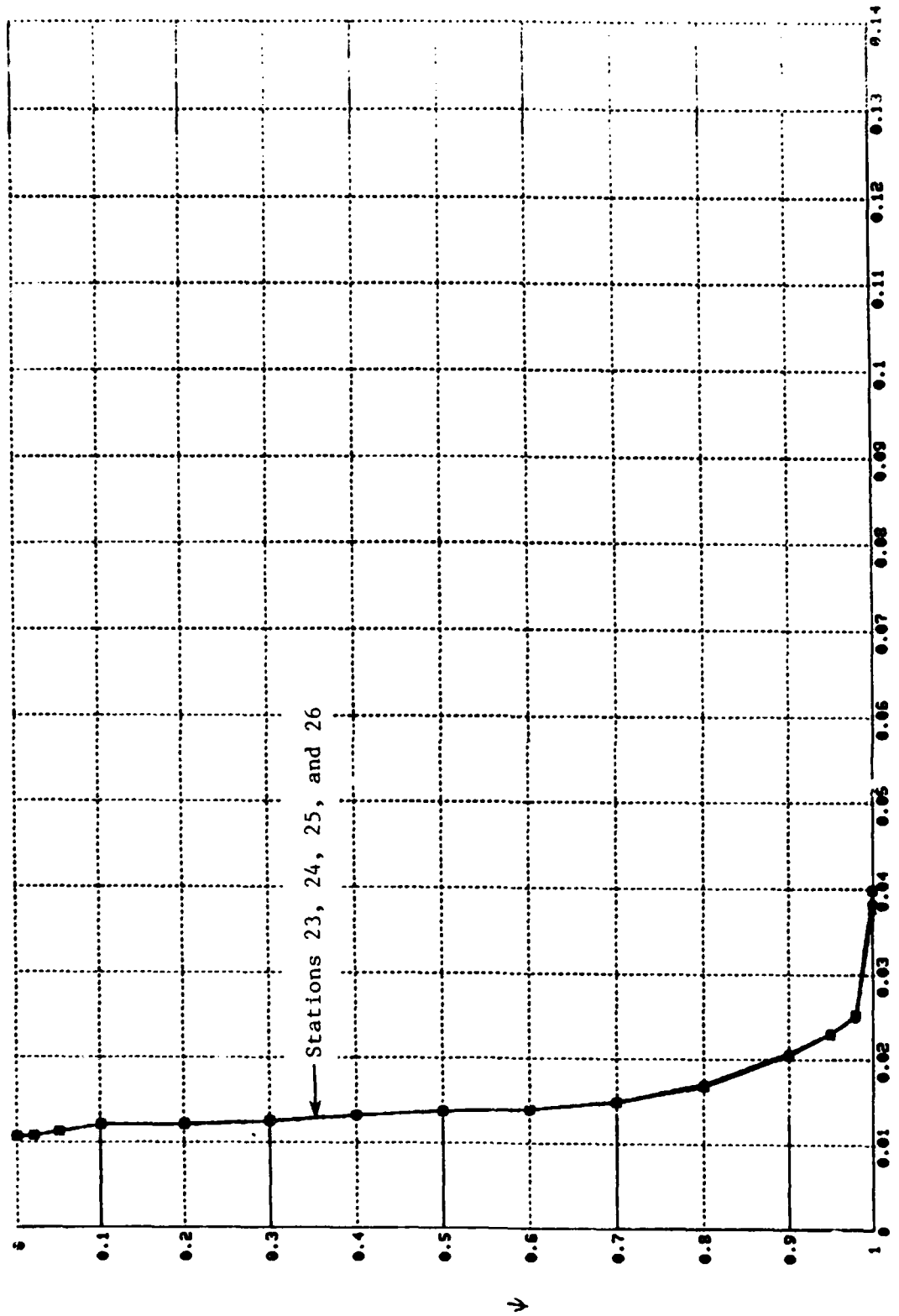

Figure 36. Spanwise and Streamwise Variation of Entropy Increment Generated by the Stator Wake, Whitfield and Keith.

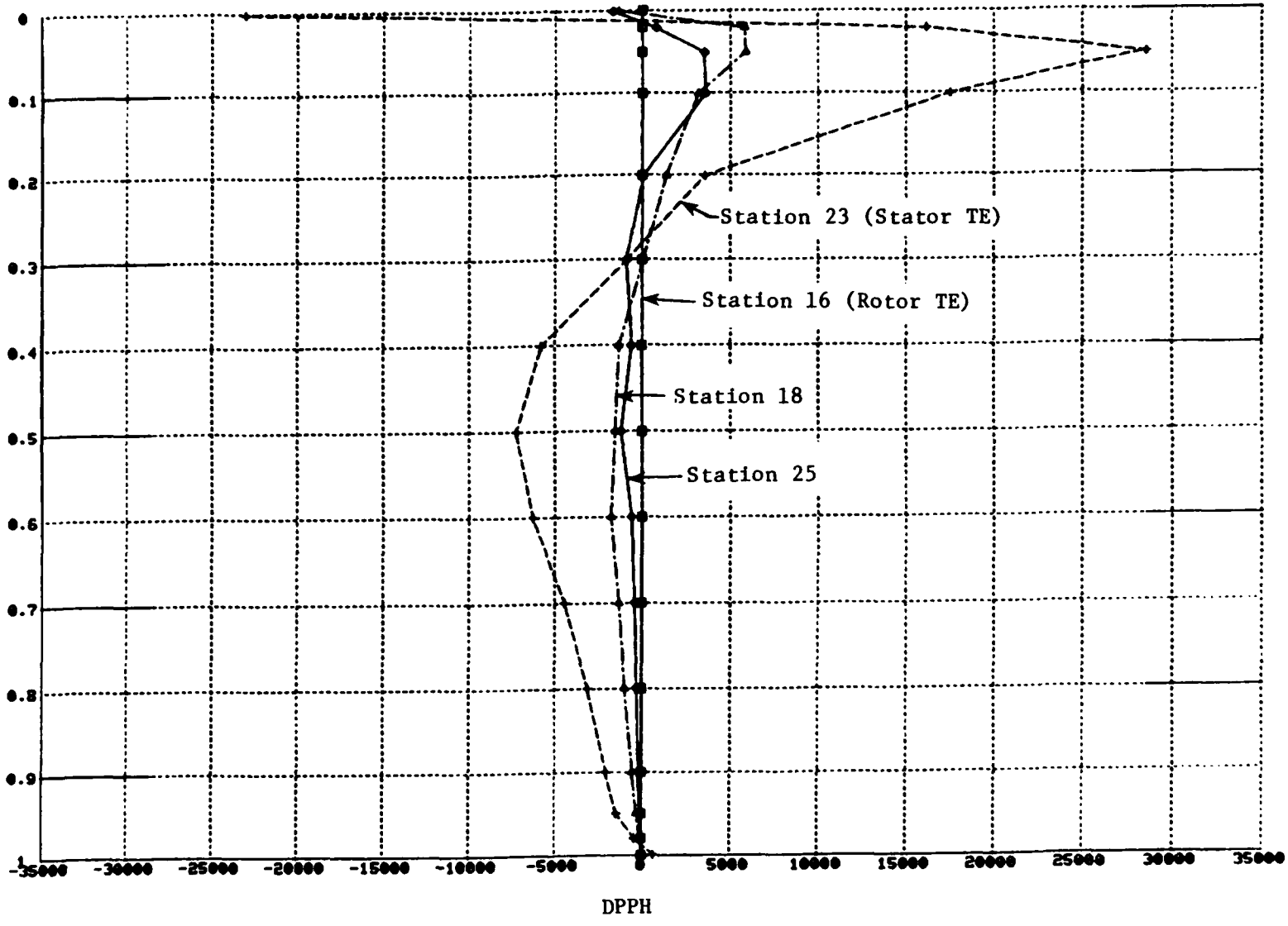

Figure 37. Right-Hand-Side Source Term for the Discretized Form of Equation 40, Whitfield and Keith.

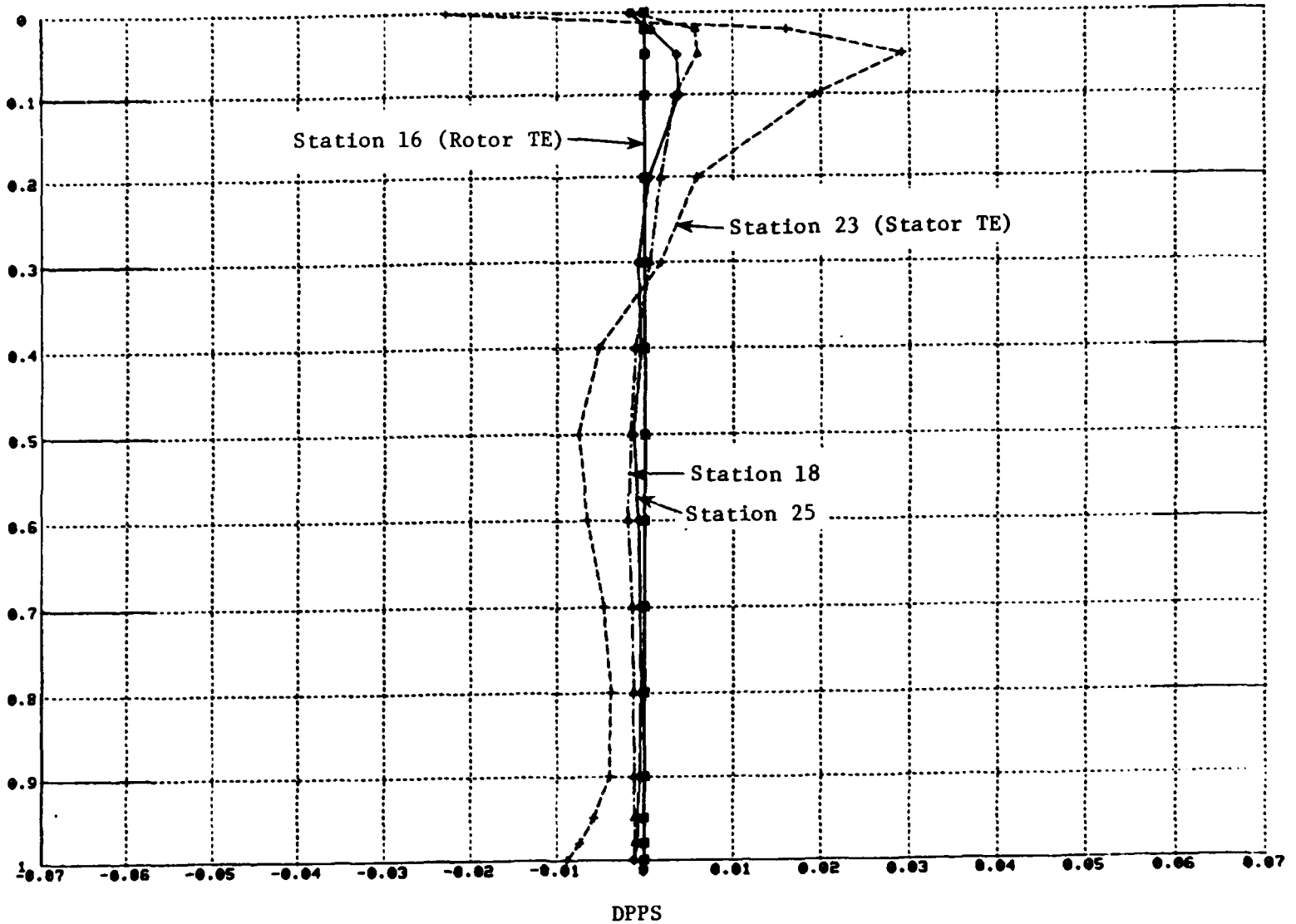

Figure 38. Right-Hand-Side Source Term for the Discretized Form of Equation 42, Whitfield and Keith.

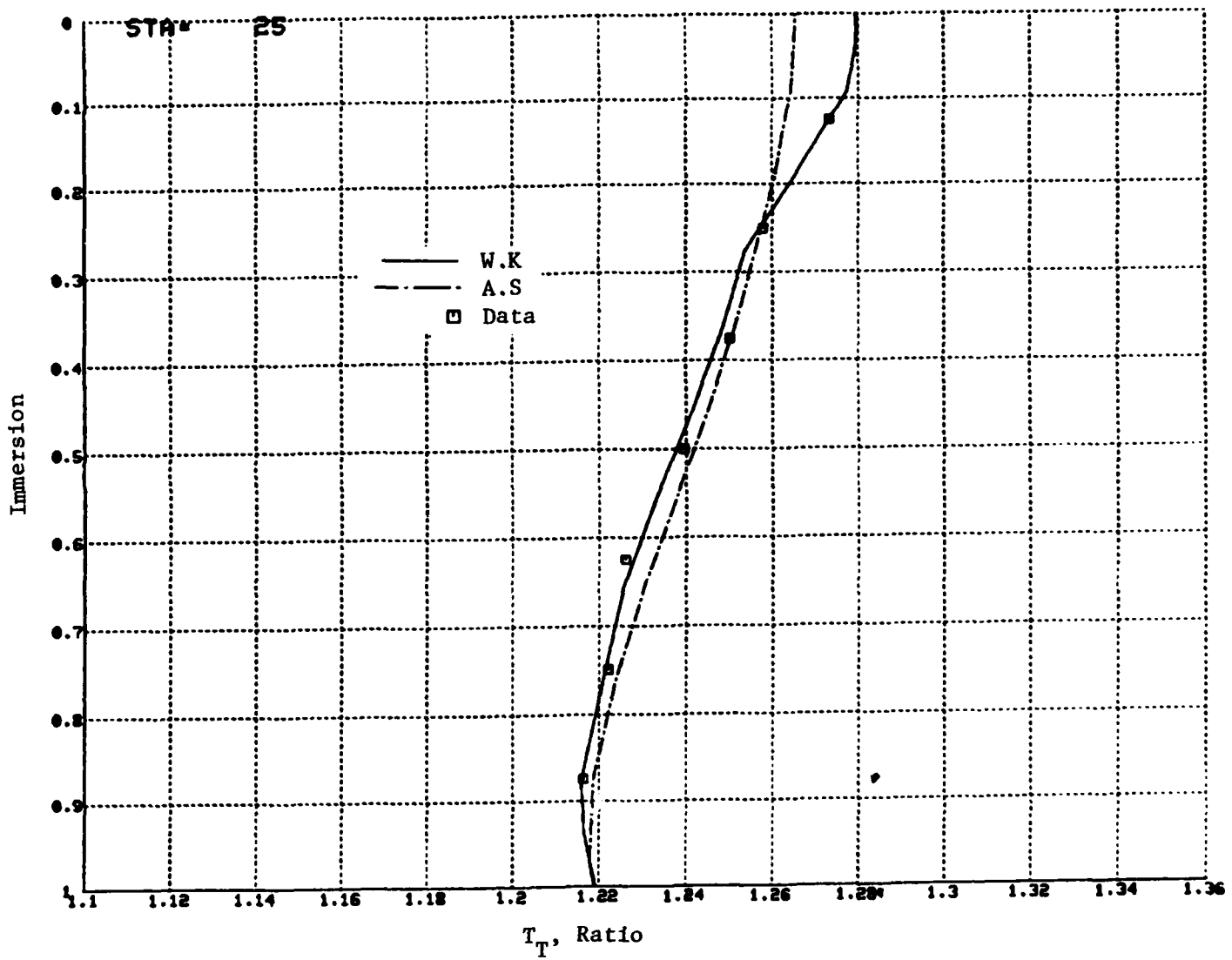

Figure 39. Comparison Between Adkins and Smith/ Whitfield and Keith Predicted Total Temperatures at Station 25 for the Same Rotor/Stator Blade Exit Primary Flow Angles and Loss Coefficients.

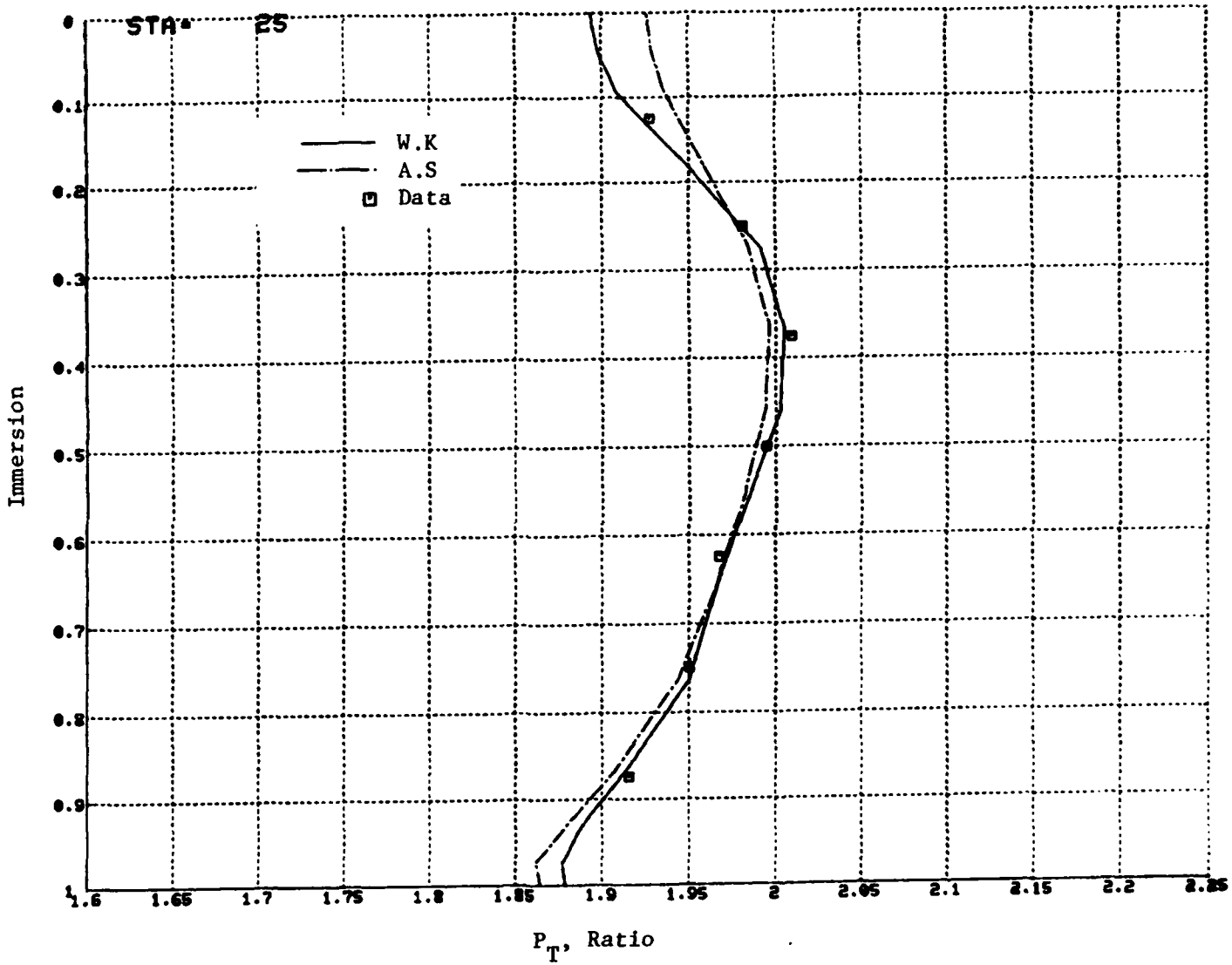

Figure 40. *Comparison* Between Adkins and Smith/Whitfield and Keith Predicted Total Pressures at Station 25 for the Same Blade Exit Primary Flow Angles and Loss Coefficients.

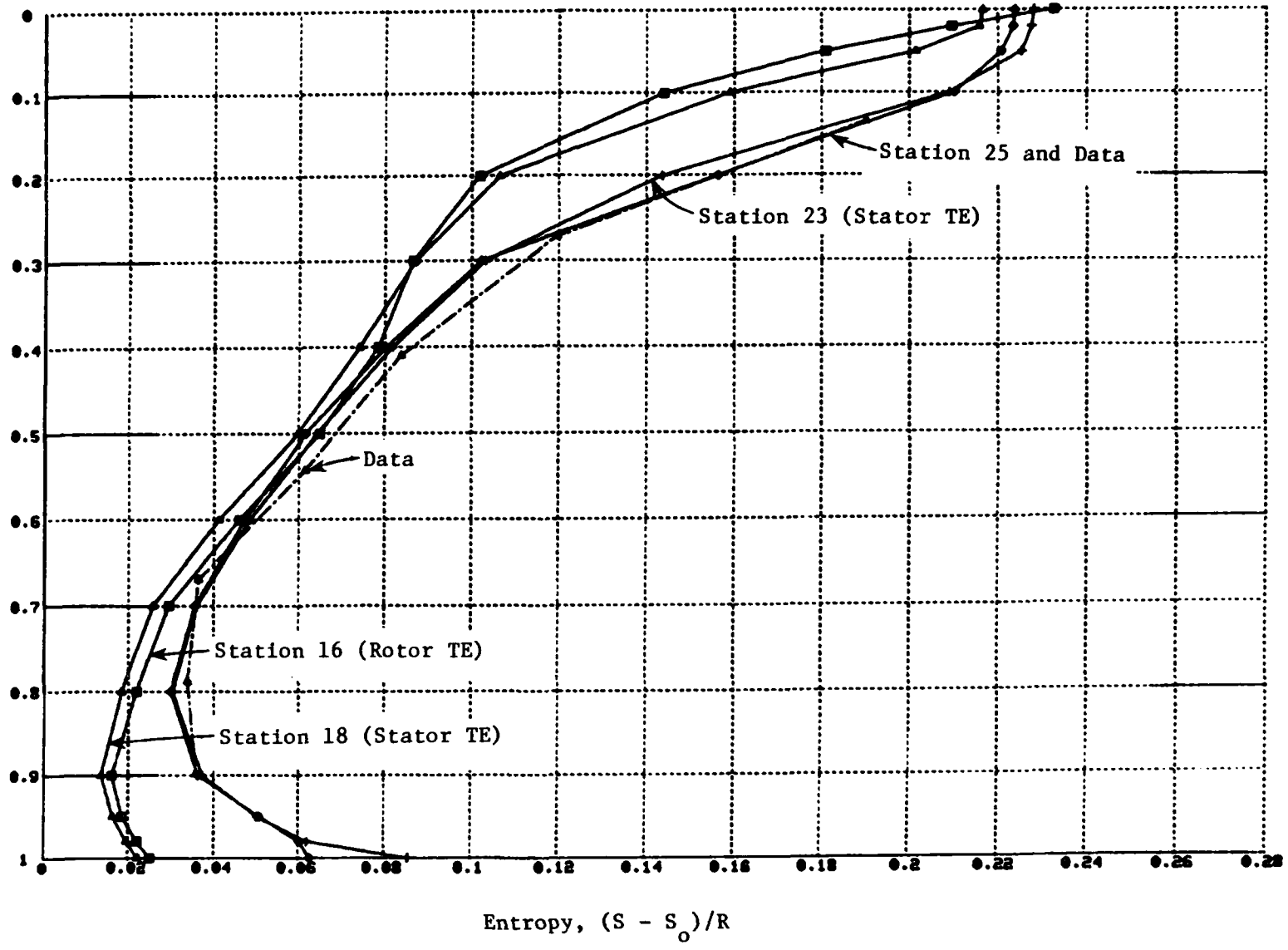

Figure 41. Variation of Entropy from Rotor Trailing Edge to Measurements Station 25 as Determined by the Solution of Equation 42 of Section 3.5.1.

the rotor and six stations in the stator. Subsequent calculations with the Adkins and Smith and Whitfield and Keith models have been performed with these through-the-blade-row stations removed. However, for consistency the latter calculations have both used the (presumed more accurate) Simonson streamline curvatures.

5.0 CONCLUSIONS

1. The peak wake radial velocity calculation of Adkins and Smith has been revised to include the effects of blade loading. Universal velocity profile shapes have been assumed for both the radial and streamwise wake profiles and these, together with simplified momentum equations in the streamwise and radial directions and the knowledge of the trailing edge form factor have been used to obtain the following:

    - Maximum streamwise deficit at the trailing edge and its decay with distance downstream
    - Decay of the peak radial velocity increment/decrement with distance downstream
    - Trailing edge wake thickness and its increase with distance downstream
    - Trailing edge momentum and displacement thicknesses.

2. Wakes have been considered as streams of energy-carrying particles which travel at mass-energy-averaged velocities in the radial and streamwise directions. At calculation stations downstream of the shedding trailing edge, the properties carried by the particles (total enthalpy behind a rotor, total rothalpy behind a stator, and entropy everywhere) are redistributed on the circumferential average streamlines for use in a revised formulation of the mixing equation as a part of the circumferential average flow determination solution iterative scheme.

3. Comparisons between the theory and available experimental data show good agreement between predicted values of both streamwise and radial peak velocity deficits in most cases. If the shedding blade boundary layer is separated, the wake appears to decay significantly more rapidly than predicted.

    The new mixing model has been applied to the Air Force High-Through-Flow Axial Flow stage where it is found that the apparent super-high efficiency near the hub of this machine is due in part to the centrifugation of wake fluid to the outer region of the annulus.

APPENDIX A: STAGGERED PARABOLIC SPLINE FORMULATION

In this appendix the equations for fitting a staggered parabolic spline curve through a given set of points are formulated. This particular curve fit is convenient because (1) either the points through which the curve must pass can be prescribed or (2) the local integral of the curve (between knots) can be prescribed. In Section A.1 the recursion relation for a spline passing through a set of points, u_i, is developed. In Section A.2 a formula for the integral across a spline segment is presented. Finally, in Section A.3 the recursion formula in terms of known integral values, rather the u values, is found.

A.1 RECURSION RELATION FOR PRESCRIBED POINT VALUES

Using the nomenclature illustrated in Figure 42, the parabolic (spline) relations are written for the i^{th} interval defined by h_i.

$$S_i = u_i + c_i\, x + \frac{1}{2}\, d_i\, x^2 \tag{A1}$$

$$S_i' = c_i + d_i\, x \tag{A2}$$

$$m_i = c_i - d_i\, f_i \tag{A3}$$

$$m_{i+1} = c_i + d_i\, g_{i+1} \tag{A4}$$

where c_i and d_i are unknown coefficients, S is the ordinate of the spline and m_i is the slope at the knot.

Subtract (3) from (4)

$$m_{i+1} - m_i = d_i\, (f_i + g_{i+1}) \tag{A5}$$

Then

$$d_i = \frac{m_{i+1} - m_i}{f_i + g_{i+1}} = \frac{r_{i+1} - m_i}{h_i} \tag{A6}$$

$$c_i = \frac{1}{h_i}\, [g_{i+1}\, m_i + f_i\, m_{i+1}] \tag{A7}$$

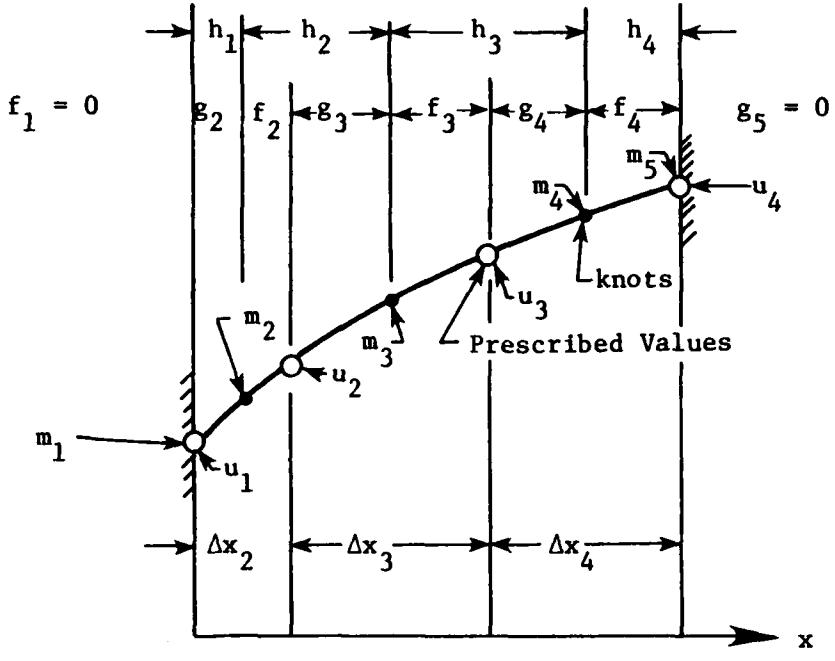

In this Example, we have:

3 Intervals
4 = N = Grid Points
5 knots
2 Boundary Conditions Required,
m_1 and m_5

Select:

$g_2 = f_2 = \Delta x_2/2$

$g_3 = f_3 = \Delta x_3/2$

$g_4 = f_4 = \Delta x_4/2$

$f_1 = 0$

$g_{n+1} = 0$

Figure 42. Illustration of Concept and Nomenclature for a Staggered Parabolic Spline.

Thus the equation for S can be written

$$S_i = u_i + [g_{i+1}\, m_i + f_i m_{i+1}] \frac{x}{h_i} + \tfrac{1}{2} [m_{i+1} - m_i] \frac{x^2}{h_i} \qquad \text{(A8)}$$

The continuity condition at knot i is:

$$-S_i(-f_i) + S_{i-1}(g_i) = 0 \qquad \text{(A9)}$$

or

$$-u_i - [g_{i+1}m_i + f_i\, m_{i+1}] \frac{(-f_i)}{h_i} - \tfrac{1}{2} [m_{i+1} - m_i] \frac{f_i^2}{h_i}$$

$$+u_{i-1} + [g_i m_{i-1} + f_{i-1}\, m_i] \frac{g_i}{h_{i-1}} + \tfrac{1}{2} [m_i - m_{i-1}] \frac{g_i^2}{h_{i-1}} = 0$$

Rearrangement gives:

$$\tfrac{1}{2} \frac{g_i^2}{h_{i-1}} m_{i-1} + \left[\frac{f_{i-1}\, g_i}{h_{i-1}} + \tfrac{1}{2} \frac{g_i^2}{h_{i-1}} + \frac{f_i g_{i+1}}{h_i} + \tfrac{1}{2} \frac{f_i^2}{h_i}\right] m_i$$

$$+\tfrac{1}{2} \frac{f_i^2}{h_i} m_{i+1} = u_i - u_{i-1}$$

or

$$\boxed{\frac{g_i^2}{h_{i-1}} m_{i-1} + \left[g_i\left(1 + \frac{f_{i-1}}{h_{i-1}}\right) + f_i\left(1 + \frac{g_{i+1}}{h_i}\right)\right] m_i + \frac{f_i^2}{h_i} m_{i+1} = 2\,(u_i - u_{i-1})} \qquad \text{(A10)}$$

A.2 REPLACEMENT OF POINT VALUE BY INTEGRAL VALUE

Over the segment h_i,

$$I_i \equiv \int_{-f_i}^{g_{i+1}} S_i dx = \int_{-f_i}^{g_{i+1}} \left\{ u_i + (g_{i+1} m_i + f_i m_{i+1}) \frac{x}{h_i} + \tfrac{1}{2}(m_{i+1} - m_i) \frac{x}{h_i} \right\} dx$$

$$= u_i (g_{i+1} + f_i) + \frac{1}{2h_i} (g_{i+1} m_i + f_i m_{i+1}) (g^2_{i+1} - f^2_i)$$

$$+ \frac{1}{6h_i} (m_{i+1} - m_i) (g^3_{i+1} - f^3_i) \qquad \text{(A11)}$$

$$I_i = u_i h_i + \frac{1}{2} (g_{i+1} m_i + f_i m_{i+1}) (g_{i+1} - f_i)$$

$$+ \frac{1}{6} (m_{i+1} - m_i) (g^2_{i+1} - g_{i+1} f_i + f^2_i)$$

$$I_i = u_i h_i + \frac{m_i}{6} [2 g^2_{i+1} - 2 f_i g_{i+1} - f^2_i]$$

$$+ \frac{m_{i+1}}{6} [-2 f^2_i + 2 f_i g_{i+1} + g^2_{i+1}] \qquad \text{(A12a)}$$

$$I_i = h_i [u_i + \frac{1}{6} (m_{i+1} - m_i) h_i] + \frac{1}{2} g^2_{i+1} m_i - \frac{1}{2} f^2_i m_{i+1} \qquad \text{(A12b)}$$

A.3 MATRIX EQUATION IN TERMS OF I RATHER THAN u

Rewrite (A12) in form to be added to (A10).

$$2u_i + \frac{m_i}{3h_i}[2g^2_{i+1} - 2f_i g_{i+1} - f^2_i] + \frac{m_{i+1}}{3h_i}[-2f^2_i + 2f_i g_{i+1} + g^2_{i+1}] = \frac{2I_i}{h_i} \tag{A13}$$

$$-2u_{i-1} + \frac{m_{i-1}}{3h_{i-1}}[-2g^2_i + 2f_{i-1} g_i + f^2_{i-1}] + \frac{m_i}{3h_{i-1}}[2f^2_{i-1} - 2f_{i-1} g_i - g^2_i] = -\frac{2I_{i-1}}{h_{i-1}} \tag{A14}$$

Add (A10), (A13), and (A14)

$$[g_i^2 + 2f_{i-1}g_i + f^2_{i-1}]\frac{m_{i-1}}{3h_{i-1}}$$

$$+ \left\{[2f^2_{i-1} - 2f_{i-1}g_i - g_i^2 + 3g_i h_{i-1} + 3f_{i-1}g_i]\frac{1}{3h_{i-1}}\right.$$

$$\left. +[2g^2_{i+1} - 2f_i g_{i+1} - f^2_i + 3f_i^2 + 6f_i g_{i+1}]\frac{1}{3h_i}\right\} m_i$$

$$+ [3f^2_i - 2f^2_i + 2f_i g_{i+1} + g^2_{i+1}]\frac{mi+1}{3h_i} = 2\left[\frac{I_i}{h_i} - \frac{I_{i-1}}{h_{i-1}}\right]$$

Simplifying -

$$\frac{1}{3}h_{i-1}m_{i-1} + \frac{2}{3}(h_{i-1} + h_i)\, m_i + \frac{1}{3}h_i\, m_{i+1} = 2\left[\frac{I_i}{h_i} - \frac{I_{i-1}}{h_{i-1}}\right]$$

or

$$\boxed{h_{i-1}\, m_{i-1} + 2(h_{i-1} + h_i)\, m_i + h_i\, m_{i+1} = 6\left[\frac{I_i}{h_i} - \frac{I_{i-1}}{h_{i-1}}\right]}$$

APPENDIX B: THE DIFFUSION EQUATION FOR CIRCUMFERENTIAL AVERAGE MIXING

In this section the diffusion equation for the mixing of stagnation enthalpy, rothalpy, and entropy is formulated. Unfortunately, this equation is complicated by the requirement that the computational grid used for through-flow analysis is generally a nonorthogonal one.

B.1 SECONDARY FLOW TRANSPORT

The secondary flow transport of any circumferentially averaged property, P, is assumed to be perpendicular to the streamlines in the meridional plane and is given by

$$-\varepsilon \frac{\partial P}{\partial n} \tag{B1}$$

where

$$\varepsilon = \frac{\rho m}{a V_m} \int_o^a V_s^{\,2}\, dt \tag{B2}$$

n = distance normal to streamlines
ρ = density
m = distance in the meridional direction
t = coordinate in the blade-to-blade direction
a = blade spacing
V_m = meridional component of circumferential average velocity
V_s = spanwise component of secondary and wake flow (in the n-direction)
P = circumferential mass-weighted average property. (In this section the overbars on $\bar{P}$ are omitted.)

In terms of the nonorthogonal coordinates, q and m, shown in Figure 43, the normal derivative is given by:

$$\frac{\partial P}{\partial n} = \frac{1}{\cos\,(\phi - \sigma)} \frac{dP}{dq} - \tan\,(\phi - \sigma) \frac{\partial P}{\partial m} \tag{B3}$$

AD-A159 312 SPANWISE REDISTRIBUTION OF ENERGY AND LOSS IN AN AXIAL FLOW COMPRESSOR BY..(U) GENERAL ELECTRIC CO CINCINNATI OH AIRCRAFT ENGINE BUSINESS GR.. C W WHITFIELD ET AL. 2/2

UNCLASSIFIED MAY 85 R84AEB460 AFWAL-TR-84-2109 F/G 20/4 NL

END

FILMED

DTIC

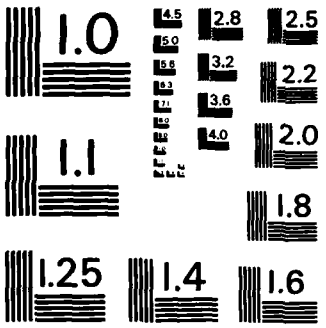

MICROCOPY RESOLUTION TEST CHART
NATIONAL BUREAU OF STANDARDS-1963-A

$$dq = h_2 \, d\xi_2$$

$$dm = h_1 \, d\xi_1$$

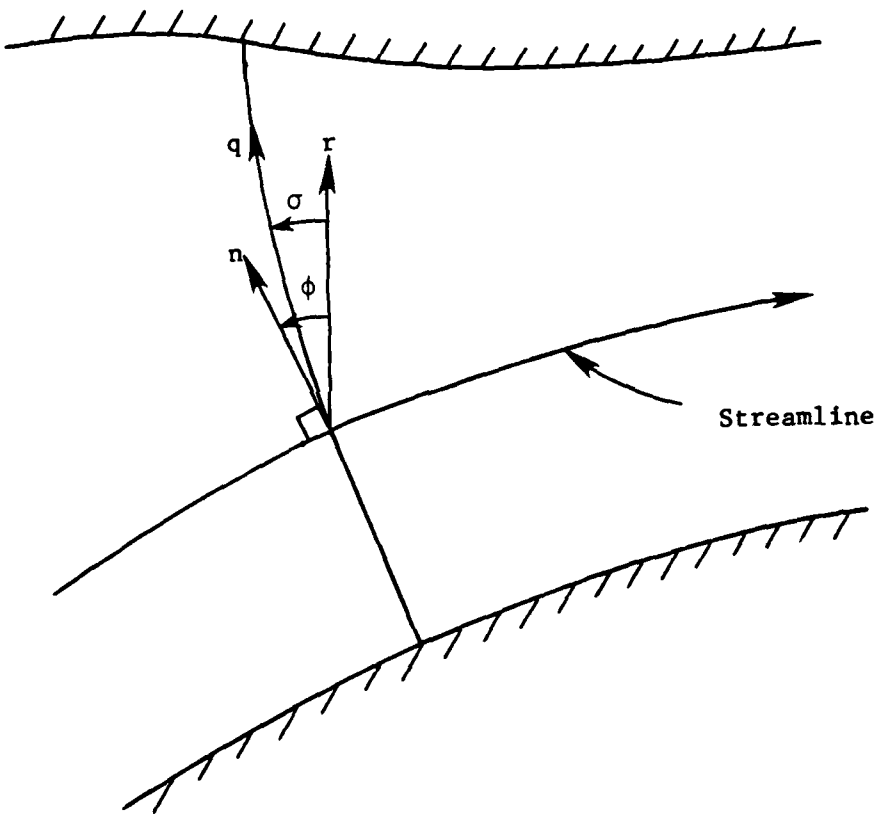

Figure 43. m - q Grid System.

The second term on the right of (B3) is generally small since $(\phi-\sigma)$ is small, and, if included, it would make the parabolic marching solution procedure impossible. Therefore, it is dropped. So:

$$\frac{\partial P}{\partial n} \approx \frac{1}{\cos(\phi - \sigma)} \frac{\partial P}{\partial q} \tag{B4}$$

B.2 DIFFERENTIAL FORM OF THE DIFFUSION EQUATION

Reference is now made to Figure 44. Considering the rectangular torus bounded by the faces labeled as i, j, i-1, j-1, it is required that the net flux of P through all of these faces be equal to the source of P integrated over the volume. As noted in the previous section, the flux normal to the streamlines is

$$\varepsilon P_n = \varepsilon \frac{\partial P}{\partial n} \approx \frac{\varepsilon}{\cos(\phi - \sigma)} \frac{\partial P}{\partial q} \tag{B5}$$

The transport of P parallel to the streamlines, carried by the fluid, is

$$\rho V_m P \tag{B6}$$

times the area normal to the streamlines.

The flux balance then is:

$$\begin{aligned} &[2\pi r\lambda h_2 \Delta\xi_2 \cos(\phi - \sigma)\rho V_m P]_i - [2\pi r\lambda h_2 \Delta\xi_2 \cos(\phi - \sigma)\rho V_m P]_{i-1} \\ &+ [2\pi r\lambda h_2 \Delta\xi_2 \sin(\phi - \sigma)\varepsilon P_n]_i - [2\pi r\lambda h_2 \Delta\xi_2 \sin(\phi - \sigma)\varepsilon P_n]_{i-1} \\ &- [2\pi r\lambda h_1 \Delta\xi_1 \varepsilon P_n]_j + [2\pi r\lambda h_1 \Delta\xi_1 \varepsilon P_n]_{j-1} \end{aligned} \tag{B7}$$

$$= \int_{j-1}^{j} \int_{i-1}^{i} S_c \, 2\pi r\lambda h_1 d\xi_1 \cos(\phi - \sigma) h_2 d\xi_2$$

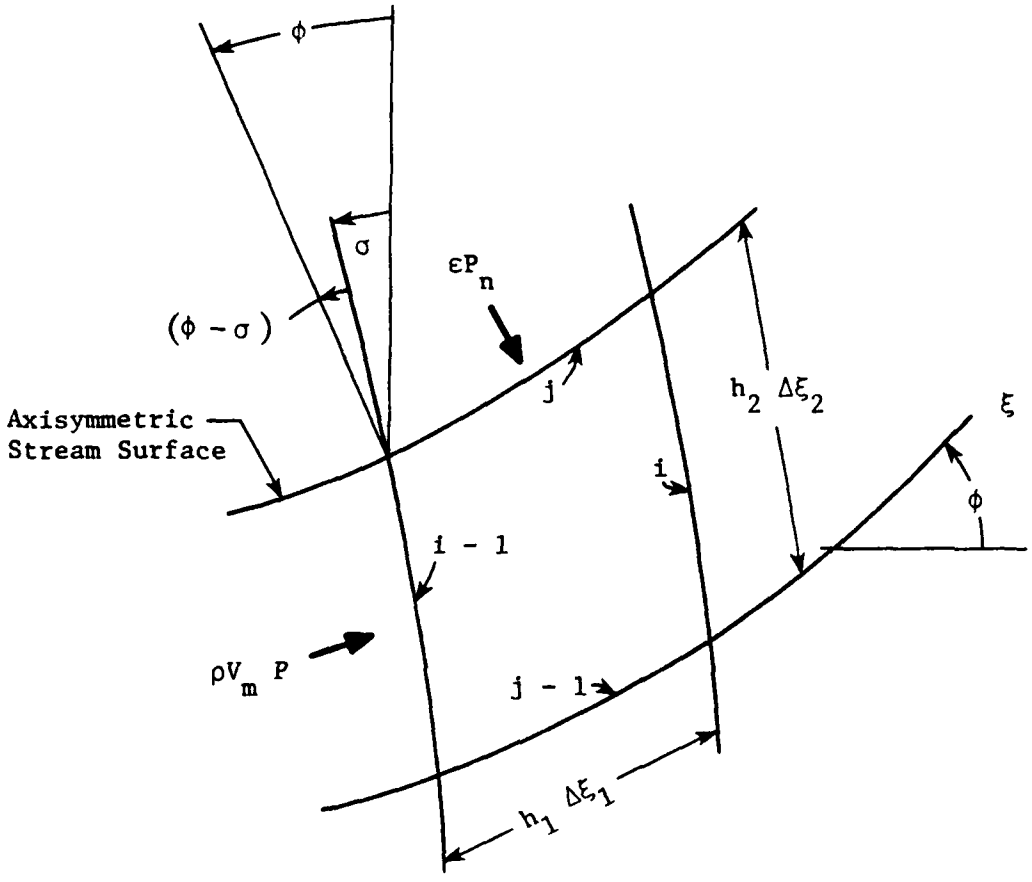

Figure 44. Designation of Cell Faces for the Derivation of the Diffusion Equation in Nonorthogonal Coordinates.

where S_c is a source term per unit volume.

To simplify this somewhat, substitute

$$f_2 = 2\pi r\lambda h_2 \cos(\phi - \sigma)\rho V_m \tag{B8a}$$

$$g_1 = \frac{2\pi r\lambda h_1 \varepsilon}{\cos(\phi - \sigma)} \tag{B8b}$$

$$g_2 = 2\pi r\lambda h_2 \tan(\phi - \sigma)\varepsilon \tag{B8c}$$

into (B7). Using (B5), the result is:

$$[f_2\Delta\xi_2 P]_i - [f_2\Delta\xi_2 P]_{i-1} + [g_2\Delta\xi_2 P_q]_i - [g_2\Delta\xi_2 P_q]_{i-1}$$
$$- [g_1\Delta\xi_1 P_q]_j + [g_1\Delta\xi_1 P_q]_{j-1} = RHS \tag{B9}$$

where RHS signifies the right-hand-side term of Equation (B7). Since $\Delta\xi_2$ is the same at faces i and i-1 and $\Delta\xi_1$ is the same at faces j and j-1, these values can be divided out. The first line of (B9) will become

$$\frac{[f_2P + g_2P_q]_i - [f_2P + g_2P_q]_{i-1}}{\Delta\xi_1}$$

which in differential form will be

$$\frac{\partial}{\partial\xi_1}[f_2P + g_2P_q]$$

By similar arguments for the 2nd line of (B9), the following differential equation is written:

$$\frac{\partial}{\partial \xi_1} [f_2 P + g_2 P_q] - \frac{\partial}{\partial \xi_2} [g_1 P_q] = 2\pi r \lambda \cos (\phi - \sigma) h_1 h_2 S_c \qquad \text{(B10)}$$

B.3 TRANSFORMATION TO STREAM FUNCTION COORDINATE

A somewhat more convenient form of the differential equation is obtained by replacing the ξ_2 coordinate with the stream function coordinate, ψ. The variable f_2, defined by Equation (B8a) relates $d\xi_2$ with $d\psi$.

$$d\psi = 2\pi r \lambda h_2 \cos (\phi - \sigma) \rho V_m \, d\xi_2$$

$$= f_2 \, d\xi_2$$

Also notice that if the continuity equation is satisfied, which it is, then f_2 is constant in the ξ-direction. With this in mind, Equation (B10) can be divided by f_2 with the following result:

$$\frac{\partial}{\partial \xi_1} [P + g_s P_q] - \frac{\partial}{\partial \psi} [g h_1 P_q] = \frac{h_1 S_c}{\rho V_m} \qquad \text{(B11)}$$

where

$$g = \frac{2\pi r \lambda \varepsilon}{\cos (\phi - \sigma)} \qquad \text{(B12a)}$$

$$g_s = \frac{\tan (\phi - \sigma)}{\cos (\phi - \sigma)} \frac{\varepsilon}{\rho V_m} = \frac{g_2}{f_2} \qquad \text{(B12b)}$$

B.4 DIFFUSION EQUATION SOURCE TERM

The source term in Equation (B11) is determined indirectly. As discussed in Section 3.5.1, wake centrifugation effects, in the absence of a spanwise variation of P (that is, $P_n = P_q = 0$), led to a circumferential average value of P equal to $\Delta P'$. Therefore, the differential equation must have the form:

$$\frac{\partial}{\partial \xi_1} [P + g_s P_q] - \frac{\partial}{\partial \psi} [g h_1 P_q] = \frac{\partial \Delta P'}{\partial \xi_1} \tag{B13}$$

so that when $P_q = 0$, it follows that

$$\frac{\partial P}{\partial \xi_1} = \frac{\partial \Delta P'}{\partial \xi_1}$$

Therefore, the source term by deducton is

$$S_c = \frac{\rho V_m}{h_1} \frac{\partial \Delta P'}{\partial \xi_1}$$

Equation (B13), together with the definition

$$P_q \equiv \frac{1}{h_2} \frac{\partial P}{\partial \xi_2} , \tag{B14}$$

is the form of the diffusion equation to be solved in the through-flow analysis program. This equation is linear for prescribed values of g and g_s, both defined by Equation (B12).

APPENDIX C: NUMERICAL SOLUTION TO THE DIFFUSION EQUATION IN NONORTHOGONAL COORDINATES

No claim is made that the mathematical model described in this report is a highly accurate one. In fact, the model is inherently an approximate one. Nevertheless, we chose a good quality numerical scheme for integretating the diffusion equation, derived in the previous section, because the hub-to-tip streamline grid spacings may be very nonuniformly distributed. In fact, a high concentration of grid lines near the hub and tip and a sparse midspan distribution is preferred. To prevent a solution that is largely dependent on the number of spanwise grid points, a second order accurate algorithm is a requirement. Another requirement is global conservation of the property P.

To meet these two requirements, a general spline scheme is formulated wherein an integral form, as well as the differential form of the conservation equation, is employed. The basic differential equation, as developed in the previous section, is

$$\frac{\partial}{\partial \xi_1} [P + g_s P_q] - \frac{\partial}{\partial \psi} [g h_1 P_q] = \frac{\partial \Delta P'}{\partial \xi_1} \tag{C1}$$

where

$$g = \frac{2\pi r \lambda \varepsilon}{\cos(\phi - \sigma)} \tag{C2a}$$

$$g_s = \frac{\tan(\phi - \sigma)}{\cos(\phi - \sigma)} \frac{\varepsilon}{\rho V_m} \tag{C2b}$$

and for later reference:

$$f = 2\pi r \lambda \cos(\phi - \sigma) \rho V_m \tag{C2c}$$

Equation (C1) is first discretized in the ξ_1 direction.

$$[P + g_s P_q]_i - [P + g_s P_q]_{i-1} - \theta\left[\frac{\partial}{\partial\psi}\,(gh_1 P_q)\right]_i$$

$$- (1 - \theta)\,\frac{\partial}{\partial\psi}\,(g_{i-1}\, h_{1i}\, P_{q_{i-1}}) = \Delta P'_i - \Delta P'_{i-1} \qquad \text{(C3)}$$

For convenience, we have chosen $\Delta\xi = 1$. Note that the distance between adjacent grid points is

$$m_i - m_{i-1} = h_{1i} \quad \Delta\xi_1 = h_{1i} \qquad \text{(C4)}$$

Because the integration is between i-1 and i, where (C4) applies, it is appropriate to use h_{1i} where h_1 appears. Hence, $h_{1\ i-1}$ does not appear in (C3). Also, the parameter, θ, is the Crank-Nicholson weighting parameter. Ideally, θ is one half. However, a value slightly larger than one half is generally chosen for stability.

Rearrangement of (C3), to put the "knowns" on the right-hand side, gives:

$$[P + g_s\, P_q]_i - \theta\left[\frac{\partial}{\partial\psi}\,(gh_1\, P_q)\right]_i$$

$$= [P + g_s\, P_q]_{i-1} + (1 - \theta)\,\frac{\partial}{\partial\psi}\,(g_{i-1}\, h_{1i}\, P_{q_{i-1}}) + \Delta P'_i - \Delta P'_{i-1} \qquad \text{(C5)}$$

This equation is now integrated with respect to ψ using the trapezoidal rule:

$$\left|\left[\frac{\partial}{\partial\psi}\,(gh_1\, P_q)\right]_{j-1} + \left[\frac{\partial}{\partial\psi}\,(gh_1\, P_q)\right]_j\right| \frac{\Delta\psi_j}{2} = (gh_1\, P_q)_j - (gh_1\, P_q)_{j-1} \qquad \text{(C6)}$$

The result is:

$$\frac{1}{2}\Delta\psi_j \left\{[P + g_s P_q]_{i,j} + [P + g_s P_q]_{i,j-1}\right\}$$
$$- \theta\left\{(gh_1 P_q)_{i,j} - (gh_1 P_q)_{i,j-1}\right\}$$
$$= \frac{1}{2}\Delta\psi_j \left\{[P + g_s P_q]_{i-1,j} + [P + g_s P_q]_{i-1,j-1}\right.$$
$$\left. + \Delta P'_{i,j} + \Delta P'_{i,j-1} - \Delta P'_{i-1,j} - \Delta P'_{i-1,j-1}\right\} \qquad (C7)$$
$$+ (1 - \theta)\left\{h_{1i,j}\,(gP_q)_{i-1,j} - h_{1i,j-1}\,(gP_q)_{i-1,j-1}\right\}$$

Equation (C7) provides one relationship between P and P_q. One additional relation is needed to complete the system. This relation is:

$$P_j - P_{j-1} - (P_{qj} + P_{qj-1})\frac{h_{2j}}{2} + \lambda\left[P_{qq_j} - P_{qq_{j-1}}\right]\frac{h_{2j}^2}{12} = 0 \qquad (C8)$$

Equation (C8), with λ=1, is based on a quartic polynomial for P between points j-1 and j. The quartic is reduced to a parabola by setting λ=0. The second derivative, P_{qq}, is related to terms in the differential equation (C5) in the following way:

$$gh_1 P_{qq} = gh_1 \frac{\partial 2P}{\partial q^2} = \frac{\partial}{\partial q}(gh_1 P_q) - P_q \frac{\partial}{\partial q}(gh_1)$$

$$P_{qq} = \frac{1}{gh_1}\left[f \frac{\partial}{\partial \psi}(gh_1 P_q) - P_q \frac{\partial}{\partial q}(gh_1)\right] \qquad (C9)$$

Substitution of (C9) into (C8) yields:

$$P_j - P_{j-1} - (P_{q_j} + P_{q_{j-1}}) \frac{h_{2j}}{2} + \frac{\lambda h_{2j}^2}{12} \left\{ \frac{1}{(gh_1)_j} \left[f_j \frac{\partial}{\partial \psi} (gh_1 P_q)_j - P_{q_j} \frac{\partial}{\partial q} (gh_1)_j \right] - \frac{1}{(gh_1)_{j-1}} \left[f_{j-1} \frac{\partial}{\partial \psi} (gh_1 P_q)_{j-1} - P_{q_{j-1}} \frac{\partial}{\partial q} (gh_1)_{j-1} \right] \right\} = 0 \quad \text{(C10)}$$

Thus we have three equations, (C5), (C7), and (C10), for the system matrix equation. The three unknowns at each mode are P_q, P, and

$$\frac{\partial}{\partial \psi} (gh_1 Pq) .$$

To conserve property P, the boundary conditions are:

$P_q = 0$ for $j = 1$ and $j = NJ$

where $j = 1$ and NJ corresponds to the casing and hub boundaries.

The parameter λ appears in Equation (C9). If $\lambda=0$, this scheme is known as the Keller-Box method. Unfortunately, for small values of ϵ (that is, small secondary flow) the Keller-Box method produces wiggles. The wiggles disappear where $\lambda=1$, in which case the method is a cubic spline method. Intermediate values of λ are also permitted.

REFERENCES

1. Adkins, G.G., Jr. and Smith. L.H., Jr., "Spanwise Mixing in Axial-Flow Turbomachines," Trans. ASME, Journal of Engineering for Power, Vol. 104, pp 97-110, January 1982.

2.* Smith, L.H., Jr., "Three-Dimensional Flow in Axial-Flow Turbomachinery, Part I. Theoretical Determination of Secondary Flow," Report I-14, Inst. for Coop. Res., Mechanical Engineering Department, The John Hopkins University, Baltimore, Md., November 1953.

3.* Smith, L.H., Jr., "Three-Dimensional Flow in Axial-Flow Turbomachinery, Part II. Experimental Investigations," Report I-16, Inst. for Coop. Res., Mechanical Engineering Department, The John Hopkins University, Baltimore, Md., May 1954.

4. Smith, L.H., Jr., "Secondary Flow in Axial-Flow Turbomachinery," Trans. ASME, vol. 77, No. 7, p 1065, October 1955.

5. Smith, L.H., Jr., "Casing Boundary Layers in Multistage Axial-Flow Compressors," Flow Research on Blading, L.S. Dzung, ed., Elsevier Publishing, Amsterdam, 1970, p 275.

6. Lakshminarayana, B. and Horlock, J.H., "Leakage and Secondary Flows in Compressor Cascades," ARC, R&M No. 3483, March 1965.

7. Koch, C.C. and Smith, L.H., Jr., "Loss Sources and Magnitudes in Axial-Flow Compressors," Trans. ASME, Journal of Engineering for Power, Vol. 98, p 411, July 1976.

8. Whitfield, C.E., "Wake Centrifugation - Quarterly R&D Status Report and Program Schedule No. 1," Contract F33615-81-C-2090, R82AEB143.

9. Whitfield, C.E., "Wake Centrifugation - Quarterly R&D Status Report and Program Schedule No. 2," Contract F33615-81-C-2090, R82AEB308.

10. Whitfield, C.E., "Wake Centrifugation - Quarterly R&D Status Report and Program Schedule No. 3," Contract F33615-81-C-2090.

11. Whitfield, C.E., "Wake Centrifugation - Quarterly R&D Status Report and Program Schedule No. 4," Contract F33615-81-C-2090, R82AEB499.

12. Whitfield, C.E., "Wake Centrifugation - Quarterly R&D Status Report and Program Schedule No. 5," Contract F33615-81-C-2090, R83AEB130.

*References 2 and 3 have been combined and published under the title "Three-Dimensional Flow in Axial-Flow Turbomachinery" as Wright Air Development Center Technical Report 55-348, August 1955.

13. Whitfield, C.E., "Wake Centrifugation - Quarterly R&D Status Report and Program Schedule No. 6," Contract F33615-81-C-2090, R83AEB307.

14. Johnston, J.P., "On the Three-Dimensional Turbulent Boundary Layer Generated by Secondary Flow," Trans. ASME, Series D, Journal of Basic Engineering, Vol. 82, p 233, March 1960.

15. Dring, R.P., Joslyn, H.D., and Hardin, L.W., "An Investigation of Axial Compressor Rotor Aerodynamics," Trans. ASME, Journal of Engineering for Power, Vol. 104, pp 85-96, January 1982.

16. Larguier, R., "Experimental Analysis Methods for Unsteady Flows in Turbomachinery," Measurement Methods in Rotating Components of Turbomachinery, p 71, presented at ASME Joint Fluids Engineering, Gas Turbine Conference and Products Show, New Orleans, Louisiana, March 10-13, 1980.

17. Larguier, R. and deSievers, A., "Methodes de Mesures Instationnaires dans Les Turbomachines," (in French), presented at AAAF 10th Colloquium on Applied Aerodynamics, Lille, France, 7-9 November, 1973.

18. Ravindranath, A. and Lakshminarayana, B., "Mean Velocity and Decay Characteristics of the Near-and-Far Wake of a Compressor Rotor Blade of Moderate Loading," Trans. ASME, Journal of Engineering for Power, Vol. 102, pp 535-548, July 1980.

19. Reynolds, B. and Lakshminarayana, B., "Characteristics of Lightly Loaded Fan Rotor Blade Wakes," NASA CR-3188, October 1979.

20. Wennerstrom, A.J., Law, C.H., Buzzell, W.A., and Derose, R.D., "Investigation of a 1500 ft/s Transonic, High-Through-Flow, Single-Stage Axial Flow Compressor with Low Hub/Tip Ratio," AFAPL-TR-76-92," October 1976.

21. Simonson, M.R., "Data Match Pass for USAF 1500 ft/sec, Transonic, High-Through-Flow, Single Stage Axial-Flow Compressor," Technical Memo TM 77-175, Aircraft Engine Business Group., General Electric Co.

22. Smith, L.H., Jr., "Casing Boundary Layers in Multistage Axial Flow Compressors," Flow Research on Blading, L.S. Dzung, ed., Elsevier, Amsterdam, p 275, 1970.

U.S.Government Printing Office: 1985 — 559-065/20920

END

FILMED

11-85

DTIC